Carsten Henkel

Coherence theory of atomic de Broglie waves and electromagnetic near fields

Habilitationsschrift

Universität Potsdam, Juni 2004

Contents

Acknowledgement

I would like to thank numerous colleagues with whom I learned a significant fraction of the physics summarized in this thesis. I am indebted to my *directeur de thèse*, Alain Aspect (Orsay), and to the physicists in Paris (among them Claude Cohen-Tannoudji, Philippe Grangier, Jean-Jacques Greffet, Robin Kaiser, Astrid Lambrecht, and Serge Reynaud), who shaped my way of working, helping to merge *le précis* and *das Anschauliche*. Klaus Mølmer (Aarhus) and Martin Wilkens (Potsdam) are both responsible for the fine tuning of my theoretical toolbox. I gratefully acknowledge Martin for granting space and freedom to acquire experience in teaching, fund raising and research management. Thanks is due to the reviewers of this thesis, Dirk-Gunnar Welsch (Jena) and Pierre Meystre (Tucson). Colleagues from experimental physics continue to provide questions and stimulus for theoretical research, and I thank particularly Ron Folman (Beer Sheva), Tilman Pfau (Stuttgart), Vahid Sandoghdar (Zürich), and Jörg Schmiedmayer (Heidelberg). Thanks to Jacques Baudon and Martial Ducloy (Paris), Jürgen Mlynek (Berlin), Wolfgang Schleich (Ulm), Robert Spreeuw (Amsterdam), Bart Van Tiggelen (Grenoble), and John Weiner (Toulouse) for invitations to interesting laboratories. I thank Fernando Sols (Madrid) and Paolo Tombesi (Camerino) for providing cross-road posts pointing towards new and exciting realms of research.

My work has been supported financially by the Deutsche Forschungsgemeinschaft DFG, by the Deutscher Akademischer Austauschdienst DAAD, and by the European Union through Research Networks.

I would like to acknowledge the companionship of young researchers who have become more than colleagues over the last years: Isabelle Bouchoule (Orsay), Rémi Carminati (Paris), Peter Domokos (Budapest), Jens Eisert (Potsdam), Karl Joulain (Poitiers), Mathias Nest (Potsdam), Lukas Novotny (Rochester), and Stefan Scheel (London).

Among the staff at Universität Potsdam, I would like to thank Arkadi Pikovski for sharing faithfully the Tuesday afternoon seminar, Ralf Menzel for continuously pulling discussions to the experimentally relevant level, and Reimund Gerhard-Multhaupt for his open-minded chairing of the jury. Thanks to the work kindly done and well done by Jutta Mainitz, Marlies Path, and Timo Felbinger on the quantum optics floor, this thesis could be finished in

excellent conditions.

These students have worked and are working closely with me in Potsdam and remotely, and I thank them for their valuable input: Geesche Boedecker, Dörte Blischke, Sébastien Clodong, Axel Friedenauer, Andreas Jacob, Peter Krüger (Heidelberg), Jean-Philippe Mulet (Paris), Antonio Negretti, Sierk Pötting, Lavinia Rogobete (Zürich), and Bo Zhang.

Finalement, merci à ma femme Valérie. Sans tes questions et ton soutien, cette étape aurait été moins fluide à franchir.

Abstract

We theoretically discuss the interaction of neutral particles (atoms, molecules) with surfaces in the regime where it is mediated by the electromagnetic field. A thorough characterization of the field at sub-wavelength distances is worked out, including energy density spectra and coherence functions. The results are applied to typical situations in integrated atom optics, where ultracold atoms are coupled to a thermal surface, and to single molecule probes in near field optics, where sub-wavelength resolution can be achieved.

Key words: coherence theory, quantum optics, quantum electrodynamics (QED), atom optics, atom chip, spectroscopy, surface, near field optics, nano optics

Die Arbeit untersucht theoretisch die Wechselwirkung neutraler Teilchen (Atome, Moleküle) mit Oberflächen, soweit sie durch das elektromagnetische Feld vermittelt wird. Spektrale Energiedichten und Kohärenzfunktionen werden hergeleitet und liefern eine umfassende Charakterisierung des Felds auf der sub-Wellenlängen-Skala. Die Ergebnisse finden auf zwei Teilgebieten Anwendung: in der integrierten Atomoptik, wo ultrakalte Atome an thermische Oberflächen koppeln, und in der Nahfeldoptik, wo eine Auflösung unterhalb der Beugungsbegrenzung mit einzelnen Molekülen als Sonden und Detektoren erzielt werden kann.

Schlüsselbegriffe: Kohärenztheorie, Quantenoptik, Quanten-Elektrodynamik (QED), Atomoptik, Atomchip, Spektroskopie, Oberfläche, Nahfeldoptik, Nano-Optik

Thesen

1. Die Wechselwirkung von Licht mit Materie hat in der Geschichte der Physik wiederholt das Feld geliefert, auf dem bedeutende Meilensteine gesetzt wurden. Dazu gehören die Entdeckung der Elektrodynamik und der Quantentheorie.

2. Die Beschreibung eines Lichtfelds bei endlicher Temperatur erfordert Begriffe aus der Gleichgewichts-Thermodynamik. Charakteristische Größen wie die spektrale Energiedichte werden aus Korrelationsfunktionen der elektrischen und magnetischen Felder im kanonischen Ensemble gewonnen. Bei hohen Frequenzen (sichtbares Spektrum) oder verschwindender Temperatur können die Quanten-Fluktuationen der Felder durch die Korrelationsfunktionen der quantisierten Feldoperatoren charakterisiert werden. Das Fluktuations-Dissipations-Theorem liefert in beiden Fällen eine Verknüpfung zu den entsprechenden Green'schen Funktionen. Für bosonische Felder wie das elektromagnetische Feld können diese aus den (klassischen) Feldgleichungen berechnet werden.

3. Die Korrelationsfunktionen des elektromagnetischen Feldes bestimmen dessen Kohärenzeigenschaften und damit seine 'Interferenzfähigkeit'. Der Kontrast eines Interferenzmusters etwa wird durch den Betrag einer geeigneten Korrelationsfunktion gegeben. Sind zwei Punkte im Feld durch einen Abstand größer als die Kohärenzlänge getrennt, kann die Strahlung, die von ihnen ausgeht, keine signifikante Interferenz zeigen. Im freien Raum, nach Filterung eines schmalbandigen Frequenzbereichs, ist die Kohärenzlänge von der Größenordnung der Wellenlänge.

4. Materielle Objekte streuen, reflektieren oder beugen Licht und sind bei endlicher Temperatur selbst Quellen von elektromagnetischer Strahlung. Die Materie-Licht-Wechselwirkung kann auf geeigneten Längenskalen mit Hilfe der makroskopischen Maxwell'schen Gleichungen beschrieben werden. Aufgrund der Kleinheit der atomaren Dimensionen im Vergleich zu typischen Wellenlängen erlauben es die makroskopischen Gleichungen, das Lichtfeld

auf Skalen kleiner als die Wellenlänge zu charakterisieren, und dies bis hinauf in den sichtbaren Spektralbereich. Dass dies möglich ist, ist letztendlich auf die Kleinheit der Feinstrukturkonstante zurückzuführen. Experimentell ist dieses Regime seit den 1980er Jahren durch die optische Raster-Mikroskopie zugänglich geworden.

5. Im 'Nahfeld' eines Objektes, bei Abständen kleiner als die Wellenlänge, zeigt das Lichtfeld deutlich andere Eigenschaften als im freien Raum. Die spektrale Energiedichte hängt von den Eigenschaften der Materie (Brechungsindex, Absorption) ab. Sie liegt bei endlicher Absorption um Größenordnungen oberhalb der Planck'schen Strahlungsformel. Metallische Objekte zeigen ein deutliches Ungleichgewicht zugunsten der magnetischen Energiedichte bei Abständen um die elektromagnetische Eindringtiefe (*skin depth*).

6. Die Kohärenzeigenschaften der Emission eines thermischen Objekts variieren im Nahfeld mit dem Abstand von der Quelle. Im Grenzfall sehr kleiner Abstände hängt die normierte räumliche Kohärenzfunktion allein von der Geometrie von Quelle und Beobachtungspunkten ab: Abstand des Beobachters und Kohärenzlänge sind gleich. Ist der Abstand vergleichbar mit der Wellenlänge und das Objekt metallisch, sind elektromagnetische Oberflächen-Resonanzen thermisch angeregt und führen zu einer Kohärenzlänge jenseits der Vakuum-Wellenlänge. Diese Regimes können durch einfache asymptotische Formeln quantitativ beschrieben werden [C. Henkel, K. Joulain, R. Carminati und J.-J. Greffet, *Opt. Commun.* **186** (2000) 57].

7. Atome und Moleküle koppeln über ihre elektrischen und magnetischen Dipolmomente an das elektromagnetische Feld. Die (thermischen oder quantenmechanischen) Fluktuationen des Felds erfordern eine statistische Beschreibung der entsprechenden Wechselwirkungen. Mastergleichungen bilden das Werkzeug dazu, so lange die Felder in einem breiten Spektralbereich fluktuieren.

8. Die Wechselwirkung von Atomen oder Molekülen mit einem Objekt wird auf Abständen oberhalb der atomaren Skala durch das elektromagnetische Feld vermittelt. Die Gegenwart des Objekts verschiebt die Energieniveaus der Teilchen und erhöht typischerweise die spontane Zerfallsrate von angeregten Zuständen. Die entsprechenden Zeit- und Frequenz-Skalen werden durch die Korrelationsfunktionen der elektrischen und magnetischen Felder in der Nähe des Objekts bestimmt.

9. Im Nahfeld einer dielektrischen Oberfläche, die auf der sub-Wellenlängenskala strukturiert ist, ist die Linienbreite eines elektrischen Dipolübergangs ebenfalls auf kleinen Skalen ortsabhängig. Dies kann dazu benutzt werden, die Topographie und die lokale dielektrische Funktion der

Oberfläche mit hoher Ortsauflösung zu vermessen. Die Auflösung ist nur durch den mittleren Abstand des Atoms oder Moleküls von der Probe begrenzt [C. Henkel und V. Sandoghdar, *Opt. Commun.* **158** (1998) 250].

10. Einzelne Moleküle, die in kleine, dielektrische Objekte von Nanometergröße implantiert sind, haben eine längere radiative Lebensdauer, weil Polarisationsladungen an der Oberfläche des Objekts das Dipolmoment des Moleküls abschirmen. Die Form des Objekts und die Position des Moleküls können die Lebensdauer stark beeinflussen [L. Rogobete, H. Schniepp, V. Sandoghdar und C. Henkel, *Opt. Lett.* **28** (2003) 1736].

11. Mikrostrukturierte Substrate sind ein wichtiges Element für die Realisierung von 'Atom-Chips', mit deren Hilfe atomoptische Elemente miniaturisiert werden und möglicherweise ein skalierbarer Quantencomputer auf der Basis neutraler Atome implementiert werden kann. Metallische Strukturen in Atom-Chips sind eine Quelle thermischer Magnetfelder, die den Spin paramagnetischer Atome umklappen und zu Verlusten aus der Mikrofalle führen [C. Henkel, S. Pötting und M. Wilkens, *Appl. Phys. B* **69** (1999) 379]. Die entsprechenden Verlustraten wurden von nicht weniger als vier experimentellen Gruppen qualitativ beziehungsweise quantitativ nachgewiesen.

12. Thermische Magnetfelder und fluktuierende Ströme tragen in Atom-Chips auch zur Erwärmung der gefangenen Atome auf einer Zeitskala von Sekunden bei. In aktuellen Experimenten ist technisches Stromrauschen die dominante Wärmequelle. Die Kopplung an das Magnetfeld wird für spinlose Atome irrelevant. Dann vermitteln Fluktuationen der van der Waals-Wechselwirkung aufgrund der Phononen-Anregungen der Chip-Oberfläche den Wärmeübertrag [C. Henkel und M. Wilkens, *Europhys. Lett.* **47** (1999) 414].

13. Atome in stark anisotropen Mikrofallen, die in der Nähe eines Substrates an thermische elektromagnetische Felder koppeln, sind ein relativ gut charakterisiertes Modellsystem, um die Dekohärenz von Materiewellen nachzuweisen. Die atomaren de Broglie-Wellen verlieren ihre räumliche Kohärenz auf einer typischen Zeitskala von Sekunden. Die Dekohärenzrate steigt mit dem Abstand zwischen zwei Punkten im Wellenfeld an, sättigt aber auf Distanzen größer als der typische Abstand der Mikrofalle von der Substrat-Oberfläche [C. Henkel, P. Krüger, R. Folman und J. Schmiedmayer, *Appl. Phys. B* **76** (2003) 173]. Dies kann etwa durch ein Atom-Interferometer nachgewiesen werden, in dem ein kaltes Ensemble oder ein Bose-Einstein-Kondensat in einem zeitabhängigen Potential aufgespalten und wieder vereinigt wird.

14. Zusammenfassend läßt sich sagen, dass die Kohärenz-Eigenschaften elektromagnetischer Nahfelder durch die Geometrie und die dielektrischen Eigenschaften der benachbarten Materie charakterisiert sind. Die Felder verhalten

sich quasi-statisch, Retardierung und Beugungsbegrenzung spielen eine untergeordnete Rolle. Das Nahfeld fluktuiert aufgrund der thermischen Anregungen der Materie. Nicht-propagierende ('evaneszente') Felder sind dominant und führen zu einer überhöhten lokalen Zustands- und Energiedichte. Im Nahfeld gefangene Atome und Moleküle sind eine empfindliche Sonde für elektromagnetische Fluktuationen.

Part I

Introduction

Chapter 1

Background

Free space is a highly symmetric medium for the propagation of light. This symmetry is broken by material objects that interact with the light field. The understanding of these interactions which often complicate the analysis, has also led to many breakthroughs in modern physics. A brief historical review may serve to illustrate this.

When James Clerk Maxwell (around 1860) adds the displacement current to the Faraday law, it becomes clear that electromagnetic waves propagate even through free space. The idea that empty space is not filled with any material substance gets widely accepted only after the null result of the Michelson-Morley experiment (1887) and its interpretation by Einstein (1905). That electromagnetic waves themselves do exist is demonstrated in 1888, when Heinrich Hertz uses objects like books and paraffine blocks as refractive elements. Sub-wavelength holes in an opaque screen are put forward in a visionary proposal by E. H. Synge (1928) as a detector of the near field close to a sample whose resolution is not limited by diffraction.

Max Planck (1900) invokes thermal equilibrium between the walls of a cavity and the field it contains to derive the spectral density of blackbody radiation. The proof of the same law by Albert Einstein (1917) is based on a more detailed picture of the interaction between light and matter. The concepts of spontaneous and stimulated emission are combined with Boltzmann statistics for an atom modelled by a two-level system, a model that becomes a 'working horse' for quantum optical processes. In the same paper, Einstein shows that the quantized momentum exchanges between atoms and the light field lead to Brownian motion in momentum space where the diffusion coefficient is linked to a radiative friction force via a fluctuation-dissipation theorem (the 'Einstein relation'). Eugene Wigner and Victor Weisskopf (1930) track spontaneous emission back to the dissipation an atom suffers when it is coupled to a

reservoir, *viz.* the quantized radiation field. At zero temperature, spontaneous emission can be interpreted as being stimulated by the quantum fluctuations of the field. The same fluctuations give rise to energy shifts the computation of which becomes an art in quantum electrodynamics. One of the first examples is the prediction of H. B. Casimir and D. Polder (1948) that close to a perfectly reflecting mirror, atomic ground states show a distance-dependent energy shift featuring different power laws, depending on the distance compared to the dominant transition wavelength.

This deliberately incomplete survey does not only illustrate the paradigmatic role of matter-light interactions, but also highlights the major impact of thermodynamical and statistical physics arguments. New developments continue to be reported and follow a similar route. A recent example from the theoretical side is the formulation in the 1990s of a consistent quantum electrodynamics for the macroscopic Maxwell equations, i.e. for dispersive and absorbing media (Huttner & al., 1991; Gruner & Welsch, 1995; Tip, 1997; Stefano & al., 1999). This theory draws on the 'fluctuation electrodynamics' developed by S. M. Rytov (1953) and is consistent with the work of G. S. Agarwal (1975) who characterized the quantized electromagnetic field near dielectric objects using the fluctuation-dissipation theorem. On the experimental side, the fundamental concepts of spontaneous emission and photon recoil have turned since the 1980s into operational tools that allow modern experimenters to reach unprecedentedly low temperatures in atomic gases (Nobel prize 1997 awarded to S. Chu, C. Cohen-Tannoudji, and W. D. Phillips). The interaction with light, in particular from laser sources, has played a key role along the way of cooling and controlling the motion of atoms and is still a tool of choice to perform coherent quantum operations with trapped atoms.

The light-matter interaction is a generic example of system-reservoir dynamics, and non equilibrium processes are handled in a natural way in this context. This can be illustrated with a simple situation taken right from the pioneering works mentioned above, namely the evolution of a two-level atom (the 'system') coupled to the quantized radiation field (the 'reservoir'). An important piece of information about the system is given by the occupation probabilities of two orthogonal states, $|\mathrm{g}\rangle$ and $|\mathrm{e}\rangle$, say. Typically these are eigenstates of the isolated system Hamiltonian and become 'dressed' and renormalized in energy when coupled to the field. The modelling of the field as a reservoir enforces a probabilistic description of the state occupations. The concept of a statistical ensemble (for example, Boltzmann factors for the reservoir states) thus merges with quantum expectation values for system observables (the population inversion for example). The reservoir-induced dynamics of the occupation probabilities is described in terms of rate equations, similar to those used by Einstein (1917). Their key ingredient are transition rates be-

tween the system states, that can be calculated using Wigner-Weisskopf theory in terms of correlation functions of the reservoir observable the system couples to. Let us convene that the usual weak-coupling, electric dipole, and rotating wave approximations are made. Then, the rate of (spontaneous plus stimulated) emission is given by the local spectral density of the electric field, i.e. the temporal Fourier transform of the field correlation function $\langle E(x,t)E(x,t')\rangle$, with respect to $t-t'$, taken at the (renormalized) atomic transition frequency and evaluated at the atomic position x. (E is the electric field projection along the atomic electric dipole moment.) Second-order field correlations of this type thus determine the time scale for reservoir-induced dynamical processes. Their evaluation plays a crucial role in this thesis. While the results are well-known in free space, they will also be required in the near field of macroscopic objects where a strong position dependence occurs. In addition, we shall be interested in situations where the field is not in thermal equilibrium, but generated by objects held at nonzero temperature. Situations of this kind occur in different sub-fields, but can be summarized in the generic setting of an atom located at sub-wavelength distance from some macroscopic object. A brief introduction is given in Chapter 2.

Rate equations and population dynamics do not exhaust the information potentially available in a quantum system. Superposition states also exist and evolve in time. A typical question that arises is: in the course of time, to what extent does the contact with the reservoir preserve the 'quantum' character of the superposition (the system being in one *and* another state[1]), and on what timescale and in which basis is it replaced by 'classical' alternatives (the system in one *or* another state[2])? To decide this question operationally, interference measurements have to be performed. The superposition state is still discernable as long as interference fringes can be seen — classical alternatives do not interfere. A quantitative measure of the 'quantum superposition' character is hence the fringe contrast. For the two-level-atom introduced above, the corresponding key quantity is the magnitude of the average value $\rho_{\mathrm{eg}}(t) \equiv \langle |\mathrm{g}\rangle\langle \mathrm{e}|\rangle$ where $|\mathrm{g}\rangle$ and $|\mathrm{e}\rangle$ are the basis states of the superposition and the angular brackets denote the average with respect to the system+reservoir ensemble. This quantity (an off-diagonal element of the density matrix) is called a *coherence*, and it is quite analoguous to the reservoir correlation functions mentioned above. Indeed, if the system is described by probability amplitudes $\psi_{\mathrm{g,\,e}}(t)$ (see footnote 1), the coherence can be written as $\rho_{\mathrm{ge}}(t) = \langle \psi_{\mathrm{g}}^*(t)\psi_{\mathrm{e}}(t)\rangle$. The average here takes into account that the system+reservoir dynamics cannot reduce to a pure Schrödinger evolution of the system wave function. For example, one can formulate a stochastic dynamics where 'quantum jumps' interrrupt at ran-

[1] Mathematically, in terms of a state vector, $|\psi(t)\rangle = \psi_{\mathrm{g}}(t)|\mathrm{g}\rangle + \psi_{\mathrm{e}}(t)|\mathrm{e}\rangle$.
[2] In terms of a density operator, $\rho(t) = p_{\mathrm{g}}(t)|\mathrm{g}\rangle\langle \mathrm{g}| + p_{\mathrm{e}}(t)|\mathrm{e}\rangle\langle \mathrm{e}|$.

dom times an otherwise continuous evolution. Averaging over a sample of stochastic wave functions then reproduces (or 'unravels') the dynamics of the system density matrix. We note that, again, one faces a second-order correlation function: coherences are correlation functions of state amplitudes or field operators.

To summarize, one is led to describe the dynamics of atoms or molecules interacting with the quantized light field in terms of a coherence theory. Depending on the relevant degrees of freedom in the system, this theory generates different kinds of equations. In the example above, the non-equilibrium dynamics of a few-level atom is typically described by a master equation for the reduced density matrix, in the simplest case in Lindblad form and with the Markov property. The characteristic scales in time and space for the master equation are determined by the electromagnetic field correlation functions. The radiation generated by some source is described by Maxwell equations in macroscopic media, combined with a suitable source correlation function. From this starting point, equations of motion for the field coherence functions can be derived. If the medium properties are only partially known and require statistical modelling, light scattering can be described with some approximations in terms of radiative transfer theory, and optical coherence functions can be retrieved. Another example of such a statistical wave optics is provided by ultracold atomic matter waves that interact with quantum or thermal electromagnetic field fluctuations. Their dynamics even gets nonlinear if the atoms degenerate at low temperatures into a Bose-Einstein condensate.

The aim of this habilitation thesis is to put into use a coupled coherence theory of atoms and light in order to formulate and answer basic questions that originate in the rapidly evolving fields of integrated atom optics and subwavelength optics. An introduction to these is given in Chapter 2. We rise to the challenge of describing systems at finite temperature or partially out of thermodynamic equilibrium, and focus on a typical setting where macroscopic, solid materials, with dimensions of at least a few nanometers, interact with the electromagnetic field by generating, scattering, or absorbing photons. The research in this context may be loosely organized around two types of questions: (i) what is the relevance of electromagnetic perturbations generated by a solid structure when an ultracold atomic sample is approached at nanometer distances?, and (ii) what kind of information about a nanostructure can be extracted via the electromagnetic field, possibly with high spatial resolution using small quantum systems like atoms or molecules? The research projects summarized in Chapter 3 illustrate that the coherence theory of the quantized near field formulated here provides insight into both issues.

Chapter 2

Motivation

The physics of light-matter interactions is typically focussed on either matter or light. If we consider for example a laser, the quantity of interest is the radiation output. Even the simplest laser theory aims at predicting and optimizing the laser emission. The laser medium is then often effectively eliminated and reduced to a dielectric background, hopefully with gain. Its properties are of interest in so far as they determine the radiation output: *matter is instrumental to harvest light*. The reverse viewpoint is also possible: *light is a tool to characterize matter*. In a laser, a significant amount of information about the relevant medium properties can indeed be extracted from the emitted radiation.

The theoretical questions dealt with in this thesis share this double face. They are rooted in two sub-fields that may be labelled by the focus they set on either matter or light: (i) integrated atom optics, where matter wave trapping and manipulation is the objective, for which the electromagnetic field provides the basic tool; and (ii) sub-wavelength optics, where the focus is on matter properties on short scales which become accessible when the electromagnetic near field is probed with high spatial resolution. Both sub-fields merge for some questions discussed here, as illustrated in Fig. 2.1:

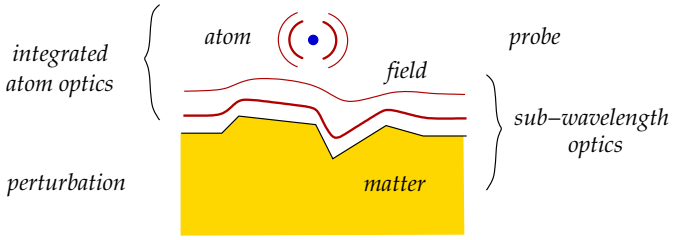

Figure 2.1: Typical setting considered in this thesis with two different points of view.

For integrated atom optics, microstructured material objects are instrumental to create tightly confined electromagnetic trapping fields. But the same object also perturbs the atoms via the near fields it generates. For sub-wavelength optics, information about the near field above a microstructure can be probed with high spatial resolution using the quasi point-like detector provided by a single atom or molecule.

2.1 Integrated atom optics

The field of atom optics has emerged in the last two decades (Meystre, 2001). It transposes basic concepts of light optics (beamsplitters, mirrors, diffraction gratings, interferometers, lasers) to matter or de Broglie waves. A two-fold motivation continues to drive the rapid evolution of the field: the exploration of fundamental wave mechanics and the demonstration of devices where atoms turn out to perform superior to photons or other particles. Atom interferometers, for example, are sensitive to rotations and give a phase shift of order $\Omega A/(\lambda v)$ (Bordé, 1989; Riehle & al., 1991; Gustavson & al., 1997; Lenef & al., 1997) At a fixed enclosed area A, the matter wave is much more phase-shifted because typically both wavelength λ and velocity v are small: relative to a light interferometer operating at a wavelength $\lambda_{\rm L}$, the shift is larger by the factor $mc\lambda_{\rm L}/h \sim 10^9\, m[\mathrm{amu}]\, \lambda_{\rm L}[\mu\mathrm{m}]$. The accuracy achieved in current experiments suggests that tiny relativistic corrections (e.g., the Lense-Thirring effect[1]) or the gravitational constant G can be measured in the near future (Kasevich & Chu, 1992; Bordé, 1997; Peters & al., 1999).

As in light optics, a major step towards practical applications is integration: miniaturize the device and combine it with source and detection system in a single, preferably solid setup. A natural solution, inspired by electromagnetic optics, is to replace free space by a waveguide for the propagation of an atomic beam. In matter wave optics, this corresponds to a confining potential and can be implemented easily with electromagnetic fields. One example are optical fields provided by hollow fibres, hollow laser beams, or complex standing wave patterns. The corresponding 'atom fibres' are expected to boost applications like lithography, i.e. the deposition of atoms on a substrate with high resolution and high flux. Another atom guide is based on the magnetic field minimum formed when the azimuthal field from a current filament is superimposed on a homogeneous 'bias' field (Fig. 2.2), as put forward by Frisch & Segré (1933). A whole network of waveguides can be realized with static magnetic or electric fields generated by nanostructures written onto a solid substrate (for a

[1]This effect, predicted by general relativity, is due to the 'dragging' of the space-time metric by a rotating body.

review, see Hinds & Hughes (1999); Reichel & al. (2001); Folman & al. (2002)). This concept offers strong confinement, highly versatile structure design and is potentially scalable when using nanofabrication technologies.

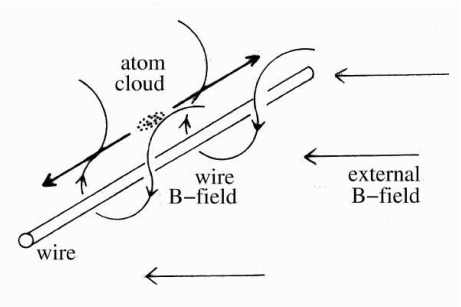

Wire current $I_{\rm w}$
External 'bias' field $B_{\rm b}$
Height $z = \dfrac{\mu_0 I_{\rm w}}{2\pi B_{\rm b}}$
Field along wire $B_{\rm IP}$
Trapping frequency
$\Omega^2 = \dfrac{-\mu_{\rm eff}}{m} \dfrac{B_{\rm b}^2}{B_{\rm IP} z^2}$

Figure 2.2: The magnetic 'side guide'. The superposition of a homogeneous field with the azimuthal field from a current filament forms a magnetic quadrupole field. Atoms with an antiparallel magnetic moment $\mu_{\rm eff} < 0$ are trapped in the zero field region at a height z above the current. If the homogeneous field has a component along the current, the field has nonzero minimum magnitude and the trapping potential is harmonic in the plane transverse to the guide axis ('Ioffe-Pritchard trap').

In addition to robust and compact interferometers, integrated atom optics may provide the 'hardware' for a quantum computer based on neutral atoms. Bits of quantum information can be encoded in atomic spin or hyperfine states as well as in the vibrational levels of the trapping potential. Quantum gates have been proposed based on collisions in state-dependent potentials or switchable dipole-dipole interactions between atoms. Quantum information can be exchanged by transporting the atoms through a network of waveguides, or by using as a 'data bus' either the collective motion of an array of trapped atoms or a light mode confined in an optical waveguide integrated into the atom trap.

Fundamental physics will also be encountered on the way, for example the alteration of atomic levels and transition rates in the near field of a solid substrate, a special case of cavity quantum electrodynamics. One can realize model systems to study 'decoherence', i.e., the loss of quantum coherence due to the interaction with the microtrap environment, by controlling or enhancing electromagnetic field fluctuations in the trapping potential. The propagation through a disordered waveguide is particularly interesting to study with degenerate ensembles (e.g., Bose-Einstein condensates), as a controlled model system for similar processes in mesoscopic electron transport. Many-body physics like Josephson oscillations can also be investigated in great detail with Bose-Einstein condensates, using multi-well potentials separated by tunnelling barriers.

The issues that are addressed in this thesis focus on the interactions of atoms with the solid substrate that are mediated at sub-wavelength distances (i.e., in the 'near field') by the electromagnetic field. Regarding the atoms, we shall adopt the usual dipole couplings, ignoring the chemical physics that occurs on the scale of the Bohr radius $a_{\rm B}$ when the electron clouds of atoms and substrate overlap. The distance range $a_{\rm B} \ldots \lambda_{\rm L}$ is non-empty even for the shortest field wavelengths $\lambda_{\rm L}$ in question (the optical range), because one has $\lambda_{\rm L} \gg a_{\rm B} \sim \alpha\,\lambda_{\rm L} \approx \lambda_{\rm L}/137$. The field, on the other hand, is strongly coupled to the solid substrate and behaves very differently on the sub-wavelength scale compared to free space. The electromagnetic energy density, for example, increases orders of magnitude above the Planck law because of the contribution of non-radiative modes. We shall evaluate in detail near field correlation functions and discuss their impact on atom dynamics in microtraps. This can be done in a system+reservoir framework even if the field itself is not in thermal equilibrium: at the very least, we can reasonably describe the macroscopic solid and its thermal excitations in terms of a reservoir.

2.2 Sub-wavelength optics

A prominent trend throughout the history of optics is to improve the spatial resolution of optical instruments. For a long time, resolution in the visible domain has been limited by diffraction. The adaptation of scanning probe techniques to optical microscopy provided a breakthrough over two decades ago. With sharp fibre tips and distance servo loops based on molecular forces, scanning near field optical microscopes have pushed our 'vision' into the nanometer range (see for example the special issue of *J. Microscopy* (2003)). Although their spatial resolution is not as high as with conventional scanning probes (electron tunnelling, atomic force), optical techniques have some advantages, for example the access to local spectroscopic information (refractive index, absorption).

It has been anticipated since the field took off that spatial resolution can be further enhanced by using single molecules as detectors or emitters (Dunn, 1999). Indeed, these are among the smallest implementations of point-like dipoles that Nature provides. Experiments have started in the 1990s and first used the fluorescence signal of single molecules deposited on a substrate to map the field distribution around the illuminating tip (Betzig & Chichester, 1993; Michaelis & al., 1999). The key idea is that the fluorescent emission is proportional, for low intensities, to the local electric field intensity at the molecule's absorption frequency. The spontaneous decay rate of the molecule, a more intrinsic property which is independent of the illumination and detection modes, is also modified by the electromagnetic environment. It can be

measured using the temporal decay of the fluorescence signal after pulsed excitation, from the antibunching of the fluorescence intensity correlations, or in some cases directly from the emitted power. The spontaneous decay rate is related to the local density of field modes (or local density of states, LDOS) at the molecule position and at its emission frequency.

In the following, we list a few current trends in the field to which the present thesis has made contributions. It is a priori not clear what kind of links exist between the surrounding nanostructures and the LDOS measured for example via the molecular lifetime, but it is essential to know to what extent this link is local when the molecule is to be used as a high-resolution imaging probe. Along the same direction arises the question how the surrounding structure and its local material parameters modulate the exchange of energy, heat, or momentum with the molecule on short scales. If there is a significant impact, one can anticipate to 'taylor' properties of the molecule by a suitable design of its environment. This idea has lent a large impact to the field of photonic band gap materials or 'photonic crystals'. In these artificial materials, structures with feature sizes comparable to or smaller than the wavelength redistribute profoundly the optical modes in frequency space. Accurate predictions for the molecular emission in these structures require the characterization of the field on the nanometer scale; this can be achieved by solving a scattering problem in the framework of the macroscopic Maxwell equations. Finally, coming back to the transfer of heat, the usual modelling of this process, using 'radiative transfer theory', generally neglects interferences in the light field, assuming an effectively zero coherence length. Thermal light in free space, in the far field of any source, is indeed incoherent on scales exceeding the wavelength so that radiative transfer is valid on larger scales, but it has to be replaced by a wave theory on smaller scales. We show here that this limiting scale is no longer given by the wavelength in the near field of a source and, more explicitly, that the coherence length of thermal radiation shifts to smaller values at short distances.

Chapter 3

Achievements

3.1 Summary

The achievements reported in the present thesis can be summarized as follows.

i. We analyze the non-equilibrium dynamics of microscopic particles (atoms, ions) weakly coupled to a fluctuating environment with an emphasis on the coherence theory of atoms trapped in the near field of nanostructures. The dominant processes and sources of fluctuations are identified. Timescales for the loss of coherence are estimated in the context of current experiments in integrated atom optics.

ii. A thorough characterization is obtained for the electromagnetic near field at sub-wavelength distances to planar structures made from linear dielectrics. To a large extent and with reasonable approximations, this is possible analytically, but numerical tools for a full calculation are also provided. We elaborate the consequences for sub-wavelength optical coherence theory, for mechanical effects on nearby objects due to both quantum and thermal field fluctuations, and for the radiation dynamics of fluorescent molecules.

Both points are obviously linked; advances in the characterization of the field have direct implications for the dynamics of atoms trapped in the near field.

3.2 Atom coherence

In the present section, we briefly introduce the projects focussing on atoms and documented in the research papers listed in Appendix C. The idea behind the ordering is roughly to go from the simple to the complicated.

Trapped ions

Carsten Henkel and Martin Wilkens (1999), 'Heating of trapped atoms near thermal surfaces,' *Europhysics Letters* **47**, 414.

Carsten Henkel, Sierk Pötting, and M. Wilkens (1999a), 'Loss and heating of particles in small and noisy traps,' *Applied Physics B* **69**, 379, selected paper of the DPG quantum optics meeting in Heidelberg (1999).

Any charged particle can be trapped in the time-dependent electric field configuration invented by Wolfgang Paul (Nobel prize 1989 shared with Norman F. Ramsey and Hans G. Dehmelt). Ion traps are currently one of the most rapidly advancing implementations of a quantum computer (Schmidt-Kaler & al., 2003) because the ion centre of mass motion can be efficiently cooled using laser light and used to exchange quantum information that is stably encoded in internal states.

In experiments performed by the group of David J. Wineland (JILA Boulder), the vibrational motion of the ion in its effective harmonic potential has shown an unusually large heating rate when the trap dimensions are scaled down to tens or hundreds of micrometers (Wineland & al., 1998; Turchette & al., 2000). We have suggested that this may be due to the coupling to thermal electric field fluctuations that 'leak' out of the room-temperature electrode. We evaluated the spectral density of the electric near field and found a transition rate between the trap vibration levels in qualitative agreement with the experimental data. In the master equation for the ion's vibrational motion, the same rate also governs the decoherence of superposition states between different trap levels, a figure of large interest for quantum computing applications.

Further investigations of the Wineland group indicate a slightly different exponent for the power law dependence of the heating rate on the ion–electrode distance. The observed behaviour can be modelled in terms of field fluctuations originating from patch charges on the electrode surfaces (Turchette & al., 2000). For a detailed understanding, more involved surface physics will be required. The issue is currently open and limits the smallness of ion traps. Experimentally, excessive heating rates are simply reduced by coming back to sufficiently large trap designs.

Free atoms in optical near fields

Carsten Henkel and Jean-Yves Courtois (1998), 'Atomic recoil and momentum diffusion close to a vacuum–dielectric interface,' *The European Physical Journal D* **3**, 129.

Neutral atoms interact strongly with the electromagnetic field via electric dipole transitions in the optical frequency range. In this context, the field can be assumed at zero temperature because thermal mode populations essentially

vanish at the relevant transition frequencies. Only vacuum fluctuations then remain and lead to the spontaneous decay of excited atomic states. The decay rates (and accompanying level shifts) become position-dependent in the near field of any scattering object.

We focus in this project on a model geometry that occurs in atom reflection experiments: a planar interface between vacuum and a dielectric. Well-known expressions for the spontaneous decay rates are recovered, and the theory is elaborated to describe the radiative forces acting on an atom that is driven by an inhogeneous light field (an evanescent wave) at sub-wavelength distance from the dielectric surface. We introduce the spatial coherence function of the atomic de Broglie wave and derive an approximate equation of motion for it (a Fokker-Planck equation for the Wigner transform). Momentum diffusion coefficients are computed and give access to the reduction of the spatial coherence length: an increasingly broad momentum distribution (width Δp) translates into a loss of spatial coherence (coherence length $\approx \hbar/\Delta p$). In the near field of the surface, coherence is more rapidly lost than in free space because of the steep spatial gradients of both the driving field intensity and of the spontaneous decay rates. We also demonstrate a peculiar behaviour of the average optical force (the radiation pressure): for a circularly polarized driving, its direction is tilted and is no longer parallel to the field propagation direction, nor to the Poynting vector. This can be attributed to the breaking of the usual symmetry of the dipole radiation pattern by the surface: unlike in free space, spontaneously emitted photons then lead to a net recoil momentum. The theory is generalized to an atom with spin $1/2$ in the ground state, and reveals spin-dependent momentum exchanges associated to optical pumping processes. An important theoretical tool for the project is the expansion of the vacuum field correlation function in terms of irreducible tensor operators. Compared to free space, this expansion contains only a few additional terms whose coefficients transform as scalars under the reduced (cylindrical) symmetry group.

Free particles in thermal near fields

Carsten Henkel, Karl Joulain, Jean-Philippe Mulet, and Jean-Jacques Greffet (2002), 'Radiation forces on small particles in thermal near fields,' *Journal of Optics A: Pure and Applied Optics* **4**, S109.

Room temperature thermal radiation peaks in the infrared range, and couples strongly to materials like polar crystals because of the resonant absorption by transverse optical phonon modes ('phonon polaritons', Ashcroft & Mermin, 1976). This is the background for a project on the radiation force in the near field of a thermal source. We consider a sub-wavelength test particle and describe it as a point dipole with the well-known Clausius-Mossotti polarizabil-

ity. The radiation force is given by (Gordon & Ashkin, 1980)

$$\mathbf{F}(\mathbf{x}) = \sum_{i\,=\,x,\,y,\,z} \langle d_i \boldsymbol{\nabla} E_i(\mathbf{x}) \rangle$$

where the average $\langle \cdots \rangle$ is taken over the (quantum and thermal) fluctuations of both dipole and field. We develop a theory that recovers the standard van der Waals–Casimir–Polder force at zero temperature (Casimir & Polder, 1948) and yields an explicit correction due to finite temperature. It is possible to describe non-equilibrium states of the field by computing the radiation a 'hot' source emits into a 'cold' vacuum. The energy flowing out of the source leads to a 'radiation wind' that repels the sub-wavelength particle, the thermal analogue of the radiation pressure force. The thermal force also contains a second contribution, analogous to the 'dipole force' of atom-light interactions (proportional to intensity gradients). It depends indeed on the distance to the source and involves the overlap between the source emission bands and the particle's refractive index (more precisely, the dispersive part of its polarizability). We introduce a frequency spectrum of the radiation force where these contributions show up as prominent peaks. They can be assigned to electromagnetic surface resonances ('surface phonon polaritons') on both the source and the particle.[1] A similar analysis can be carried out for the Casimir force between two non perfect mirrors: see the project Henkel & al. (2004b) summarized on page 35.

Atom loss in magnetic microtraps

Carsten Henkel, Sierk Pötting, and Martin Wilkens (1999b), 'Loss and heating of particles in small and noisy traps,' *Applied Physics B* **69**, 379, selected paper of the DPG quantum optics meeting in Heidelberg (1999).

This and the following projects focus on atoms confined in miniaturized traps and exposed to thermal near fields. The situation is generic for microtraps in integrated atom optics (Hinds & Hughes, 1999; Reichel & al., 2001; Folman & al., 2002). It is essential to include a finite temperature as much lower transition frequencies become relevant.

To begin with, we consider magnetic traps and estimate the loss rate due to thermal magnetic near fields. These traps are based on the linear Zeeman effect. In the adiabatic approximation, the angle between the atomic magnetic moment $\boldsymbol{\mu} = \mu_{\mathrm{B}} g \mathbf{J}$ and the local magnetic field direction $\hat{\mathbf{B}}(\mathbf{x})$ (i.e., the magnetic quantum number $m_J = \langle \hat{\mathbf{B}}(\mathbf{x}) \cdot \mathbf{J} \rangle$) is conserved, and the Zeeman shift reduces to the effective potential $-\mu_{\mathrm{B}} g m_J |\mathbf{B}(\mathbf{x})|$. Magnetic field minima provide traps for atoms with an antiparallel magnetic moment ($g m_J < 0$); recall

[1] For a planar source and a spherical particle of the same material, these resonances have slightly different frequency asymptotes determined by $\mathrm{Re}\,\varepsilon(\omega) = -1,\, -2$, respectively.

that field maxima are forbidden by the Maxwell equation $\boldsymbol{\nabla} \cdot \mathbf{B} = 0$. After a transition that changes the sign of m_J, potential minima have turned into maxima and the atom is expelled from the trap. Even if another transition back to the trapping potential happens sufficiently fast, the kinetic energy gain leads to heating.

As is well known from magnetic resonance spectroscopy, transitions between magnetic sublevels ('spin flips') are induced by time-dependent, magnetic fields transverse to the trapping field. The spin flip rate is proportional to the field's spectral density at the Larmor frequency $\hbar\omega_{\mathrm{L}} = \mu_{\mathrm{B}} g |\mathbf{B}(\mathbf{x})|$ which typically ranges in the 1–100 MHz domain. In the present project, we focus on one source of field fluctuations and spin flip loss: thermally excited currents in the microstructures surrounding the trap minimum ('near field noise'). Fluctuations of the electric currents that create the trapping fields ('current noise') are considered in Henkel & al. (2003c). We mention already here that the contribution of current noise is surprisingly large: taking a thin, straight wire and current fluctuations at the shot noise level, the spin life time is of the order of a few seconds for typical microtrap parameters.

Near field noise turns out to be a more significant source of spin flips. Two methods have been developed to characterize it. In equilibrium, the fluctuation–dissipation theorem yields the magnetic field's spectral density in terms of the magnetic field Green function (see Section 5.3.2 and Agarwal (1975a)). This method has been used in the present project. Alternatively, the radiation emitted by the 'hot' microstructures can be calculated directly as done by Varpula & Poutanen (1984); Sidles & al. (2003) and in the previous project (Henkel & al., 2002, see page 19). We have shown that when the field propagation is described in the quasistatic limit, the scattering problem at the interfaces can be avoided and one is led to a simple summation over the volume filled by conducting microstructures (Henkel & Pötting, 2001). For a thin layer of thickness d, for example, the spin flip loss rate is of the order of

$$\gamma \sim \mu_0^2 k_{\mathrm{B}} T_{\mathrm{s}} \sigma_{\mathrm{s}} \frac{d}{z(z+d)} \sim 100\,\mathrm{s}^{-1} T_{\mathrm{s}}[300\,\mathrm{K}]\, \sigma_{\mathrm{s}}[\sigma_{\mathrm{Cu}}] \frac{d}{(z+d) z[\mu\mathrm{m}]} \tag{3.1}$$

where T_{s}, σ_{s} are temperature and conductivity of the layer.[2] The simple summation method is a useful tool to predict the scaling with material parameters and geometry for quite arbitrary microstructures. It shows that the loss rate decays algebraically with distance z, and that the smaller the volume of the conducting material, the faster the decay. Thermally induced spin flips can hence be reduced along two avenues: employ the least possible amount of conducting material or reduce the product $T_{\mathrm{s}}\sigma_{\mathrm{s}}$. Alternatively, one can increase the

[2] Eq.(3.1) is not valid in the perfect conductor limit $\sigma_{\mathrm{s}} \to \infty$ because it assumes $d, z \ll \delta$ where $\delta \propto 1/\sqrt{\sigma}$ is the skin depth.

distance to the microstructure or increase the skin depth $\delta = (2\varepsilon_0 c^2/\sigma_s\omega_L)^{1/2}$, applying larger magnetic fields. We have indeed found that the spin flip rate decays faster with z, as one enters the regime $z \gg \delta$.

In magnetic traps, spin flips also occur because an atom moving in the trap experiences a time-dependent magnetic field. Taking into account corrections to the adiabatic approximation, flip rates have been estimated by Sukumar & Brink (1997) in Oxford and by the group of H. Thomas (Basel) and colleagues (Gov & al., 1998, 2000a,b). One gets an exponential suppression $\propto \exp(-\omega_L/\Omega)$ with the ratio between Larmor frequency and trap vibration frequency Ω. Nonadiabatic flips are thus easily ruled out in experimentally realized microtraps by increasing the trapping field.

The first measurements of microtrap loss rates performed in Claus Zimmermann's group (Tübingen) gave a reduced lifetime at short distance and have been interpreted as interactions with the surface (Fortágh & al., 2002). Experimental difficulties, however, made a direct comparison to theory unsatisfactory, as Wolfgang Ketterle's group (MIT) pointed out in a careful cross-check experiment (Leanhardt & al., 2003). The loss rates observed recently in the groups of Ed A. Hinds (Sussex/London), Eric A. Cornell (JILA Boulder), and Vladan Vuletić (Stanford/Harvard) are on the contrary consistent with the thermally induced flips introduced here (Jones & al., 2003; Harber & al., 2003; Lin & al., 2004), see Figure 3.1. By varying the trap distance and the substrate material, the scaling laws predicted in 1999 as well as the overall magnitude of the loss rate could be confirmed in 2003.

Ultimate sources of trapped atom heating

Carsten Henkel and Martin Wilkens (1999), 'Heating of trapped atoms near thermal surfaces,' *Europhysics Letters* **47**, 414.

Paramagnetic atoms experience a force in magnetic field gradients — this is the basic principle of magnetic trapping. Now, if fluctuating fields that vary in space are present, they act like a random force and heat the atomic motion. The noise strength of this force is related to the heating rate (the kinetic energy gained per unit time and per atom). The relevant quantity is the noise spectral density at the vibration frequency if the atom is trapped in a harmonic well. In integrated atom optics, trap miniaturization leads to steep potentials and large vibration frequencies, with typical values approaching the MHz range.

We have estimated the spectrum of magnetic field gradients starting from the field's spatial correlation function (Henkel & Wilkens, 1999; Henkel & al., 1999b). The corresponding heating rate has been compared to a random force due to another source: thermal or technical current noise that shifts the location of the trap minimum (Folman & al., 2002; Henkel & al., 2003c; Schroll & al.,

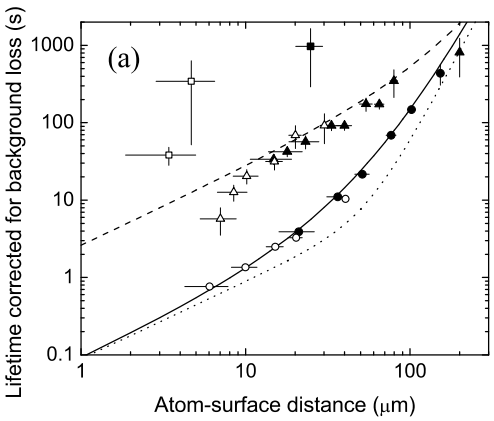

Figure 3.1: Loss rate due to thermal magnetic noise vs. trap distance for difference surface materials. Symbols: experimental data for condensed (open) and non-condensed (filled) gases. Lines: theoretical predictions (dotted: interpolation, solid: numerically evaluated integral for magnetic noise spectrum). Communicated by D. M. Harber (2003).

2003). It has been shown that for typical experiments in integrated atom optics, this second source actually dominates. One reason is the large spring constant in strongly confined traps that associates large forces with small trap displacements. Another reason is that in this range of frequencies, technical noise dominates the current noise, raising it well above the shot noise level. This is consistent with experimental observations of Jakob Reichel's and Theodor W. Hänsch's group in München (Hänsel & al., 2001).

Obviously, heating due to magnetic noise can be eliminated by working with spinless atoms. These can be trapped, for example, in optical dipole traps (Grimm & al., 2000). We have compared different couplings to the microtrap environment that could still provide heating in that case. Thermal electric field fluctuations and the corresponding time-dependent Stark shift turn out to be subdominant compared to elastic excitations of the substrate surface (phonons) that couple to the atom via the van der Waals-London-Casimir-Polder interaction (Haroche, 1992). We have adopted a simple model for the corresponding time-dependent corrections to the interaction with a planar surface (Hill & al., 1982; Franchini & Bartolani, 1994) and derived the heating rate by describing the surface fluctuations in terms of a thermal phonon reservoir. The result is again a power law in the distance z, decreasing here like $1/z^{10}$. With typical parameters, we predict that for spinless atoms, the ground state in a harmonic trap is indeed stable with respect to heating on timescales exceeding minutes. The group of Rudi Grimm (Innsbruck) where Cesium atoms are trapped in an

evanescent wave above a glass substrate (Hammes & al., 2003) and cooled below the Bose-Einstein condensation temperature (Rychtarik & al., 2004), may soon achieve trapping times where van der Waals heating is observable.

We finally note that one gets the depletion rate of the trap ground state by normalizing the heating rate to the vibrational energy quantum. This rate also relates to the timescale over which a prepared quantum state persists resp. 'decoheres' in the microtrap environment (Henkel & al., 1999b). One can thus identify practical limitations for the storage of quantum information in the atomic centre of mass motion.

Decoherence of guided matter waves

Carsten Henkel and Sierk Pötting (2001), 'Coherent transport of matter waves,' *Applied Physics B* **72**, 73, selected paper of the DPG quantum optics meeting in Bonn (2000).

Carsten Henkel, Peter Krüger, Ron Folman, and Jörg Schmiedmayer (2003c), 'Fundamental limits for coherent manipulation on atom chips,' *Applied Physics B* **76**, 173, selected paper of the DPG quantum optics meeting in Osnabrück (2002).

In atomic waveguides similar to the 'side guide' shown in Figure 2.2, the confinement along the guide axis is much weaker than perpendicular to it, and one can assume the motion in this direction to be 'quasi free'. In the project presented here, we turn to the impact of time-dependent perturbations on matter wave propagation in these low-dimensional geometries. The physics is very similar to the decoherence model popularized by Woyciech H. Zurek (1991) that was originally intended to explain the non-observation of spatial superposition states for macroscopic objects.[3] In atomic microtraps, a more detailed characterization of decoherence is possible because the coupling to the environment is microscopically known and determined by the magnetic noise correlation functions obtained previously. One may thus consider cold trapped atoms as a model system to investigate decoherence on a mesoscopic scale, since the noise parameters can be varied experimentally to some extent.

We have derived a master equation for the density operator of quasi free matter waves in the weak-coupling approximation (Henkel & Pötting, 2001). The Markov approximation applies for magnetic near field noise because one has a reservoir spectral density that is frequency-independent in the relevant range. By taking into account the spatial correlation function of the noise field, we are able to write the master equation in the form of a radiative transfer equation (Chandrasekhar, 1960) where the interaction with the noise field is described by a (differential) scattering cross section. Details of the derivation

[3] Zurek considers a 'test particle' whose position coordinate couples to a 'quantum field' that is treated as a reservoir in thermal equilibrium, thus modelling the interaction with the environment. The particle-field coupling is fixed in the high-temperature limit in terms of the macroscopically observed damping rate.

are given in the paper Henkel (2001) that is reproduced in Appendix B. In the limit that the scattered momenta are small, a Fokker-Planck equation is found and we recover the framework developed by Zurek (1991).

For atoms that are quasi free or subject to a linear potential, we solve the radiative transfer equation analytically (Henkel & Pötting, 2001). The resulting matter wave density operator is consistent with earlier results (Jayannavar & Kumar, 1982) and shows exponential decoherence in position space. The off-diagonal elements or coherences $\langle \mathbf{x}|\rho(t)|\mathbf{x}+\mathbf{s}\rangle$ decay for $s > 0$ with a rate $\gamma(\mathbf{s})$ that increases with distance. Confirming results by Cheng & Raymer (1999), the decoherence rate saturates if the 'off-diagonality parameter' s is much larger than the noise correlation length.[4]

We have estimated the decoherence rate due to magnetic noise for typical integrated atom traps and find that it is limited from above by approximately the spin flip loss rate (Henkel, 2001; Folman & al., 2002; Henkel & al., 2003c). Any strategy to reduce trap loss will hence avoid spatial decoherence as well. It is shown as well that the correlation length of near field magnetic noise is comparable to the trap height z. This is true both for noise induced by the thermal surface (Henkel & al., 2000, summarized on page 29) and by fluctuations of a wire current at the shot noise level (Henkel & al., 2003c). A similar result has been obtained by Christoph Bruder's group in Basel for thermal wire current fluctuations (Schroll & al., 2003). In a miniaturized network of atom guides, the small noise correlation length has the following consequences: on spatial scales larger than the correlation length ($\sim z$), spatial decoherence is governed by a single time constant, the saturated rate $\gamma(\mathbf{s} \to \infty)$, comparable to the spin flip rate. In addition, noise with short spatial correlations is 'rough': the momentum diffusion coefficient or, equivalently, the heating rate increases faster with smaller trap height than the spin flip rate itself, by a factor $1/z^2$.

BEC decoherence

Carsten Henkel and Simon A. Gardiner (2004), 'Decoherence of Bose-Einstein condensates in microtraps,' *Physical Review A* **69**, 043602.

Carsten Henkel, Simon A. Gardiner, and Antonio Negretti (2004a), '(De)coherence physics with condensates in microtraps,' *Laser Physics* **14**, 615–20, proceedings of the 12th International Workshop on Laser Physics, Hamburg 2003.

In 2001, Bose-Einstein condensation has been achieved with miniaturized surface traps in nearly simultaneous experiments performed by the groups of Jakob Reichel in München (Hänsel & al., 2001) and of Claus Zimmermann in Tübingen (Ott & al., 2001). Let us recall that below the condensation tempera-

[4]This feature is absent from Zurek's model because it does not contain a cutoff at large momenta for the quantum field that couples to the test particle.

ture, a macroscopic number of atoms occupy a single quantum state of the trapping potential and form the Bose-Einstein condensate (BEC). The interatomic interactions in these dense samples lead to a spatial broadening of the 'condensate wave function' with respect to single-particle quantum mechanics. The simplest description of BEC dynamics is in terms of a nonlinear Schrödinger equation where the interactions are taken into account by a density-dependent potential; this is called the 'mean field approximation'. More refined theories include also condensate excitations and non-condensed atoms and model them as a quantum fluid surrounding the BEC and interacting with it (Fetter, 1999; Stoof, 1999). This approach is attributed to Lev Landau and called the 'two-fluid model'.

Using the mean field approximation, we have extended the decoherence theory of the previous projects to a trapped BEC. This allows to explore the impact of interactions and nonlinearity on the scenario of decohering matter waves. We have focussed on a pure condensate that is released into a quasi one-dimensional waveguide and expands while interacting with a weak, time-dependent potential. In a first step, we neglect interactions in the non-condensed or 'normal' fluid. The corresponding (single particle) density operator then satisfies the master equation of the previously presented project, augmented by a source term coming from the condensate. Indeed, the scattering off the noise potential depletes the condensate and creates atoms in higher-energy states. In this approximation, the BEC wave function itself evolves according to a nonlinear Schrödinger equation with a corresponding loss term.

This simple theory can be solved analytically and qualitatively reproduces Monte Carlo simulations of the nonlinear Schrödinger equation with a noise potential, provided the interatomic interactions are not too strong. The agreement becomes quantitative if two key parameters for the noise potential (strength and correlation length) are renormalized. This can be traced back to the superfluidity of the condensate, more precisely, to the suppression of long-wavelength excitations. This intuitive picture is confirmed by preliminary calculations that describe the excitations in the local-density approximation and assume a slowly-varying condensate profile, see Fig. 3.2.

In a regime of stronger interactions which would be typical for experiments with Bose-Einstein condensates in microtraps, numerical simulations predict that the condensate becomes unstable during the expansion. Fig. 3.3 shows that the condensed fraction collapses on a time scale much shorter than expected from the noise strength. We suspect that this is due to the quite sensible perturbation provided by a small normal fluid fraction. The subject is currently under investigation.

Decoherence of condensates in microtraps has not been directly observed as yet, to our knowledge. Indirect evidence is provided by the heating process

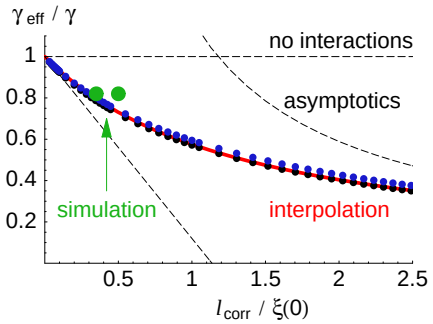

Figure 3.2: Renormalization of decoherence in a Bose-Einstein condensate. We plot the ratio between the 'bare' and the renormalized decoherence rate $\gamma(s \to \infty)$ for different ratios between the noise correlation length $\ell_{\rm corr}$ and the healing length $\xi(0)$ in the condensate centre. Large dots: numerical simulation. Small dots: renormalized decoherence rate for condensate density profiles of Thomas-Fermi shape (lower curve) and gaussian shape (upper curve). Solid line: interpolation formula. Dashed lines: asymptotics for large and small healing lengths, corresponding to weak and strong interactions, respectively.

attributed to technical noise in the München atom chip experiment (Hänsel & al., 2001). A number of other microtraps suffer from a static, inhomogeneous potential that leads to BEC fragmentation (Fortágh & al., 2002; Kraft & al., 2002; Leanhardt & al., 2003; Jones & al., 2003). This makes the experiments differ from our model because the free expansion in these traps is perturbed. In a recent paper, the inhomogeneous potential is attributed to random lateral displacements of the wire current (Wang & al., 2003), and investigations of the corresponding disordered multi-condensate sample (a 'Bose glass') are suggested.

Atom optical diffraction gratings

Carsten Henkel, Hartmut Wallis, Nathalie Westbrook, Chris I. Westbrook, Alain Aspect, Klaus Sengstock, and Wolfgang Ertmer (1999b), 'Theory of atomic diffraction from evanescent waves,' *Applied Physics B* **69**, 277.

This review paper summarizes the results of my Ph.D. thesis[5] on the diffraction of cold atoms from optical reflection gratings. The gratings under consideration are made with partially standing evanescent waves. We identify the relevant diffraction mechanisms and compare the theory to experimental realizations achieved in the groups of W. Ertmer (Bonn/Hannover), V. Lorent (Villetaneuse), and A. Aspect (Orsay).

[5] 'Réflexion et diffraction d'atomes lents par un miroir à onde évanescente,' Université Paris-Sud, France, 11 December 1996.

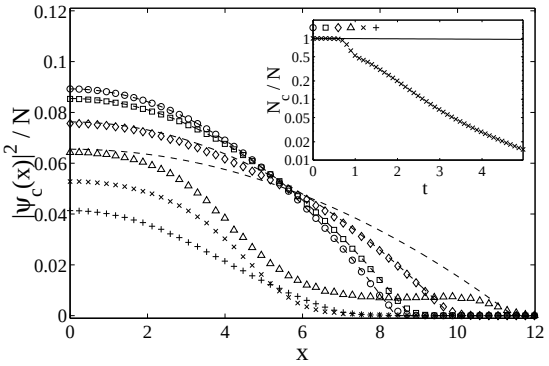

Figure 3.3: Condensate density profiles upon release from a harmonic trap into a noisy one-dimensional waveguide. Symbols: noise-averaged Gross-Pitaevskii field for $\Omega t = 0,\, 0.3, \ldots 1.5$ where Ω is the initial trap frequency. Dashed lines: time-dependent Thomas-Fermi profile (Castin & Dum, 1996). Solid line (inset): exponential decay $\mathrm{e}^{-\gamma t}$. The parameters correspond to the microtrap experiment of the J. Reichel group (Hänsel & al., 2001): distance $10\,\mu\mathrm{m}$, noise strength $\gamma = 0.0075\,\Omega$, correlation length $\ell_{\mathrm{corr}} = 0.66$ oscillator units, interaction strength $gN \approx 400$ oscillator units.

Mesoscopic atom optics with atom chips

Ron Folman, Peter Krüger, Jörg Schmiedmayer, Johannes H. Denschlag, and Carsten Henkel (2002), 'Microscopic atom optics: from wires to an atom chip,' *Advances in Atomic, Molecular, and Optical Physics* **48**, 263, edited by B. Bederson (Academic Press, New York).

Recent developments and current perspectives of integrated atom optics are discussed in this review article. A chapter on loss and decoherence in atom chip traps summarizes the results obtained in several projects described here. We sketch the vision of a scalable quantum computer implemented with neutral atoms.

3.3 Optical coherence

The following projects focus on the electromagnetic field and its coherence in the vicinity of a possibly nanostructured substrate. The presentation starts with a the characterization of the spatial coherence length of thermal light and then addresses questions of single-molecule fluorescence in a inhogeneous environment. The last topic touched upon is the Casimir force, the electromagnetically induced attraction between macroscopic mirrors separated by a vacuum gap.

Near field of a planar source

Carsten Henkel, Karl Joulain, Rémi Carminati, and Jean-Jacques Greffet (2000), 'Spatial coherence of thermal near fields,' *Optics Communications* **186**, 57.

What is the energy spectrum of a thermal radiation field and how coherent is it? The Planck formula provides the answer in the far field, *i.e.*, in a spectral region where the wavelength λ is smaller than the distance z to any scattering or radiating objects. In the near field, the answer is less universal because one has to describe the material objects and the radiation source itself. A natural framework is provided by 'fluctuation electrodynamics': the macroscopic Maxwell equations including polarization noise sources whose statistics is given in terms of the source temperature. This theory is able to generalize the Planck law down to the atomic scale. It has been developed in the 1950s by the groups around S. M. Rytov and L. Landau (Rytov & al., 1989). In the 1990s, fluctuation electrodynamics was identified as a natural framework to consistently quantize the electrodynamics of absorbing and dispersive media (Huttner & al., 1991; Gruner & Welsch, 1995; Tip, 1997; Stefano & al., 1999).

The group of Jean-Jacques Greffet (Paris) applied the Rytov theory to characterize the non-equilibrium field in the 'cold' vacuum above a 'hot' planar source (a metal-filled half space) and obtained numerical results for its spatial coherence and its energy spectrum (Carminati & Greffet, 1999; Shchegrov & al., 2000). In particular, the coherence length ℓ_{coh} (measured in a plane parallel to the source) depends on the distance of observation z, and there are regimes where it becomes much smaller or larger than the wavelength. In the present project, we have worked out analytical approximations that explicitly exhibit the relevant physical processes that determine ℓ_{coh}. At short distance $z \ll \lambda$, for example, the coherence length is fixed by the geometry and is of the order of z; it is not limited from below by the skin depth of the source material, as put forward by Carminati & Greffet (1999). Approaching the source, the near field thus becomes spatially more and more incoherent; a limit is only reached when the concept of a local dielectric susceptibility breaks down. This happens, depending on the material, on the atomic scale or somewhat above it (Feibelman, 1982; Ford & Weber, 1984). If the source material supports electromagnetic surface resonances[6], these dominate the electromagnetic energy density in a distance range $z \sim \lambda$. We show that the energy density then has a nearly exponential variation because the surface resonance corresponds to evanescent fields with a well-defined decay length perpendicular to the plane. Parallel to the surface, the coherence length is equal to the extinction length

[6] In metals with a relative permittivity $\mathrm{Re}\,\varepsilon(\omega) < -1$, a collective surface charge oscillation couples to the electromagnetic field to combine into a so-called 'surface plasmon' resonance (Raether, 1988). 'Surface phonon polaritons' correspond to an optical phonon coupled to the field; they occur in many polar crystals.

of the resonance which is made finite by material losses; it can exceed many wavelengths.

Regarding the polarization properties of the thermal near field, the group of Ari T. Friberg (Stockholm/Kista) has generalized the concept of a degree of polarization. This is needed because there is no longer a preferred direction of propagation with respect to which the field is transverse (Setälä & al., 2002a,b). In the regime of distances where surface resonances dominate the field energy, they lead to a net degree of polarization. But also in the very near field, $z \ll \lambda$, the surface breaks spatial isotropy and the thermal radiation field is partially polarized. On the experimental side, the group of J.-J. Greffet designed a thermal source to emit narrow angular lobes of radiation by patterning its surface with a grating optimized for the conversion of surface modes into propagating modes. The high directivity of this source can be regarded as a proof of a spatial coherence length larger than the wavelength (Gall & al., 1997; Greffet & al., 2001).

The results of this project provide a complete, analytical characterization of the thermal near field also at low frequencies. Magnetic field coherence functions can be obtained in a similar way and are discussed in Section 5.2. We use them extensively in this thesis to predict loss and decoherence rates for atoms held in near field traps.

Single-molecule fluorescence above a nanostructured substrate

Carsten Henkel and Vahid Sandoghdar (1998), 'Single-molecule spectroscopy near structured dielectrics,' *Optics Communications* **158**, 250.

The spontaneous decay rate of an excited two-level system is proportional to the electric field correlation spectrum evaluated at the system transition frequency and its position in space (Agarwal, 1975c). In the present project, we use this link to establish molecular fluorescence as a high-resolution probe for the vacuum field fluctuations. The focus is on the scattering of the vacuum field from a dielectric sample with sub-wavelength structures and on the question to what extent the spontaneous decay rate allows to 'image' these structures. In other words, what can the molecule tell about the nanostructured substrate below, while there is just vacuum between both?

The spontaneous decay rate in the near field of objects with simple shapes has been calculated since the 1970s (see, *e.g.*, Chance & al. (1978)). More complicated shapes require numerical methods that have become available with improved computer power in the 1990s (Girard & al., 1995; Novotny, 1996). In order to get insight into the resolution limit, we have developed an analytical treatment. The strength of the vacuum fluctuations is computed as a function of the molecule position and the orientation of its transition dipole

moment. The price to pay for the analytical approach is the requirement of an essentially planar substrate, whose corrugation amplitude is small compared to both the wavelength and the molecular distance. The field scattered from the nanoscale corrugation is then calculated perturbatively to first order in the corrugation, using the so-called Rayleigh expansion (Rayleigh, 1907). Similar approaches have been reported for scattering problems by Agarwal (1977); Nieto-Vesperinas (1982); Greffet (1988); Labeke & Barchiesi (1993). One thus gets a position-dependent correction to the decay rate whose Fourier transform is proportional to the corrugation spectrum of the substrate. This answers the question of resolution, since the wavenumber-dependent ratio between the decay rate and the corrugation provides, in the language of optical imaging, the 'transfer function' of the device. Its knowledge allows to deconvolve the spatial modulations of the fluorescence rate and to retrieve the surface profile.[7] We have worked out simple asymptotic formulas for the limit of small-scale corrugations that allow to show analytically that the resolution is only limited by the molecule-substrate distance.

Nearly simultaneously although independently, the group of Daniel Van Labeke in Besançon proposed a similar approach (Parent & al., 1999a,b) and computed two-dimensional fluorescence images that demonstrate numerically a sub-wavelength resolution. In Dijon, the group of Frédérique de Fornel has developed numerical calculations including scattering to all orders to assess the validity of fluorescence imaging (Rahmani & al., 1997, 2001). A similar transfer function has been put forward by the Greffet group (Paris) for the images obtained by a scanning near-field optical microscope (SNOM) (Greffet & al., 1995; Carminati & Greffet, 1995b). The physics of both concepts is very similar, the essential difference comes from the illuminating field used in a SNOM. A direct comparison to experiments where the fluorescence lifetime is measured as a function of molecule position, is not straightforward due to the influence of the nearby probe tip (see Novotny (1996) and the review by Dunn (1999)). Promising results with single molecules as point-like detectors or sources have been achieved by the group of Vahid Sandoghdar in Zürich (Michaelis & al., 1999, 2000).

Fluorescence dynamics inside nanoparticles

Lavinia Rogobete, Hannes Schniepp, Vahid Sandoghdar, and Carsten Henkel (2003b), 'Spontaneous emission in nanoscopic dielectric particles,' *Optics Letters* **28**, 1736.

[7] More precisely, the signal depends on the deviation of the substrate permittivity from a flat reference geometry, integrated along a line perpendicular to the substrate (Carminati & Greffet, 1995a). A spatially varying refractive index is thus indistinguishable, in this approach, from a corrugated topography. Topographic information, however, is routinely accessible in scanning near field devices from the feedback loop that monitors the probe-sample distance (Dunn, 1999).

Lavinia Rogobete, Vahid Sandoghdar, and Carsten Henkel, 'Modification of spontaneous emission in nanoscopic environments,' unpublished (2003a).

The previous project assumed the probe molecule to be held in vacuum, while in many experiments it is embedded in a thin film or a sub-wavelength size particle. The impact of the local environment on the fluorescent emission is addressed here, taking as an example a small dielectric host surrounding the molecule. The particle size is below the regime of Mie resonances that enhance the emission (Chew, 1988): we are not dealing with a cavity but with a scatterer.

We model the host particle in terms of a spatially constant permittivity; this allows to cover scales down to the mesosopic regime (smaller than the wavelength but larger than the atomic scale). Given this restriction, it is clear that one does *not* recover the molecule in vacuum by taking the limit of vanishing particle size. The molecule is modelled as an electric point dipole and thus occurs as a source term in the wave equations for the electromagnetic field. The radiative decay rate is determined from the power emitted into the far field provided the source dipole is identified with the matrix element of the molecular dipole operator (see for example Haroche (1992) and Eq.(6.9)). To find the emitted radiation, the wave equation is solved numerically, and we focus on a simplified two-dimensional geometry for reasons of computer power. The solution allows for any shape and size of the host particle; its surface enters via the boundary conditions for the electric field vector. We take advantage of this by reformulating the Helmholtz equation as a surface integral equation using Green's theorem (Born & Wolf, 1959; Nieto-Vesperinas, 1991). The integral equation is then solved with the method of moments: the kernel of this equation is regularized and the field approximated by piecewise constant functions on discrete boundary elements as described in the textbooks by Bancroft (1996) and Harrington (1993).

We find that the host particle reduces the molecular decay rate compared to an unbounded dielectric environment (Rogobete & al., 2003b). This reduction can be understood from electrostatic arguments: the molecular dipole is partially 'screened' by the polarization charges it induces on the particle boundaries. At large distances, the multipole expansion of the field contains a dipole component with a reduced amplitude — and it is this component that dominates the emitted power for sub-wavelength hosts. An interesting result is that the relevant parameters of the host particle are its overall area (in our two-dimensional model) and its aspect ratio, but not its geometrical details. For 'round' hosts with a molecule at the center, different polygonal shapes lead to the same decay rate. Sharp corners do matter, of course, if an off-centered molecule approaches them: it then couples to stronger electric fields and we retrieve an enhanced emission. Elongated shapes also give a different distribution of polarization charges. We find nearly no reduction of decay for a

molecular dipole parallel to the long axis of a rectangle because the continuity of the tangential electric field makes the host surface nearly 'transparent'. A very good agreement is found with an analytical solution for elongated elliptical particles (Rogobete & al., 2003a).

Our findings give a complementary contribution to the ongoing debate on local field corrections. These are usually defined for a dipole in an empty cavity surrounded by an unbounded dielectric: on a larger scale, our model just reverses optically thin and thick media. The empty-cavity model dates back to the 19th century: Lorentz and Lorenz used it in their derivation of the connection between the (macroscopic) permittivity and the (microscopic) polarizability of the material constituents, the Clausius–Mossotti formula. A similar model is required for quantum electrodynamics in dielectrics because one has to connect the macroscopic field to the 'local' field at the molecule's position. Surprisingly, different models for the molecule's surroundings[8] lead to different local fields. As a consequence, the dependence of the spontaneous emission rate in a dielectric on the medium permittivity is as yet unsettled (Glauber & Lewenstein, 1991; Lagendijk & al., 1997; Scheel & al., 1999; Dung & al., 2000; Crenshaw & Bowden, 2000; Schuurmans & al., 2000; Rahmani, 2002). From our results, one can conclude that the rather arbitrary choice between quasi-spherical and elongated cavities leads to different local fields, suggesting that the problem may be ill-posed.

On the experimental side, the group of Johan P. Woerdman (Leiden) has measured local field effects in dense gases: atomic transition frequencies are shifted at high density because the atoms get partially excited, leading to a change in their polarizability (van Kampen & al., 1999). In Zürich, Schniepp & Sandoghdar (2002) have performed an experiment similar to our model: they measure the lifetime of Europium complexes that homogeneously fill sub-wavelength spheres and find agreement with the local field correction for a 'real cavity', as discussed by Chew (1988). The Leiden and Zürich experiments are limited, however, to rather small values of the relative permittivity between cavity and surrounding medium. The group of Philippe Grangier (Orsay) studied individual color centers embedded in diamond nanocrystals with $\varepsilon \approx 5$. The radiative decay rates they measure are consistent with no particle depolarization (or local field correction) at all (Beveratos & al., 2001). A quantitative understanding of these results is a current challenge; it may be that the gradual change of the refractive index at the surface of the nanocrystals (surrounded by a polymer layer) plays a role. Otherwise, one may have to invoke less well-characterized parameters of the emitters like their chemical environment or non-radiative decay.

[8] Prominent models are known as 'virtual cavity' or 'real cavity', see Glauber & Lewenstein (1991) and Schuurmans & al. (2000).

Radiative relaxation in photonic crystals

Geesche Boedecker and Carsten Henkel (2003), 'All-frequency effective medium theory for a photonic crystal,' *Optics Express* **11**, 1590.

Geesche Boedecker, Carsten Henkel, Christian Hermann, and Ortwin Hess (2004), 'Spontaneous emission in photonic structures: theory and simulation,' chapter 2 of *Photonic crystals – advances in design, fabrication and characterization*, edited by Kurt Busch, S. Lölkes, R. Wehrspohn, and H. Föll (Wiley-VCH, Berlin, scheduled for 2004), invited book chapter.

Photonic crystals are a class of artificial materials that diffract electromagnetic waves due to a periodic modulation of their refractive index. They have been proposed by Eli Yablonovitch (1987) with the perspective of designing the dispersion relation and mode density of light. The applications aimed at involve the suppression of spontaneous emission when a 'photonic band gap' opens around the emitter's transition frequency, the guiding of light along chains of defect structures on a sub-wavelength scale, and highly dispersive refraction ('superprism'), see the textbooks by Joannopoulos & al. (1995) and Sakoda (2001). Sajeev John (1987) in Toronto suggested that disordered photonic crystals provide a setting to observe the long-sought phenomenon of Anderson localization of light (1958). The topic evolves rapidly as shown by a number of recently published proceedings and special issues (Soukoulis, 2001; *Opt. Express*, 2001; *IEEE J. Quant. El.*, 2002; *Opt. Quantum Electr.*, 2002; *phys. stat. sol. (a)*, 2003).

The field in a photonic crystal provides an example of a reservoir with a strongly modulated spectral density and this leads to non Markovian dynamics for spontaneous emission. In a series of papers, Maciej Lewenstein and the S. John group showed that as a consequence, excited states decay in a non exponential, oscillatory way and can trap a fractional population even at long times, see Lewenstein & al. (1988); John & Wang (1990); John & Quang (1994) and the review by Woldeyohannes & John (2003). In recent times, these calculations have been refined by taking into account dispersion relations taken from more realistic band structure calculations (Zhu & al., 2000; Busch & al., 2000). It has been found that non Markovian dynamics is quite sensitive to the shape of the spectral mode density around the transition frequency, but it is not clear whether it survives in real crystals. Finite samples or residual disorder smoothe out any singular features of the mode density, leading back to exponential decay because the system gets effectively amenable to a Wigner-Weisskopf approximation.

We have investigated a simple one-dimensional Kronig-Penney model for a photonic crystal and derived an analytical formula for the spectral mode density (Boedecker & Henkel, 2003). It describes both finite and infinite systems and also covers the case of a nonzero absorption where standard band structure calculations get into trouble because the mode frequencies or Bloch vectors

become complex (Tip & al., 2000). The frequencies of modes localized at crystal defects can also be calculated easily with our approach. These modes are sharply peaked in space and frequency and can be used to concentrate the fluorescence of an emitter. The key idea of our theory is to replace the structured crystal by a homogeneous 'effective medium' where the field propagation is described in terms of Bloch waves. Finite samples are described by matching Bloch waves to plane waves at the boundaries, and this leads to reflection and transmission coefficients that can be compared to experimental data.

In our review chapter on spontaneous emission in photonic strctures (Boedecker & al., 2004), an overview of the current theory is given and numerical calculations of the spectral mode density are discussed. We elaborate a classical model for the emission of a dipole coupled to a square-root singular mode density that is generic for three-dimensional band edge, complementing quantum calculations of a similar system by Woldeyohannes & John (2003).

Casimir force

Carsten Henkel, Karl Joulain, Jean-Philippe Mulet, and Jean-Jacques Greffet (2004b), 'Coupled surface polaritons and the Casimir force,' *Physical Review A* **69**, 023808.

In the last project presented in this thesis, we calculate coherence functions of the electromagnetic field between two mirrors made from real materials to point out a particular aspect of their Casimir interaction. This force, predicted in 1948, arises because material objects redistribute the field modes in space and frequency and lead to an unbalanced radiation pressure. An alternative interpretation involves the change in the field's zero-point energy due to changes in the mode frequencies or their spectral density. For two perfect mirrors, the force (per unit area) is attractive and proportional to $\hbar c/z^4$ where z is the mirror separation. Early calculations indicated that the Casimir energy of a spherical, perfectly conducting cavity decreases with radius. This raised the hope of constructing a 'mechanical' model for the electron where the Casimir energy balances the electrostatic self-repulsion (Mostepanenko & Trunov, 1997). Intense investigations in the context of quantum field theory ensued, but the model was eventually abandoned (Lambrecht, 2002).

Theoretical activity has recently shifted towards a better description of realistic objects, since Lamoreaux (1997) and Mohideen & Roy (1998) improved the experimental resolution to a few percent and evidence in micromechanical systems has been found (Buks & Roukes, 2001; Chan & al., 2001). Our contribution follows this line of thought: we focus on mirrors made from realistic metals and derive a correction due to metallic absorption in the short-distance regime (Henkel & al., 2004b). This is achieved by elaborating on early suggestions by Kampen & al. (1968) and Gerlach (1971) that electromagnetic surface

modes are responsible for the Casimir attraction. When the metallic mirrors approach each other, these surface modes start to overlap and split into even and odd superpositions with slightly different frequencies. We show that their contributions to the Maxwell stress tensor are of opposite sign, and it is known since the seminal work by Lifshitz (1956) that the Casimir force can be retrieved from this tensor. It turns out that the Casimir effect can be attributed to the attractive force exerted by the *even* superposition of surface modes, similar to molecular binding in quantum mechanics.

For a quantitative estimate, we observe that at short distances[9], the spectrum of the force indeed peaks at the frequencies of the coupled surface modes. An asymptotic formula is found by expanding the spectrum around these peaks. We recover an attractive force proportional to $\hbar\Omega/z^3$ where Ω is the single-mirror surface resonance frequency, and compute the first order correction with respect to the absorption rate of the material. This agrees with previous results obtained by Lambrecht & Reynaud (2000), when absorption is neglected, and is very similar to the short-distance calculation performed by the group of D.-G. Welsch in Jena (Raabe & al., 2003).

Our analysis suggests that it may be possible to tune the magnitude and sign of the Casimir force with suitable thin coatings on the mirrors. If these provide a phase shift at the frequency of the surface resonances, they may modify the relative weights of even and odd modes. The possibility of a repulsive Casimir force for magnetic materials (permeability $\mu \neq 1$) has recently been demonstrated by Kenneth & al. (2002). An alternative, as yet unexplored road are materials with a negative index of refraction (permittivity and permeability both negative). The electrodynamics in these materials has been studied in 1967 by Veselago who pointed out that they show an inverted radiation pressure. Negative index materials are in the focus of a recent debate raised by Pendry (2000) about the possibility of a 'perfect lens'. For a review of the theory, see Ziolkowski & Heyman (2001) and Haldane (2002). Experimental details on metamaterials currently employed to realize a negative index in the microwave range are given by Markoš & Soukoulis (2003).

[9]More precisely, $z \ll \lambda_{\rm SP}$, where $\lambda_{\rm SP}$ is the wavelength of the electromagnetic surface mode. Perfect mirrors correspond to the limit $\lambda_{\rm SP} \to 0$.

Chapter 4

Outlook

The advances in the understanding of electromagnetic near field coherence reported here have identified the relevant processes and parameters and thus point towards new avenues of research. Some ideas helped to shape the scientific content of current projects funded by the Deutsche Forschungsgemeinschaft[1] and the European Union[2], and results will be reported on a scale of one to three years. Other ideas are still in an exploratory stage and are sketched in the following. They may be loosely organized around three major goals:

— control and reduction of electromagnetic noise in atom chips

— improved understanding of coherence in trapped Bose-Einstein condensates

— demonstration of quantum electrodynamic effects in realistic photonic structures

4.1 Atom chips

Spin flip and heating rates due to thermal magnetic fields are small, but they significantly bar the route towards large scale, sub-μm integrated atom optics. We now know that the choice of the substrate material for atom chips is one critical issue. Low noise alternatives to conventional metals are provided by permanently magnetized thin films and superconductors. Magnetic noise control thus becomes an issue of material science. The key specifications are set by

[1] Project 'Photonic Crystal Quantum Optics' funded 2001–04 in the *Schwerpunktprogramm* 1113 'Photonic Crystals'.

[2] Network 'Field Atom Surface Interactions Training Network', coordinated by J. Weiner (Toulouse), funded 2002–05 by the TMR programme. Network 'Atom Chip Quantum Processor', coordinated by J. Schmiedmayer (Heidelberg), funded 2003–05 by the IST programme.

the results reported here: the electromagnetic response of the materials must show weak dissipation in the kHz–GHz frequency range.

Another issue to be explored is the 'robustness' of the adiabatic approximation in magnetic traps with weak perturbations. Many calculations use the adiabatic potential and separate time scales between the Larmor precession, trap motion, and noise-induced transitions. If magnetic noise couples, for example, Zeeman states, one can imagine that the large Zeeman energy becomes available for the conversion into kinetic energy. Heating or a significant renormalization of the trap potential would be the consequences. Insight into this problem can be provided from quadrupole models studied by Hinds & Eberlein (2000) and Gov & al. (2000b). A simple estimate shows that the adiabaticity in these traps scales with the same parameter as the anharmonicity of the adiabatic potential. In practice, nonadiabatic corrections thus cannot be separated from nonlinear aspects of the atomic motion. A beautiful experimental demonstration of corrections to the adiabatic approximation has been achieved by the group of Ennio Arimondo (Pisa): they have shown that a condensate is subject to a 'geometric' force that arises when the atom spin tries to follow a time-dependent magnetic field (Aharonov & Stern, 1992; Müller & al., 2000).

4.2 Coherent condensate dynamics

Numerical simulations of expanding condensates that we have performed indicate an instability in the presence of noise, already at a very weak level. To understand this phenomenon, an analysis in terms of collective and quasiparticle excitations would be helpful. An interesting aspect of the problem is that the expansion velocity in the laboratory frame can exceed the local sound velocity in the condensate wings. This implies that the centre and the wings of the condensate cannot exchange signals using sound waves — an intriguing situation that resembles the cosmological period of inflation in the early stages of the Universe.

If a condensate is held for long times in a microtrap or split and recombined, one can also expect that quantum corrections beyond the mean field approximation become relevant (see for example Menotti & al. (2001)). Their impact on integrated condensate interferometers would be worth examining with realistic trapping potentials, including weak noise fields. The role of fluctuations in the condensate phase for physics beyond the mean field remains to be explored, for example in the context of the Josephson effect (the atom current across a tunnelling barrier, driven by the quantized phase difference of the matter wave field). Experimental efforts are already underway, and unexpected observations will surely open new challenges.

4.3 Quantum electrodynamics

We have pointed out several consequences of modified vacuum fluctuations for atoms that move in the near field of a solid surface: for example enhanced, position-dependent spontaneous emission rates and peculiar radiation forces (see page 18). A direct experimental verification is missing so far, however, because these effects are delicate. We expect that there is an impact on the stationary state of atoms trapped in evanescent fields where distances of the order of a micron become feasible (Dowling & Gea-Banacloche, 1997; Grimm & al., 2000; Hammes & al., 2003). In particular, by exploiting different polarization states of the evanescent light, it should be possible to demonstrate that spontaneous emission rates in the near field depend on the dipole orientation. Measurements of this effect have mostly been performed with randomly oriented samples, see Chance & al. (1978); Snoeks & al. (1995); Worthing & al. (1999), and the review by Barnes (1998). Near field experiments with single molecule resolution have shown a strong polarization dependence, but typically the molecular dipole is fixed and steep gradients occur in the illuminating field. Cold, trapped atoms may offer here an improved control because their dipole moment is linked to the polarization of the trapping light. For long trapping times, one may finally ask whether temperature-dependent fluctuations of the van der Waals force may become relevant for heating or decoherence. This has so far been estimated for the Casimir force between macroscopic objects (Barton, 1991; Eberlein, 1992).[3]

Realistic photonic structures where light propagation is more profoundly modified are alternative candidates to demonstrate quantum effects beyond the standard approximations. Whether the structural quality of current finite-size samples is sufficient to reach a non Markovian regime of spontaneous decay, remains to be seen, and the answer will require nontrivial numerical calculations of the field. Disordered photonic crystals are interesting in their own right, however. For example, what is the impact of 'hopping transport' between defect sites on the fluorescence light emitted in the bandgap of the ordered structure? If light propagation slows down and travel times acquire a significant statistical spread, what happens to the 'anti-bunching' dip seen in the photon correlation signal of single-molecule fluorescence? Finally, can solid-state emitters that are easily implanted in photonic structures, reach the level of coherence required for QED physics? The combination of semiconductor physics with electrodynamics in complex structures will provide the clues. The demonstration of single-photon emitting devices based on nanocrystals

[3] **Note added in proof** (07 June 2004). Wu, Kuo, and Ford, "Fluctuations of the retarded van der Waals force" [Phys. Rev. A 65 (2002) 062102] discuss the case of an atom in front of a perfectly conducting surface, in the long-distance regime.

by the group of Y. Yamamoto (Stanford) already opens promising perspectives (Santori & al., 2002).

In the coming years, we can surely expect that light and matter in interaction will continue to change the way we look at the world around us and to advance the technology we shape this world with.

Part II

Technical Overview

Chapter 5

Fields

The electromagnetic field is the basic vehicle that mediates interactions in quantum optics. Neutral atoms, e.g., couple to it via their electric and magnetic dipole moments, while direct, 'chemical' interactions with surrounding material can be suppressed by keeping the relevant distances above the atomic scale. It is therefore natural to start with a discussion of the coherence properties of the field. In free space, the relevant questions and answers are well-known: in the absence of sources and at thermodynamic equilibrium, the Planck formula gives the frequency spectrum of the energy density. The propagation of a partially coherent field through vacuum is described by partial differential equations for the coherence function that have been written down by E. Wolf (Mandel & Wolf, 1995). We focus in this thesis on the near field and its coherence. First of all, the very concept of 'near' fields requires a reference object to measure distance. This material object may generate the field and its boundaries will scatter it. A convenient framework that covers both possibilities are the macroscopic Maxwell equations. We quote them here in the form relevant for our purposes and explain how neutral atoms provide a source for the field. The techniques to characterize electromagnetic coherence are reviewed, and methods to compute magnetic field correlations are outlined.

5.1 Macroscopic Maxwell theory

Field equations

The equations for the electromagnetic field in a linear and local medium read in frequency space[1] (Jackson, 1975)

$$\begin{aligned} &\boldsymbol{\nabla}\cdot\mathbf{B}=0\\ &\varepsilon_0\boldsymbol{\nabla}\cdot\varepsilon\mathbf{E}=\rho\\ &\boldsymbol{\nabla}\times\mathbf{E}-\mathrm{i}\omega\,\mathbf{B}=0\\ &\boldsymbol{\nabla}\times\frac{\mathbf{B}}{\mu}+\frac{\mathrm{i}\omega}{c^2}\varepsilon\,\mathbf{E}=\mu_0\mathbf{j} \end{aligned} \tag{5.1}$$

The dielectric and magnetic response of the medium is described by the relative permittivity ε and permeability μ. The macroscopic charge and current densities are ρ and $\mathbf{j}$. In this thesis, we focus on nonmagnetic media and set $\mu = 1$. We also suppose that the system is globally neutral and express the sources of the field in terms of an ('external') polarization density: $\rho = -\boldsymbol{\nabla}\cdot\mathbf{P}$, $\mathbf{j} = -\mathrm{i}\omega\mathbf{P}$. Sometimes, we also need a magnetization current $\mathbf{j} = \boldsymbol{\nabla}\times\mathbf{M}$ where $\mathbf{M}$ is the external magnetization field. For our purposes, the macroscopic Maxwell equations thus take the form

$$\begin{aligned} &\boldsymbol{\nabla}\cdot\mathbf{B}=0\\ &\varepsilon_0\boldsymbol{\nabla}\cdot\varepsilon\mathbf{E}=-\boldsymbol{\nabla}\cdot\mathbf{P}\\ &\boldsymbol{\nabla}\times\mathbf{E}-\mathrm{i}\omega\,\mathbf{B}=0\\ &\boldsymbol{\nabla}\times\mathbf{B}+\frac{\mathrm{i}\omega}{c^2}\,\varepsilon\,\mathbf{E}=-\frac{\mathrm{i}\omega}{\varepsilon_0 c^2}\mathbf{P}+\mu_0\boldsymbol{\nabla}\times\mathbf{M}. \end{aligned} \tag{5.2}$$

Two aspects of these equations are worth recalling.

(i) The medium response that is encoded in the dielectric function $\varepsilon = \varepsilon(\mathbf{x};\omega)$ typically results from a statistical description of a large number of microscopic particles, it is an average quantity. In a liquid formed by permanent electric dipoles, for example, it depends on the local temperature (orientation polarization).

(ii) The macroscopic theory is only valid on a mesoscopic or 'coarse' length scale, typically one order of magnitude above the atomic scale at least. Only on these scales is the material response determined by a sufficiently large number of particles so that in the statistical description of $\varepsilon(\mathbf{x};\omega)$, fluctuations can

[1] The convention used here for the Fourier transform is

$$f(t) = \int \frac{\mathrm{d}\omega}{2\pi}\,\mathrm{e}^{-\mathrm{i}\omega t} f(\omega).$$

be neglected.[2] We note that the restriction to mesoscopic scales is consistent with our assumption that atoms are held at mesoscopic distances at least; being far away on the atomic scale, they do not resolve the atomic structure of the material objects.

Dipole sources

A generic example for a globally neutral charge distribution is a point-like Hertzian dipole with dipole moment $\mathbf{d}$ at the position $\mathbf{x}_0$. Its polarization field is given by (in the time domain)

$$\mathbf{P}(\mathbf{x}, t) = \mathbf{d}(t)\delta(\mathbf{x} - \mathbf{x}_0). \tag{5.3}$$

On the mesoscopic scale we will work on, this is a good approximation for an atom. The atomic electric dipole moment is given by an operator whose nonzero matrix elements connect the energy level pairs that form electric-dipole (or 'E1') transitions. In the simplest case, we just retain two levels, the ground state $|\mathrm{g}\rangle$ and the excited state $|\mathrm{e}\rangle$, and expand the dipole operator (in the Heisenberg picture) as

$$\mathbf{d}(t) = \mathbf{d}\big\{\sigma_+(t) + \sigma_-(t)\big\}, \tag{5.4}$$

where $\mathbf{d}$ is the (possibly complex) reduced dipole matrix element whose direction is fixed by the magnetic quantum numbers of the ground and excited states. In the Schrödinger picture, the fermionic ladder operators can be written $\sigma_+ = |\mathrm{g}\rangle\langle\mathrm{e}|$ and $\sigma_- = \sigma_+^\dagger = |\mathrm{e}\rangle\langle\mathrm{g}|$. The subscript denotes the positive resp. negative frequency with which these operators evolve in the Heisenberg picture.

The magnetization due to the magnetic moment of an atom can be expressed in terms of the total spin operator[3] $\mathbf{J}$ (we choose it dimensionless)

$$\mathbf{M}(\mathbf{x}, t) = \mu\mathbf{J}(t)\delta(\mathbf{x} - \mathbf{x}_0), \tag{5.5}$$

where the effective magnetic moment $\mu = \hbar\mu_\mathrm{B} g_F$ can be expressed in terms of a Landé factor g_J. The Schrödinger operator $\mathbf{J}$ has the standard angular momentum representation on the magnetic sublevels manifold of an atom.

[2] For some materials like metals or semiconductors, while a macroscopic framework is applicable, one has to use a nonlocal dielectric response. This is because the electrons accelerated by an external electric field start to move quasi-ballistically. They reach a diffusive regime on a length scale given by the electron mean free path (Ashcroft & Mermin, 1976). Beyond this scale, a local description is justified again.

[3] In atomic physics, this is sometimes written $\mathbf{F}$, including both electronic and nuclear spin contributions.

Green function

The electric field radiated by a monochromatic point dipole provides the Green function or tensor of the Maxwell equations. It encodes the essential knowledge about electromagnetic scattering and radiation problems for a given medium geometry. If we write the dipole as $\mathbf{d}(t) = \mathbf{d}\,\mathrm{e}^{-\mathrm{i}\omega t}$ with a complex amplitude $\mathbf{d}$, the electric field satisfies the wave equation

$$-\boldsymbol{\nabla}\times\boldsymbol{\nabla}\times\mathbf{E}(\mathbf{x};\omega)+\frac{\omega^2}{c^2}\,\varepsilon(\mathbf{x};\omega)\,\mathbf{E}(\mathbf{x};\omega)=-\frac{\omega^2\,\mathbf{d}}{\varepsilon_0 c^2}\delta(\mathbf{x}-\mathbf{x}'), \tag{5.6}$$

where $\mathbf{x}'$ is the dipole position and $\varepsilon(\mathbf{x};\omega)$ the medium permittivity. Since the field depends linearly on the dipole source, we can define the Green tensor via the relation[4] (Einstein's summation convention is applied)

$$E_i(\mathbf{x};\omega)=G_{ij}(\mathbf{x},\mathbf{x}';\omega)d_j. \tag{5.7}$$

An explicit solution can be given in a homogeneous dielectric. The tensor only depends on $\mathbf{r}=\mathbf{x}-\mathbf{x}'$ in this case; introducing the unit vector $\hat{\mathbf{r}}$ and the medium wave number $k=\sqrt{\omega^2\varepsilon(\omega)/c^2}$, we have

$$\begin{aligned} G_{ij}^{(\mathrm{hom})}(\mathbf{r};\omega) &= \frac{\delta_{ij}}{3\varepsilon_0\varepsilon(\omega)}\delta(\mathbf{r}) \\ &\quad+\frac{k^2\,\mathrm{e}^{\mathrm{i}kr}}{4\pi\varepsilon_0\varepsilon(\omega)}\left[\frac{\delta_{ij}-\hat{r}_i\hat{r}_j}{r}\right. \\ &\quad\left.+(\delta_{ij}-3\hat{r}_i\hat{r}_j)\left(\frac{\mathrm{i}}{kr^2}-\frac{1}{k^2r^3}\right)\right]. \end{aligned} \tag{5.8}$$

The first line proportional to the δ function ensures the 'sum rule' that the volume-averaged field is proportional to the dipole moment. The second line dominates in the far field, it is transverse with respect of the observation direction $\hat{\mathbf{r}}$. The third line has zero angular average and dominates in the near field. Note that the $1/r^3$ contribution survives in the static limit $\omega\to 0$; it then reduces to the Coulomb field generated by the dipole and screened by the dielectric medium.

Causality requires that the medium wave number k in Eq.(5.8) is taken as the square root with a positive imaginary part. In free space or an absorptionless dielectric where $\varepsilon>0$, this can be ensured by giving the frequency ω an infinitesimally positive imaginary part, $k=\sqrt{\varepsilon}(\omega+\mathrm{i}0)/c$. This prescription suffices to obtain the causal (retarded) Green function when the wave equation (5.6) is solved by a spatial Fourier transformation. It will be understood in

[4]Many other conventions exist for the prefactor of Eq.(5.7) in the literature. They originate in different factors in front of the δ function source in Eq.(5.6).

what follows that ε is complex with a positive imaginary part (passive, absorbing medium).

Under quite general assumptions, the Green tensor is symmetric and obeys reciprocity. By *symmetry*, we mean the following relation between negative and positive (real) frequencies

$$G_{ij}(\mathbf{x}, \mathbf{x}'; -\omega) = G_{ij}^*(\mathbf{x}, \mathbf{x}'; \omega) \tag{5.9}$$

This relation holds because in the time domain, $G_{ij}(t)$ is a real response function connecting the real quantities electric field and (classical) dipole moment. *Reciprocity* is tantamount to the exchange of source and detector and holds as long as the dielectric tensor is symmetric (Jackson, 1975). It thus trivially holds for the scalar permittivity we use here and reads

$$G_{ji}(\mathbf{x}', \mathbf{x}; \omega) = G_{ij}(\mathbf{x}, \mathbf{x}'; \omega). \tag{5.10}$$

An exception is provided by Faraday-active media in a static magnetic field, for example.

An alternative expression for the Green tensor, the Weyl expansion, is useful in the near field. Let us assume that the dielectric medium breaks the symmetry in such a way that the xy-plane plays a distinguished role. This is the case close to a planar interface, for example. Introducing two-dimensional in-plane vectors, we shall use the notation $\mathbf{r} = \mathbf{R} + \mathbf{n}z$ where $\mathbf{n}$ is the unit normal. Here and in the following, we assume $z \neq 0$ so that the contact contribution to the Green tensor (5.8) can be safely ignored. One then has the following Fourier expansion, also known as the 'angular spectrum representation' (Nieto-Vesperinas, 1991),

$$G_{ij}^{(\mathrm{hom})}(\mathbf{R}, z; \omega) = \frac{\mathrm{i}}{2\varepsilon_0 \varepsilon(\omega)} \int \frac{\mathrm{d}^2 Q}{(2\pi)^2} \frac{\exp \mathrm{i}(\mathbf{Q} \cdot \mathbf{R} + q_z |z|)}{q_z} \left[k^2 \delta_{ij} - q_i(z) q_j(z) \right]. \tag{5.11}$$

This is an expansion in plane waves with wave vectors $\mathbf{q}(z) = \mathbf{Q} + \mathbf{n} q_z \operatorname{sgn} z$ that propagate away from the reference plane $z = 0$. The normal wave vector component is either real or imaginary, corresponding to propagating or evanescent waves:[5]

$$q_z = \sqrt{k^2 - Q^2}, \qquad \operatorname{Im} q_z \geq 0, \operatorname{Re} q_z \geq 0. \tag{5.12}$$

In addition, each plane wave satisfies the dispersion relation $\mathbf{q}^2(z) = k^2$. The bracketed tensor in Eq.(5.11) is hence transverse with respect to $\mathbf{q}(z)$ and can

[5] This distinction applies, strictly speaking, to a nonabsorbing medium like vacuum with real and positive $\varepsilon(\omega)$. If absorption is present, q_z is always complex, and the borderline between propagating and evanescent waves is less sharply defined.

be expanded in a basis of transverse polarization vectors

$$k^2\delta_{ij} - q_i(z)q_j(z) = k^2 \sum_{\mu\,=\,\mathrm{s},\,\mathrm{p}} e_{\mu i}(z)e_{\mu j}(z), \qquad \mathbf{e}_\mu(z)\cdot\mathbf{q}(z) = 0. \tag{5.13}$$

We normalize these vectors to $\mathbf{e}_\mu^2(z) = 1$; note that no complex conjugation is involved, although the vectors are complex in general. The conventional labels s and p correspond to vectors perpendicular to and in the plane of incidence spanned by $\mathbf{Q}$ and $\mathbf{e}_z$.

5.2 Near fields

In this section, we consider the electromagnetic field close to a planar substrate and work out the corresponding Green functions. When the theory is quantized, the Green functions will provide the essential information about the near field correlation spectra.

Surface Green function

The Weyl expansion (5.11) is taylormade for scattering problems involving quasiplanar interfaces between media. We quote here for further reference the Green tensor in the vacuum above a dielectric that fills the 'lower' half space $z < 0$. If a dipole source is located at $z' > 0$ in the upper half space, the reflection from the dielectric leads to an additional field whose Green tensor can be written in close analogy to its homogeneous case counterpart (5.11)

$$z, z' > 0: \qquad G_{ij}^{(\mathrm{refl})}(\mathbf{x},\mathbf{x}';\omega) = \tag{5.14}$$
$$\frac{\mathrm{i}\omega^2}{2\varepsilon_0 c^2}\int\frac{\mathrm{d}^2Q}{(2\pi)^2}\frac{\mathrm{e}^{\mathrm{i}\mathbf{q}(+)\cdot\mathbf{x}-\mathrm{i}\mathbf{q}(-)\cdot\mathbf{x}'}}{q_z}\sum_{\mu\,=\,\mathrm{s},\,\mathrm{p}} r_\mu e_{\mu i}(+)e_{\mu j}(-),$$

where r_μ are the Fresnel reflection coefficients and where the argument $\pm$ distinguishes upward from downward propagating (or decaying) waves. The permittivity of the lower medium only enters via the Fresnel coefficients; as long as the planar symmetry is not broken, Eq.(5.14) can also be used above a multilayer medium. Note that sign conventions differ for the Fresnel coefficients; only the product of r_μ and the polarization vectors appearing under the sum in has an unambiguous meaning.

The magnetic Green tensor is defined by analogy to Eq.(5.7) as the magnetic field radiated by a point magnetic moment

$$B_i(\mathbf{x};\omega) = H_{ij}(\mathbf{x},\mathbf{x}';\omega)m_j, \tag{5.15}$$

where the magnetization density is $\mathbf{M}(\mathbf{x}) = \mathbf{m}\,\delta(\mathbf{x}-\mathbf{x}')$. From the Maxwell equations (5.2), we find that in terms of its electric counterpart, the magnetic Green tensor is given by a double curl

$$H_{ij}(\mathbf{x},\mathbf{x}';\omega) = \frac{1}{\omega^2}\epsilon_{ikl}\epsilon_{jmn}\frac{\partial}{\partial x_k}\frac{\partial}{\partial x'_m}G_{ln}(\mathbf{x},\mathbf{x}';\omega). \tag{5.16}$$

In a homogeneous dielectric, this leads to an expression similar to (5.8).

In the near field, the relevant physics is encoded in the reflected field, as given by the Green tensor (5.14). Performing the double rotation, we observe that the polarization vectors are exchanged according to

$$\mathbf{q}\times\mathbf{e}_{\rm s} = \frac{\omega}{c}\mathbf{e}_{\rm p}, \qquad \mathbf{q}\times\mathbf{e}_{\rm p} = -\frac{\omega}{c}\mathbf{e}_{\rm s} \tag{5.17}$$

because $\mathbf{q}$, $\mathbf{e}_{\rm s}$, and $\mathbf{e}_{\rm p}$ form an orthogonal *Dreibein*. Hence, up to a factor $1/c^2$, we obtain the reflected magnetic Green tensor by exchanging the reflection coefficients $r_{\rm s} \leftrightarrow r_{\rm p}$ in Eq.(5.14).

5.2.1 Short distance expansion

To illustrate the behaviour of the field at short distances, we review here asymptotic expansions for the electric and magnetic Green tensors. Our presentation collects results scattered in Henkel & Courtois (1998); Henkel & al. (1999b, 2000).

Electric field

As a first step, we show that at short distances, the reflected part (5.14) of the electric Green tensor takes a simple, electrostatic form. 'Short distance' means the limit $z, z' \ll \lambda$. The integral over the wave vector $\mathbf{Q}$ involves the factor $\mathrm{e}^{\mathrm{i}q_z(z+z')}$ which provides a cutoff for $|q_z| \geq 1/(z+z') \gg k_0 \equiv \omega/c$. Analyzing the integrand, we notice that it peaks around the cutoff value. We thus get the leading order asymptotics by using the expansion in the limit $Q, |q_z| \gg k_0$ under the integral. Assuming the more stringent condition $Q \gg k \equiv \sqrt{\varepsilon}\omega/c$ where ε is the lower medium permittivity, we obtain

$$r_{\rm p}\, e_{{\rm p}i}(+)e_{{\rm p}j}(-) \approx \frac{\varepsilon-1}{\varepsilon+1}\frac{(Q\mathbf{n}-\mathrm{i}\mathbf{Q})_i(Q\mathbf{n}+\mathrm{i}\mathbf{Q})_j}{k_0^2} \tag{5.18}$$

$$r_{\rm s}\, e_{{\rm s}i}(+)e_{{\rm s}j}(-) \approx \frac{k_0^2(\varepsilon-1)}{4Q^2}\frac{(\mathbf{n}\times\mathbf{Q})_i(\mathbf{n}\times\mathbf{Q})_j}{Q^2}, \tag{5.19}$$

where $\mathbf{n}$ is the surface normal. The polarizations behave very differently, the p-polarized part dominating for large Q by a factor $(Q/k_0)^4$. The corresponding reflection coefficient $r_{\rm p}$ tends towards the electrostatic value $r_{\rm stat} = (\varepsilon-1)/(\varepsilon+$

1) and becomes independent of Q. This means that the reflection from the surface is nondispersive, and we can use image theory to evaluate the reflected dipole field, *i.e.*, Eq.(5.14). It corresponds to the well-known field of an *image dipole* $\tilde{\mathbf{d}} = (-d_x, -d_y, d_z) r_{\mathrm{stat}}$ located at the position $\mathbf{X}' - z'\mathbf{n}$ below the surface.[6] The short-distance behaviour of the free space Green function (5.8) thus yields the tensor

$$G_{ij}^{(\mathrm{refl})}(\mathbf{X}, z, \mathbf{X}', z'; \omega) \approx -\frac{\varepsilon - 1}{\varepsilon + 1} \frac{1}{4\pi\varepsilon_0} \frac{\delta_{ik}\tilde{r}^2 - 3\tilde{r}_i\tilde{r}_k}{\tilde{r}^3} \left(-\delta_{kj} + 2n_k n_j\right), \quad (5.20)$$

$$= \frac{\varepsilon - 1}{\varepsilon + 1} \frac{1}{4\pi\varepsilon_0\, \tilde{r}^5} \begin{pmatrix} \tilde{r}^2 - 3(X - X')^2 & 0 & 3(X - X')(z + z') \\ 0 & \tilde{r}^2 & 0 \\ -3(X - X')(z + z') & 0 & 3(z + z')^2 - \tilde{r}^2 \end{pmatrix}_{ij}$$

where $\tilde{\mathbf{r}} = \mathbf{X} - \mathbf{X}' + (z + z')\mathbf{n}$ is the distance between the observation point and the image dipole. For the matrix representation, we have chosen the x-axis along $\mathbf{X} - \mathbf{X}'$.

It may be surprising that a Green tensor constructed with 'transverse' polarization vectors ($\mathbf{e}_\mu \cdot \mathbf{q} = 0$) assumes at short distances the 'longitudinal' form of an electrostatic field (the $1/r^3$ dipole field). This is due to the behaviour of the p-polarization vector at large wave vectors:

$$Q \gg k_0 : \mathbf{e}_{\mathrm{p}} \approx \frac{Q\mathbf{n} - \mathrm{i}\mathbf{Q}}{k_0} = \frac{\mathbf{q}}{\mathrm{i}k_0} \quad (5.21)$$

which is both 'longitudinal' and 'transverse' because to this order $\mathbf{q}^2 = 0$. Note also that the Green tensor (5.20) is reciprocal (5.10): exchanging $\mathbf{X}$ and $\mathbf{X}'$ flips the sign of the off-diagonal arguments, and this is undone by the matrix transpose.

In Henkel & al. (2000), it is shown that the thermal emission from a planar body has a cross correlation tensor (defined in Eq.(5.41) below) proportional to (5.20), including the nonzero off-diagonal elements. An expansion where the condition $Q \gg \sqrt{\varepsilon}k$ is relaxed is presented in Henkel & al. (1999b). This is relevant above metallic surfaces at low frequencies where $|\varepsilon|$ is very large. A careful analysis shows that the results presented here hold in a distance range $z, z' \ll \delta(\omega)$ where $\delta(\omega)$ is the skin depth in the metal.[7] In the opposite regime $z, z' \gg \delta(\omega)$, the reflection coefficient r_{stat} is close to unity and one gets a different power law in $\tilde{r}$ compared to Eq.(5.20). More details are given on page 59 where the cross correlation spectra for electric and magnetic fields are compared.

[6] This prescription is consistent with the comparison to the Weyl expansion (5.11) of the free space Green tensor. Both Eq.(5.11) and Eq.(5.14) describe the same field if the image dipole satisfies $\mathbf{e}_{\mathrm{p}}(+) \cdot \tilde{\mathrm{d}} = r_{\mathrm{stat}}\, \mathbf{e}_{\mathrm{p}}(-) \cdot \mathrm{d}$. The vectors $\mathbf{e}_{\mathrm{p}}(\pm)$ have x, y-components with different signs, and we get the rules for the image dipole.

[7] One has $\delta(\omega) = \sqrt{2\varepsilon_0 c^2/(\sigma\omega)}$ in terms of the conductivity σ.

Magnetic field

To get the magnetic Green tensor, we cannot simply take the double curl of (5.20), using the relation (5.16), because the electric field is purely longitudinal to the order we have taken. The magnetic field is determined by the next order corrections. We cannot use image theory for these because they involve dispersive (Q-dependent) reflection coefficients. An explicit integration is nevertheless possible and has been used in Henkel & al. (1999b).

We recall that the Weyl expansion of the magnetic Green tensor can be found simply by exchanging the s- and p-labels for the reflection coefficients, according to (5.17). The short-distance expansion goes through as before and leads to the large Q limit of the reflection coefficients

$$r_{\rm p} e_{{\rm s}i}(+) e_{{\rm s}j}(-) \approx \frac{\varepsilon-1}{\varepsilon+1} \frac{(\mathbf{n}\times\mathbf{Q})_i (\mathbf{n}\times\mathbf{Q})_j}{Q^2} \tag{5.22}$$

$$r_{\rm s} e_{{\rm p}i}(+) e_{{\rm p}j}(-) \approx \frac{k_0^2(\varepsilon-1)}{4Q^2} \frac{(Q\mathbf{n}-{\rm i}\mathbf{Q})_i (Q\mathbf{n}+{\rm i}\mathbf{Q})_j}{k_0^2}. \tag{5.23}$$

In this case, both polarizations scale with Q in the same way and have to be kept. If however we focus on a metallic surface with a large permittivity, then the second line dominates.

The integral over the wave vector $\mathbf{Q}$ is performed in cylindrical coordinates, with the azimuthal angle φ measured with respect to the direction of $\mathbf{R} \equiv \mathbf{X}-\mathbf{X}'$. An analogous procedure has been followed in Henkel & Courtois (1998); Henkel & al. (2000). The azimuthal integration yields Bessel functions

$$\int \frac{{\rm d}\varphi}{2\pi} {\rm e}^{{\rm i}QR\cos\varphi} \mathbf{e}_{\rm s}(+)\otimes\mathbf{e}_{\rm s}(-) = \frac{1}{2}\begin{pmatrix} J_0+J_2 & 0 & 0 \\ 0 & J_0-J_2 & 0 \\ 0 & 0 & 0 \end{pmatrix}, \tag{5.24}$$

$$\int \frac{{\rm d}\varphi}{2\pi} {\rm e}^{{\rm i}QR\cos\varphi} \mathbf{e}_{\rm p}(+)\otimes\mathbf{e}_{\rm p}(-) = \frac{Q^2}{2k^2}\begin{pmatrix} J_0-J_2 & 0 & 2J_1 \\ 0 & J_0+J_2 & 0 \\ -2J_1 & 0 & 2J_0 \end{pmatrix} \tag{5.25}$$

where the argument QR of $J_{0,1,2}$ has been suppressed everywhere for brevity. The radial integrals over Q can also be done analytically, starting from the identity

$$\int_0^\infty {\rm d}Q\, {\rm e}^{-Q\bar z} J_0(QR) = \frac{1}{\sqrt{\bar z^2+R^2}} \tag{5.26}$$

and its derivatives with respect to R and $\bar z \equiv z+z'$. The full magnetic Green tensor, which has not been discussed in Henkel & al. (1999b), is thus given by

$$H_{ij}^{(\rm refl)}(\mathbf{X},z,\mathbf{X}',z';\omega) \approx \tag{5.27}$$

$$\frac{\omega^2\mu_0}{4\pi c^2}\left\{\frac{\varepsilon-1}{4(X-X')^2\tilde{r}}\begin{pmatrix}\bar{z}(\tilde{r}-\bar{z}) & 0 & (X-X')(\tilde{r}-\bar{z})\\ 0 & \tilde{r}(\tilde{r}-\bar{z}) & 0\\ -(X-X')(\tilde{r}-\bar{z}) & 0 & (X-X')^2\end{pmatrix}_{ij}\right.$$
$$\left.+\frac{\varepsilon-1}{\varepsilon+1}\frac{1}{(X-X')^2\tilde{r}}\begin{pmatrix}\tilde{r}(\tilde{r}-\bar{z}) & 0 & 0\\ 0 & \bar{z}(\tilde{r}-\bar{z}) & 0\\ 0 & 0 & 0\end{pmatrix}_{ij}\right\}$$

where again $\tilde{\mathbf{r}} = \mathbf{X} - \mathbf{X}' + \bar{z}\mathbf{n}$ and the x-axis is chosen along $\mathbf{X} - \mathbf{X}'$. Note the limits $\tilde{r} \to \bar{z}$ and $\bar{z}(\tilde{r} - \bar{z}) \to (\mathbf{X} - \mathbf{X}')^2/2$ for $\mathbf{X} - \mathbf{X}' \to 0$. The tensor is invariant under transposition combined with the exchange $\mathbf{X} \leftrightarrow \mathbf{X}'$, ensuring reciprocity.

The magnetic Green function (5.27) shows a different dependence on frequency and on the geometry, compared to the electric image dipole (5.20). The diagonal elements, for example, decay as ω^2/z. This leads to a pronounced asymmetry between electric and magnetic noise spectra, as we discuss on page 59 below. Before, we outline a scheme that permits to calculate electric and magnetic fields in arbitrary geometries (Section 5.2.2) and introduce the quantization procedure for the macroscopic Maxwell equations (Section 5.3).

5.2.2 Arbitrary geometries

Electric dipole radiation

The Maxwell equations (5.1) can be formulated in integral form as well. This is convenient for some numerical solution schemes. We review here a formulation in terms of boundary or surface integrals that we have used in field simulations. The presentation is adapted from Boedecker & al. (2004).

We focus in the wave equation (5.6) on a geometry with dielectric nano-objects whose permittivity $\varepsilon > 1$ is locally homogeneous and isotropic. Inside and outside the objects, the problem is reduced to propagation in a homogeneous medium, and scattering occurs due to the matching of the fields at the object boundaries. This permits a reformulation in terms of a boundary integral equation (the result is called the 'extinction theorem', see Born & Wolf (1959); Nieto-Vesperinas (1991) for details).

Let us focus on the Green function outside a single nano-object and adopt for illustration purposes a two-dimensional model. The object thus corresponds to a cylinder, and the point source to a chain of dipoles. The polarization dependence separates into two cases, and the physically interesting one for near field investigations is a dipole polarized in the xy-plane, say ('p-polarization'). In that case, the problem is conveniently formulated in terms of the magnetic field $\mathbf{H}(\mathbf{x}) = \mathbf{e}_z H(x, y)$ that contains a single nonzero component.

Its wave equation reads

$$\boldsymbol{\nabla}\left(\frac{1}{\varepsilon(\mathbf{x})}\cdot\boldsymbol{\nabla}H\right)+k_0^2H=\frac{\mathrm{i}\omega}{\varepsilon(\mathbf{x}')}\mathbf{d}\cdot(\mathbf{e}_z\times\boldsymbol{\nabla})\delta(\mathbf{x}-\mathbf{x}') \tag{5.28}$$

where we switched to $\mathbf{x}=(x,y)$, $\mathbf{x}'$ is the source position and again $k_0=\omega/c$. In an infinite homogeneous dielectric, this equation can be solved in terms of a third kind Bessel function $H_0^{(1)}(z)$. This solution provides us with a particular solution to the wave equation outside the nano-object, the 'dipole field'

$$\begin{aligned} H_{\mathrm{dip}}(\mathbf{x}) &= \mathrm{i}\omega\,\mathbf{d}\cdot(\mathbf{e}_z\times\boldsymbol{\nabla})G_0(\mathbf{x}-\mathbf{x}') &(5.29)\\ G_0(\mathbf{x}-\mathbf{x}') &= \frac{\mathrm{i}}{4}H_0^{(1)}(k_0|\mathbf{x}-\mathbf{x}'|). &(5.30)\end{aligned}$$

A similar equation with $k\equiv\sqrt{\varepsilon}\omega/c$ gives the dipole field $G_\varepsilon(\mathbf{x}-\mathbf{x}')$ inside the object.

On the boundary $\mathcal{B}$ of the nano-object, the field $H(\mathbf{x})$ and the normal derivative $F(\mathbf{x})\equiv(1/\varepsilon)\partial H/\partial n$ (the tangential electric field) are continuous. The wave equation is then equivalent to the following pair of integral equations, where $\mathbf{r}\in\mathcal{B}$ is on the object boundary (Nieto-Vesperinas, 1991)

$$\begin{aligned} H(\mathbf{r}) &= 2\,\mathcal{P}\oint_{\mathcal{B}}\mathrm{d}a(\mathbf{x})\,\left[G_\varepsilon(\mathbf{x}-\mathbf{r})\varepsilon F(\mathbf{x})-H(\mathbf{x})\frac{\partial G_\varepsilon}{\partial n}(\mathbf{x}-\mathbf{r})\right], &(5.31)\\ H(\mathbf{r}) &= 2H_{\mathrm{dip}}(\mathbf{r})-2\,\mathcal{P}\oint_{\mathcal{B}}\mathrm{d}a(\mathbf{x})\,\left[G_0(\mathbf{x}-\mathbf{r})F(\mathbf{x})-H(\mathbf{x})\frac{\partial G_0}{\partial n}(\mathbf{x}-\mathbf{r})\right], &\end{aligned}$$

where $\mathrm{d}a(\mathbf{x})$ is the boundary element at the point $\mathbf{x}$, $\partial/\partial n$ is the derivative along the outward normal, and $\mathcal{P}$ denotes the principle value. A similar equation (but with all prefactors 2 replaced by unity) gives the field outside the object in terms of its values on the boundary. The far field is computed by expanding the Green function and becomes similar to a spatial Fourier transform of the boundary field.

For numerical calculations, the object boundary is discretized into surface elements Δa and the integrals replaced by Riemann sums. More refined schemes exist, for example expansions in piecewise linear functions, and are known as 'moment methods' (Bancroft, 1996; Harrington, 1993). The singularity of the derivative $\partial G/\partial n$ has already been accounted for in (5.31) and explains the factor 2 in front of the integrals. When the singularity of the Green function itself is extracted to lowest order in Δa, one gets for the integral over the boundary element containing $\mathbf{r}$:

$$\int_{\mathcal{B}(\mathbf{r})}\mathrm{d}a(\mathbf{x})\,G_\varepsilon(\mathbf{x}-\mathbf{r})\varepsilon F(\mathbf{x})\approx-\Delta a\,\varepsilon F(\mathbf{r})\left[2\log(k\Delta a/4)-2+2\gamma-\mathrm{i}\pi\right], \tag{5.32}$$

where $\gamma\approx0.577$ is the Euler constant. A similar equation holds for G_0. Once this term is taken care of, the other boundary elements can be treated as in a

Riemann sum, leading to a linear system for the boundary field and its normal derivative.

Numerical results using this scheme have been reported in Rogobete & al. (2003b) and summarized on page 31. For a dipole embedded in an object, the overall effect is a reduction of the total emission, with a significant dependence on the dipole position and orientation for non-circular objects.

Magnetic fields

Numerical calculations for magnetic fields are relevant for the context of atom chips. The radiation of a magnetic dipole (the Green tensor) gives access to the cross correlation spectrum of the field, and this quantity determines the time scales characteristic for spin flip and heating processes in magnetic surface traps. Numerical calculations are required for not too simple trap geometries. We outline here a scheme that is able to handle a two-dimensional model.

We assume a trap environment whose dielectric function is invariant along one direction, the z-axis, say. This applies to a long wire on a planar substrate, for example. We focus on fields that are constant along the z-axis as well. The corresponding Green function thus describes the field radiated by a chain of magnetic point dipoles. It is most easily described in terms of the vector potential. If the dipoles are polarized in the xy-plane, the vector potential contains a single nonzero component $\mathbf{A}(\mathbf{x}) = \mathbf{e}_z A(x, y)$. Its wave equation is very similar to (5.28)

$$\boldsymbol{\nabla}^2 A + k_0^2 \varepsilon(\mathbf{x}) A = \mu_0 \mathbf{m} \cdot (\mathbf{e}_z \times \boldsymbol{\nabla}) \delta(\mathbf{x} - \mathbf{x}') \tag{5.33}$$

where $\mathbf{m}$ is the magnetic dipole and $\mathbf{x}'$ its (two-dimensional) position.

This problem can be solved with the same methods as before. For the field on the object boundary, we get a pair of integral equations where the unknowns are the vector potential and its normal derivative $B_\mathrm{t} \equiv \partial A / \partial n$ (the tangential magnetic field) that are both continuous across the boundary. These equations differ only slightly from (5.31)

$$\begin{aligned} A(\mathbf{r}) &= 2\,\mathcal{P} \oint_{\mathcal{B}} \mathrm{d}a(\mathbf{x}) \left[G_\varepsilon(\mathbf{x} - \mathbf{r}) B_\mathrm{t}(\mathbf{x}) - A(\mathbf{x}) \frac{\partial G_\varepsilon}{\partial n}(\mathbf{x} - \mathbf{r}) \right] \\ A(\mathbf{r}) &= 2A_\mathrm{dip}(\mathbf{r}) - 2\,\mathcal{P} \oint_{\mathcal{B}} \mathrm{d}a(\mathbf{x}) \left[G_0(\mathbf{x} - \mathbf{r}) B_\mathrm{t}(\mathbf{x}) - A(\mathbf{x}) \frac{\partial G_0}{\partial n}(\mathbf{x} - \mathbf{r}) \right] \end{aligned} \tag{5.34}$$

where the same Green functions G_0, G_ε as in Eq.(5.30) appear. They determine the dipole field A_dip similar to (5.29).

The field outside is given by an equation similar to the second line of (5.34) (replace both factors 2 by unity). The first term gives the field radiated in free space, so that the interesting part, the scattering from the object, is encoded in

the second term. For typical surface traps, we can safely make the approximation that the vacuum wavelength is larger than any other characteristic scale. This is justified by the frequency range of magnetic field fluctuations relevant for typical atom traps (kHz–100 MHz). The vacuum Green function can then be replaced by its static limit

$$G_0(\mathbf{r}) \approx -\frac{1}{2\pi}\left(\log\frac{k_0|\mathbf{r}|}{2} + \gamma - \frac{\mathrm{i}\pi}{2}\right), \tag{5.35}$$

where the additive constants are kept for consistency with G_ε.

If the object permittivity is also of order unity, we can make the approximation (5.35) for the inside field. As a consequence of the continuity conditions, the object boundaries do not modify the vector potential in this case: the magnetic dipole radiates as in free space. Hence, the magnetic near field is only scattered by materials with a large permittivity, such that the medium wavelength $1/k \propto \lambda_{\mathrm{vac}}/\sqrt{\varepsilon}$ is comparable to other geometric length scales (object size, dipole distance). Details of the consequences for atom chip noise spectra and numerical results using this scheme have to be worked out and will be reported elsewhere.

5.3 Quantization

Field quantization canonically proceeds by promoting c-number valued fields to non-commuting operators. The difficulty is to ensure the consistency of the field equations for operators. In the case of the macroscopic Maxwell equations, a problem arises for a complex medium permittivity which is the generic case for a causal medium (satisfying the Kramers-Kronig relations). The decay of the fields (both in time and space) due to dissipation is incompatible with the fixed value of the field commutator in the quantized theory. The solution to this problem proceeds along a well-known line of thought in statistical physics and quantum optics: while dissipation dumps energy and information into a reservoir, the reservoir couples back to the field via fluctuations. The reservoir does not appear explicitly when the field equations are averaged over the reservoir fluctuations, saving the Maxwell equations. But fluctuations do affect field commutators and correlations and maintain in this way the nonzero commutator in the quantized theory.

5.3.1 Noise operators

The prescription to quantize the macroscopic Maxwell equations (5.2) can thus be summarized by the replacement table

$$\begin{aligned} \mathbf{E}(\mathbf{x}) &\mapsto \hat{\mathbf{E}}(\mathbf{x}) \\ \mathbf{B}(\mathbf{x}) &\mapsto \hat{\mathbf{B}}(\mathbf{x}) \\ \mathbf{P}(\mathbf{x}) &\mapsto \hat{\mathbf{P}}_{\mathrm{n}}(\mathbf{x}) + \mathbf{P}(\mathbf{x}) \end{aligned} \tag{5.36}$$

where the carets denote operators and will be dropped in the following. The 'noise polarization' field $\mathbf{P}_{\mathrm{n}}(\mathbf{x})$ is a bosonic operator with commutator[8]

$$\left[P_{\mathrm{n}i}(\mathbf{x};\omega),\, P^{\dagger}_{\mathrm{n}j}(\mathbf{x}';\omega')\right] = 4\pi\hbar\,\delta(\omega-\omega')\delta_{ij}\delta(\mathbf{x}-\mathbf{x}')\,\mathrm{Im}[\varepsilon_0\varepsilon(\mathbf{x};\omega)]. \tag{5.37}$$

The noise polarization vanishes in regions where $\mathrm{Im}\,\varepsilon(\mathbf{x};\omega) = 0$, it is thus confined within the dielectric medium. The noise strength is proportional to the medium absorption in order to compensate for the temporal decay of the solutions to the homogeneous Maxwell equations. This relation essentially amounts to the fluctuation disspation theorem for the polarization noise and implies the corresponding theorem for the fields, as discussed below.

The Kronecker δ_{ij} and the spatial delta function in (5.37) follow from the assumption of a local and isotropic permittivity. The generalization to the more general case of nonlocal media is apparent and has been discussed by the group of Salvatore Savasta in Messina (Stefano & al., 1999, 2000). The prescriptions (5.36,5.37) apply to the case of a nonmagnetic medium. If $\mu \neq 1$, one has to include a noise magnetization as well, see Knöll & al. (2001) and Dung & al. (2003). Finally, for amplifying media ($\mathrm{Im}\,\varepsilon < 0$), consistency requires the exchange of $\mathbf{P}$ and $\mathbf{P}^{\dagger}$ in (5.37). (Details can be found in Knöll & al. (2001).) Savasta & al. (2002) analyze the example of a point scatterer formed by an inverted two-level atom.

We recall that the usual mode expansion of the electric field operator does not hold in an absorbing medium. It is replaced by the expression

$$\mathbf{E}(\mathbf{x};\omega) = \mathbf{E}_{\mathrm{sc}}(\mathbf{x};\omega) + \mathbf{E}_{\mathrm{n}}(\mathbf{x};\omega) \tag{5.38}$$

$$E_{\mathrm{n}i}(\mathbf{x};\omega) = \int \mathrm{d}V(\mathbf{x}')\, G_{ij}(\mathbf{x},\mathbf{x}';\omega) P_{\mathrm{n}j}(\mathbf{x}';\omega), \tag{5.39}$$

where the mode functions occurring in the first term $\mathbf{E}_{\mathrm{sc}}(\mathbf{x})$ solve the homogeneous version of the wave equation (5.6). They describe the scattering of the vacuum field by the dielectric medium. For bounded objects, these modes may be labelled by incident plane waves and are normalized as these (Stefano & al., 1999). The second term in Eq.(5.38) is the radiation due to the noise polarization that can be found from the Green tensor $G_{ij}(\mathbf{x},\mathbf{x}';\omega)$.

[8] The prefactor 4π is related to our convention for the Fourier transformation, see the footnote on page 44.

5.3.2 Crossed field correlations

The quantities of interest in the quantized theory are the correlation functions of the electromagnetic field, but in the presence of the dielectric medium. We define the electric field cross correlation tensor by

$$\mathcal{E}_{ij}(\mathbf{x},\mathbf{x}';\omega) = \int \mathrm{d}\tau\, \mathrm{e}^{-\mathrm{i}\omega\tau} \langle E_i(\mathbf{x},t+\tau) E_j(\mathbf{x}',t)\rangle \tag{5.40}$$

where the average is taken with respect to the ensemble for the combined system 'field and noise polarization'. We assume statistical stationarity[9] so that Eq.(5.40) does not depend on t. In frequency space, the correlation spectrum is given by

$$\langle E_i^\dagger(\mathbf{x};\omega) E_j(\mathbf{x}';\omega')\rangle = 2\pi\delta(\omega-\omega')\,\mathcal{E}_{ij}(\mathbf{x},\mathbf{x}';\omega), \tag{5.41}$$

where we have used that the fields are hermitean. The fields are delta-correlated in frequency space because they are statistically stationary. In terms of the usual operator ordering conventions, our definition corresponds, for positive frequencies, to 'normal' order: $\mathbf{E}(\omega)$ then contains the positive frequency components and the corresponding annihilation operators appear to the right of the creation operators in $\mathbf{E}^\dagger(\omega)$. At negative frequencies, $\mathcal{E}_{ij}(\omega)$ corresponds to an 'anti-normally' ordered average, since hermiticity implies the symmetry relation $\mathbf{E}(-\omega) = \mathbf{E}^\dagger(\omega)$.

Fluctuation dissipation theorem

If field and medium are in thermal equilibrium, any consistent quantization scheme leads to the *fluctuation dissipation theorem* for the field

$$\mathcal{E}_{ij}(\mathbf{x},\mathbf{x}';\omega) = \frac{2\hbar\,\mathrm{Im}\,G_{ij}(\mathbf{x},\mathbf{x}';\omega)}{\mathrm{e}^{\hbar\omega/k_\mathrm{B}T}-1}. \tag{5.42}$$

The strength of the field fluctuations is linked to the dissipative part of the field's response function (the Green tensor) and the temperature. With the fluctuation dissipation theorem, we thus obtain the spatial and spectral dependence of the field correlations by calculating the Green tensor for the dielectric environment. Recalling the basic definition of the latter – the electric field radiated by a monochromatic point dipole –, we note that the theorem reduces quantum and thermal field fluctuations to a 'classical' electrodynamics quantity.

In Appendix A, we quote elementary proofs of Eq.(5.42) for two complementary model situations: an absorptionless dielectric where standard mode expansions can be used (Glauber & Lewenstein, 1991) and a medium with dielectric function whose imaginary part is at least infinitesimally positive all

[9] This means that temporal correlation functions only depend on time differences.

over space (Knöll & al., 2001). A proof for a bounded, absorbing dielectric can be found in Stefano & al. (2000).

We note that formula (5.42) applies both to positive and negative frequencies. At zero temperature, for example, the field noise spectrum only covers negative frequencies because

$$\lim_{T\to 0} \frac{1}{\mathrm{e}^{\hbar\omega/k_{\mathrm{B}}T}-1} = \begin{cases} 0, & \omega > k_{\mathrm{B}}T/\hbar \searrow 0, \\ -1, & \omega < -k_{\mathrm{B}}T/\hbar \nearrow 0. \end{cases} \tag{5.43}$$

This is consistent with the fact that normally ordered field averages vanish in the vacuum state, while anti-normally ordered averages do not.[10] In the literature, for example Rytov's book (1989), symmetrized correlation spectra are often used that are symmetric in frequency, as for classical random fields. The fluctuation dissipation theorem for these reads

$$\begin{aligned} \mathcal{E}^{(\mathrm{S})}_{ij}(\mathbf{x},\mathbf{x}';\omega) &\equiv \tfrac{1}{2}\left\{\mathcal{E}_{ij}(\mathbf{x},\mathbf{x}';\omega) + \mathcal{E}_{ji}(\mathbf{x}',\mathbf{x};-\omega)\right\} \\ &= \hbar\coth(\hbar\omega/2k_{\mathrm{B}}T)\,\mathrm{Im}\,G_{ij}(\mathbf{x},\mathbf{x}';\omega), \end{aligned} \tag{5.44}$$

where we have used the symmetry and reciprocity of the Green tensor (Eqs.(5.9, 5.10)). At high temperatures, $\hbar\coth(\hbar\omega/2k_{\mathrm{B}}T) \to 2k_{\mathrm{B}}T/\omega$, so that Planck's constant disappears and we recover the Einstein relation (a 'classical' fluctuation dissipation theorem).

Example: Planck formula

Planck's formula for the spectral density of blackbody radiation can be found from Eq.(5.42) using the free space Green function (5.8). One finds that the electric and magnetic energy densities are equal:[11]

$$u_E(\omega) \equiv \frac{\varepsilon_0}{2}\,\mathrm{tr}\,\mathcal{E}_{ij}(\mathbf{x},\mathbf{x};\omega) = \frac{\hbar\omega^3/(2\pi c^3)}{\mathrm{e}^{\hbar\omega/k_{\mathrm{B}}T}-1} = u_B(\omega). \tag{5.45}$$

Non equilibrium radiation

At thermal equilibrium, one could ignore noise operators and use the field characterization provided by the fluctuation dissipation theorem. The quantization scheme really becomes operational in non equilibrium situations, for example, when the dielectric medium has a locally varying temperature. We can thus model the emission from a thermal source (Carminati & Greffet, 1999; Henkel & al., 2000). Throughout this thesis, we assume that the medium is, at

[10] The spectrum of the energy density remains positive because the symmetry relation (5.9) implies that $\mathrm{Im}\,G_{ii}(\mathbf{x},\mathbf{x};\omega) < 0$ for negative frequencies.

[11] The limit $\mathbf{x} \to \mathbf{x}'$ requires some care for the Green tensor (5.8), see de Vries & al. (1998). Fortunately, its imaginary part does not present any singularities.

least locally, in thermal equilibrium[12] and use Bose-Einstein statistics to compute the expectation value of the noise operators. In terms of a cross correlation tensor $\mathcal{P}_{ij}(\mathbf{x},\mathbf{x}';\omega)$ defined similar to (5.41), the polarization noise is characterized by the local spectrum

$$\mathcal{P}_{ij}(\mathbf{x},\mathbf{x}';\omega) = \delta_{ij}\delta(\mathbf{x}-\mathbf{x}')\,\frac{2\hbar\,\mathrm{Im}[\varepsilon_0\varepsilon(\mathbf{x};\omega)]}{\mathrm{e}^{\hbar\omega/k_\mathrm{B}T(\mathbf{x})}-1}, \tag{5.46}$$

where $T(\mathbf{x})$ is the local temperature. Let us assume that $\mathbf{E}_\mathrm{sc}$, the field incident from infinity in (5.38), is at zero temperature.[13] This leads to the emission spectrum (at $\omega > 0$):

$$\mathcal{E}_{ij}(\mathbf{x},\mathbf{x}';\omega) = 2\hbar\int_{\mathcal{S}}\mathrm{d}V(\mathbf{x}_1)G^*_{ik}(\mathbf{x},\mathbf{x}_1;\omega)G_{jk}(\mathbf{x}',\mathbf{x}_1;\omega)\frac{\mathrm{Im}[\varepsilon_0\varepsilon(\mathbf{x}_1;\omega)]}{\mathrm{e}^{\hbar\omega/k_\mathrm{B}T(\mathbf{x}_1)}-1}, \tag{5.47}$$

where $\mathcal{S}$ is the volume occupied by the source. In the equilibrium case, an electrodynamic identity allows to reduce this integral to the imaginary part of the Green tensor (see Appendix A.2).

An alternative formulation of (5.47) has been given by Sidles & al. (2003) who consider the radiation of a point source and its absorption in the microstructures. Due to the reciprocity of the Green tensor, this approach yields equivalent results.

5.3.3 Near field correlation spectra

We review here the cross correlation spectra for electric and magnetic fields in the near field of a planar substrate. Assuming the field in equilibrium with the substrate, we shall use the fluctuation-dissipation theorem (5.42) and its magnetic equivalent

$$\mathcal{B}_{ij}(\mathbf{x},\mathbf{x}';\omega) = \frac{2\hbar\,\mathrm{Im}\,H_{ij}(\mathbf{x},\mathbf{x}';\omega)}{\mathrm{e}^{\hbar\omega/k_\mathrm{B}T}-1}. \tag{5.48}$$

Energy densities

As a first example, let us compute the ratio between the electric and magnetic spectral energy densities u_E and u_B in the near field. This is plotted in Figure 5.1, as calculated from the exact formulas in Henkel & al. (1999b). In the far

[12] The assumption of local equilibrium is reasonable on the mesoscopic length scale we work on, since on this scale the object contains a macroscopic number of particles. Note that local equilibrium does not exclude that a field induces a medium polarization, as described by the dielectric function. As pointed out by Callen & Welton (1951), the latter in general depends on the state of the medium (its local temperature, for example). To quote an example, a partially excited two-level medium shows a reduced absorption due to saturation.

[13] Formally, one can consider that the vacuum around the object is closed in the far field by a 'cold absorber' held at zero temperature. This maintains the non-equilibrium situation, see Henry & Kazarinov (1996).

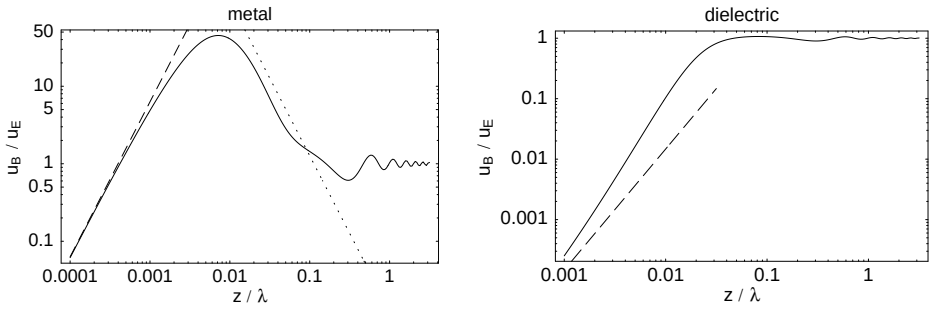

Figure 5.1: Ratio of magnetic to electric energy density vs. distance from a medium-filled half-space, normalized to the wavelength λ. Left panel: metal with $\varepsilon = 1 + 800\,\mathrm{i}$ (skin depth $\delta = 0.008\,\lambda$). Right panel: dielectric ($\varepsilon = 2.3 + 0.1\,\mathrm{i}$, $\delta > \lambda$). The dashed and dotted lines correspond to Eqs.(5.50, 5.51), as discussed in the text.

field, both are given by the Planck formula (5.45). At short distance from the substrate, the reflected field encoded in the Green tensors (5.20) and (5.27) provides the near field correction. We find that these scale like $1/z^3$ and $1/(\lambda\!\!\!^{-2} z)$ at short distances, respectively, and dominate both over the far field value $\propto 1/\lambda\!\!\!^{-3}$ where $\lambda\!\!\!^{-} \equiv c/\omega$. For the magnetic noise spectrum, this is consistent with Varpula & Poutanen (1984); Sidles & al. (2003). We thus get a ratio

$$\frac{u_B}{u_E} \approx \frac{z^2}{2\lambda\!\!\!^{-2}} \frac{\mathrm{Im}\,\varepsilon + 2\,\mathrm{Im}\,\dfrac{\varepsilon-1}{\varepsilon+1}}{\mathrm{Im}\,\dfrac{\varepsilon-1}{\varepsilon+1}}. \tag{5.49}$$

This is plotted as dashed lines in Fig. 5.1. We observe that depending on the substrate permittivity ε, the field energy is stored predominantly in the magnetic or in the electric field.

Of interest for integrated atom optics is the case of metallic substrates at low frequencies where $\varepsilon \approx \mathrm{i}\sigma/(\varepsilon_0\omega)$ is dominated by the DC conductivity σ. We then have $|\varepsilon| \gg 1$, and to leading order, the ratio (5.49) becomes

$$\frac{u_B}{u_E} \approx \frac{\sigma^2 z^2}{4\varepsilon_0^2 c^2} \gg 1. \tag{5.50}$$

The characteristic length $\varepsilon_0 c/\sigma$ has a value $10^{-10}\,\mathrm{m}$ for typical metal conductivities so that the field energy becomes more and more 'magnetic' as one recedes from the substrate. This trend continues up to the skin depth $\delta = \sqrt{2\varepsilon_0 c^2/(\sigma\omega)}$ where the near field expansions used here do not hold any longer. Using the results of Henkel & al. (1999b), we find in the regime $\delta \ll z \ll \lambda\!\!\!^{-}$ (the dotted line in Fig.5.1)

$$\frac{u_B}{u_E} \approx \frac{\lambda\!\!\!^{-2}}{2z^2} \gg 1. \tag{5.51}$$

At a distance $z \sim \lambda$, the far field energy density takes over compared to the near field correction, and we then recover $u_B \sim u_E$. The spatial modulations of u_B and u_E in this range have a period $\approx \lambda/2$, they arise due to the reflection from the substrate.

A more detailed discussion of the electric and magnetic energy densities, including electromagnetic surface resonances, is given in a recent paper by Joulain & al. (2003).

Correlation length

As a second example, we demonstrate that magnetic near field noise is spatially 'rough' on a scale given by the observation distance. This result has been mentioned without proof in Henkel & al. (2003c).

The quantity of interest is the spatial correlation function for a particular component of the magnetic field. The context is that of a quasi one-dimensional atom trap, a 'side guide' above a planar substrate (see Fig.2.2). At the guide centre, the magnetic field is oriented along the guide axis due to a superimposed homogeneous field. Magnetic fluctuations along this axis dominate the fluctuations of the adiabatic trapping potential (6.17) and lead to heating and scattering of the trapped atoms. If we choose the x-axis along the guide, we thus have to compute the correlation function $B_{xx}(x, z, x', z; \omega)$ for two points in the guide.

In the far field where Planck's blackbody theory applies, the correlation length is given by the wavelength, but we focus here on the limit where the guide distance z is much smaller than the wavelength. As in the previous example, we model the substrate by a metallic half-space[14] , focus on distances smaller than the skin depth and use the near field contribution (5.27) to the magnetic Green tensor. The fluctuation dissipation theorem (5.48) then gives

$$B_{xx}(x, z, x', z; \omega) = \frac{\hbar\omega\mu_0^2\sigma}{4\pi(\mathrm{e}^{\hbar\omega/k_\mathrm{B}T} - 1)} \frac{z(\tilde{r} - 2z)}{\tilde{r}(x - x')^2}, \tag{5.52}$$

where again $\tilde{r}^2 = (x - x')^2 + 4z^2$ is the distance to the image dipole. For low frequencies ($\hbar\omega \ll k_\mathrm{B}T$), we find a flat spectrum

$$B_{xx}(x, z, x, z; \omega) = \frac{\sigma k_\mathrm{B} T \mu_0^2}{32\pi\, z}. \tag{5.53}$$

Normalizing the correlation function (5.52) to this value, we get Eq.(33) of Henkel & al. (2003c),

$$C_{xx}(x - x'; z) = \frac{8z^2}{\sqrt{(x - x')^2 + 4z^2}(\sqrt{(x - x')^2 + 4z^2} + 2z)}. \tag{5.54}$$

[14]Calculations of the magnetic Green function for a thin layer turn out to reproduce the correlation length found here.

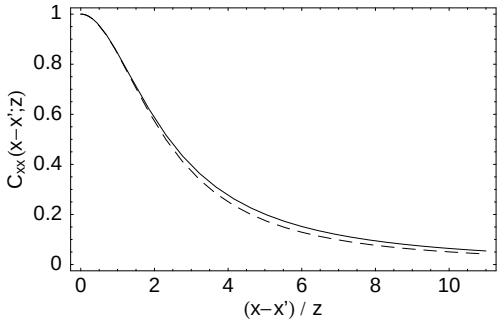

Figure 5.2: Normalized correlation function (5.54) for thermal magnetic fields in the short distance limit. The dashed curve corresponds to the Lorentzian $C(x-x') = \ell_{\rm corr}^2/[(x-x')^2+\ell_{\rm corr}^2]$ with $\ell_{\rm corr} = 4z/\sqrt{3}$. The lateral separation $x-x'$ is scaled to the distance z.

This is plotted in Fig.5.2 and compared to a Lorentzian which shows a similar asymptotics for short and large separations $x-x'$. Both expressions demonstrate that the thermal magnetic near field along the linear guide is correlated on a scale given by the distance to the substrate. The same result has been obtained by Henkel & al. (2000) for the electric field. In that paper, it is also shown that $\ell_{\rm corr}$ scales proportional to z even at distances beyond the skin depth (in the range $\delta < z \ll \lambda\!\!\!^{-}$).

Magnetostatic approximation

Henkel & Pötting (2001) develop a simplified framework for magnetic noise spectra that is able to handle arbitrary geometrical shapes. The starting point is the formula (5.47) for the radiation emitted by a hot body. The key approximation is that the Green function for the magnetic field radiated by a pointlike polarization current is replaced by its free space value,

$$B_i(\mathbf{x}) = \int {\rm d}V(\mathbf{x}') K_{ij}(\mathbf{x}-\mathbf{x}';\omega) P_j(\mathbf{x}'), \tag{5.55}$$

$$K_{ij}(\mathbf{r};\omega) \approx -\frac{{\rm i}\mu_0\omega}{4\pi}\varepsilon_{ijk}\hat{r}_k \frac{{\rm e}^{{\rm i}k_0 r}}{r^2}\left(1-{\rm i}k_0 r\right), \tag{5.56}$$

where in the near field, the magnetostatic limit $k_0 r = r/\lambda\!\!\!^{-} \to 0$ can be taken. In this approach, the magnetic field is propagated ignoring the impact of the interface. Taking the low-frequency limit $\hbar\omega \ll k_{\rm B}T$, we get close to a metallic object

$$\mathcal{B}_{ij}(\mathbf{x},\mathbf{x}';\omega) = \frac{2\sigma k_{\rm B}T}{\omega^2}\int\limits_{\mathcal{S}} {\rm d}V(\mathbf{x}_1) K^*_{ik}(\mathbf{x}-\mathbf{x}_1;\omega) K_{jk}(\mathbf{x}'-\mathbf{x}_1;\omega) \tag{5.57}$$

$$= \frac{\sigma k_{\mathrm{B}} T \mu_0^2}{8\pi^2} \int\limits_{\mathcal{S}} \mathrm{d}V(\mathbf{x}_1) \frac{\delta_{ij}(\mathbf{x}-\mathbf{x}_1)\cdot(\mathbf{x}'-\mathbf{x}_1) - (\mathbf{x}-\mathbf{x}_1)_j(\mathbf{x}'-\mathbf{x}_1)_i}{|\mathbf{x}-\mathbf{x}_1|^3 |\mathbf{x}'-\mathbf{x}_1|^3},$$

where $\mathcal{S}$ is the object volume. We recover the frequency-independent spectrum of Eq.(5.53), multiplied by a geometry-dependent integral. For simple object shapes, the integration can again be performed analytically (see Table 5.3); it can be done numerically in a straightforward way for a realistic experimental geometry. Above a half space, we recover the power law $\propto 1/z$ derived without any approximation in Eq.(5.53) in the regime $z \ll \delta$. As shown in Table 5.3, a faster decay occurs for a thin layer or a thin wire: we thus conclude that *magnetic noise is stronger the larger the amount of metallic material surrounding the microtrap*.

Object	short distance $z \ll a$	medium distance $a \ll z \ll \delta$	large distance $\delta \ll z \ll \lambda\!\!\!^{-}$
Half space (exact)	$1/z$	$1/z$	δ^3/z^4
Half space (approx.)	$1/z$	$1/z$	$1/z$
Layer (approx.)	$1/z$	a/z^2	a/z^2
Wire (approx.)	$1/z$	a^2/z^3	a^2/z^3

Table 5.3: Distance dependence of magnetic near field noise. Exact results are based on Eq.(5.27) and Eq.(22) of Henkel & al. (1999b); approximate results on Eq.(5.57). The length a specifies the layer thickness resp. the wire radius; δ is the skin depth.

Although this approximation yields correct power laws and order of magnitude estimates at short distances $z \ll \delta$, it is not exact: the magnetic cross correlation tensor above a half-space is not reproduced. We conclude this section with an explanation of this failure.

One error has an obvious reason: the change in the power law with distance around the skin depth δ can not be reproduced (see Table 5.3) because the substrate permittivity is ignored in the Green function (5.56). If the skin depth is taken into account for the propagation in the medium, we have checked that one recovers, for a planar substrate, the crossover $1/z \to 1/z^4$ in the distance dependence.

The second error occurs at distances $z \ll \delta$, where the approximation does not describe correctly the relative magnitude of the noise tensor diagonal elements. ¿¿From Eqs.(5.27, 5.48), the exact short-distance asymptotics for a half-space is

$$B_{ij}^{(\mathrm{exact})}(x,z,x,z;\omega) = \frac{\sigma k_{\mathrm{B}} T \mu_0^2}{32\pi\, z} \left(\delta_{ij} + n_i n_j\right) \tag{5.58}$$

where $\mathbf{n}$ is the unit surface normal. In the approximate result found in Henkel & Pötting (2001) using (5.57), the tensor $\delta_{ij} + n_i n_j$ is replaced by $3\delta_{ij} - n_i n_j$.

The field components parallel to the surface are thus overestimated, leading to a magnetic energy density which is too large by a factor two. This failure originates from the boundary conditions imposed by the surface that are ignored as well when using the Green function (5.56). Note that for $z \ll \delta$, the damping of the field in the medium is negligible, and one may describe the fields quasi-statically. However, the jump in the medium conductivity for a metallic object leads to the following boundary condition[15]

$$\left.\frac{\partial \mathbf{B}}{\partial n}\right|_{\text{out}} - \left.\frac{\partial \mathbf{B}}{\partial n}\right|_{\text{in}} = \mu_0 \sigma \mathbf{n} \times \mathbf{E}, \tag{5.59}$$

where $\partial/\partial n$ is the derivative along the surface normal $\mathbf{n}$ and σ the object conductivity. We have checked that with this boundary condition, a magnetostatic calculation gives the correct noise tensor (5.58) for a planar substrate. A correction to the fields inside the medium in a similar situation has been discussed by Sidles & al. (2003). The application of this refined theory to other geometries, for example cylindrical wires, is in progress.

[15] We evaluate the Faraday-Lorentz law just above and below the surface, take parallel components and use $\boldsymbol{\nabla} \cdot \mathbf{B} = 0$. A conductivity $\sigma \gg \varepsilon_0 \omega$ is assumed.

Chapter 6

Atoms

We have seen that the electromagnetic field shows intrinsic fluctuations that get strongly modified and enhanced in the near field. The spontaneous decay of atoms is hence accelerated and atomic energy levels are shifted. In the simplest framework to describe the atom-field interaction, one focusses on the atomic level populations and describes their dynamics in terms of rate equations. A more complete picture is provided by master equations that also characterize how atoms lose quantum-mechanical coherence (superposition states) due to the coupling to the field. This framework is reviewed here, with an emphasis on the connection between the field correlation functions and the typical time scales for atomic dynamics.

6.1 Electric dipole coupling to optical fields

In this section, we introduce our notation for two-level atoms that interact via an electric dipole transition with the electromagnetic field. The basic atomic observables and the non-Hamiltonian evolution in a fluctuating field are sketched.

6.1.1 Two-level atom

The Hamiltonian for a single atom driven by a near-resonant laser field can be written as

$$H_{\rm S} = H_{\rm A} + H_{\rm AL} = \frac{\hbar\omega_A}{2}\sigma_3 - (\sigma_+\mathbf{d} + \sigma_-\mathbf{d}^*)\cdot\mathbf{E}_{\rm L}(\mathbf{r},t). \tag{6.1}$$

Only two levels, $|{\rm g}\rangle$ and $|{\rm e}\rangle$, separated by the Bohr frequency $\omega_{\rm A}$ close to the laser frequency have been retained; this is the resonance or two-level approximation. The operator $\sigma_3 \equiv |{\rm e}\rangle\langle{\rm e}| - |{\rm g}\rangle\langle{\rm g}|$ is the atomic inversion, $\sigma_+ \equiv |{\rm g}\rangle\langle{\rm e}|$

and $\sigma_- = \sigma_+^\dagger = |\mathrm{e}\rangle\langle\mathrm{g}|$ are the flip operators, and $\mathbf{d}$ is the electric dipole matrix element. The laser field is described in terms of a classical field $\mathbf{E}_\mathrm{L}(\mathbf{r},t)$ to be evaluated at the atomic position $\mathbf{r}$.

In the rotating wave approximation, only slowly varying terms in an interaction picture with respect to H_A are retained in the coupling H_AL. In this picture, the flip operators evolve as $\sigma_\pm\,\mathrm{e}^{\mp\mathrm{i}\omega_\mathrm{A}t}$ (positive and negative frequency parts). For a monochromatic laser field, $\mathbf{E}_\mathrm{L}(\mathbf{r},t) = \mathbf{E}_\mathrm{L}(\mathbf{r})\,\mathrm{e}^{-\mathrm{i}\omega_\mathrm{L}t} + \mathrm{C.C.}$, with a small detuning, $|\omega_\mathrm{L}-\omega_\mathrm{A}| \ll \omega_\mathrm{A}$, the terms kept in the interaction Hamiltonian are

$$H_\mathrm{AL} = -\sigma_+\mathbf{d}\cdot\mathbf{E}_\mathrm{L}^*(\mathbf{r})\,\mathrm{e}^{+\mathrm{i}\omega_L t} - \sigma_-\mathbf{d}^*\cdot\mathbf{E}_\mathrm{L}(\mathbf{r})\,\mathrm{e}^{-\mathrm{i}\omega_L t}. \tag{6.2}$$

The explicit time dependence can be removed with a unitary transformation into a 'rotating frame' so that we finally get

$$H_\mathrm{S} = -\frac{\hbar\Delta_\mathrm{L}}{2}\sigma_3 + \frac{\hbar\Omega(\mathbf{r})}{2}\left(\sigma_+ + \sigma_-\right), \tag{6.3}$$

where $\Delta_\mathrm{L} \equiv \omega_\mathrm{L} - \omega_\mathrm{A}$ is the laser detuning and the 'Rabi frequency' $\Omega \equiv -2\mathbf{d}^*\cdot\mathbf{E}_\mathrm{L}(\mathbf{r})/\hbar$ has been made real with a suitably chosen origin of time.

6.1.2 Master equations

Due to the statistical nature of the interaction with vacuum or thermal fields, we cannot describe the atom in terms of a wave function (a two-component spinor). Instead, a reduced density matrix ρ has to be used that takes into account the average with respect to the field fluctuations. All expectation values of system operators $\mathcal{O}$ can then be computed according to $\langle\mathcal{O}\rangle = \mathrm{Tr}\,(\mathcal{O}\rho)$.

For a two-level atom weakly coupled to a broad band fluctuating field, the density matrix ρ evolves according to (in the Schrödinger picture)

$$\frac{\mathrm{d}\rho}{\mathrm{d}t} = \frac{1}{\mathrm{i}\hbar}\left[H_\mathrm{S},\,\rho\right] + \frac{1}{2}\sum_{\alpha=+,-}\Gamma_\alpha\left(2\sigma_\alpha\rho\sigma_\alpha^\dagger - \left\{\sigma_\alpha^\dagger\sigma_\alpha,\,\rho\right\}\right), \tag{6.4}$$

$$\{\mathcal{O},\,\rho\} \equiv \mathcal{O}\,\rho + \rho\,\mathcal{O}. \tag{6.5}$$

The Hamiltonian H_S generates the non-dissipative evolution of the system.[1] The rates $\Gamma_\pm$ describe transitions between the levels $|\mathrm{e}\rangle$, $|\mathrm{g}\rangle$. In our notation, Γ_+ corresponds to the process $|\mathrm{e}\rangle \to |\mathrm{g}\rangle$ (spontaneous and stimulated emission) and Γ_- to absorption.

The transition rates are given by correlation functions of the field the atom couples to. For the case of an electric dipole transition considered here,

$$\Gamma_- = \frac{d_i\,d_j^*}{\hbar^2}\int\mathrm{d}\tau\,\mathrm{e}^{-\mathrm{i}\omega_\mathrm{A}\tau}\langle E_i(\mathbf{r},t+\tau)E_j(\mathbf{r},t)\rangle_\mathrm{R}$$

[1] It includes renormalized transition frequencies where the renormalization (Lamb shift, van der Waals shift) is due to the interaction with the field.

$$= \frac{d_i\, d_j^*}{\hbar^2}\mathcal{E}_{ij}(\mathbf{r},\mathbf{r};\omega_\mathrm{A}) \qquad \text{(absorption)}, \tag{6.6}$$

$$\Gamma_+ = \frac{d_i\, d_j^*}{\hbar^2}\mathcal{E}_{ij}(\mathbf{r},\mathbf{r};-\omega_\mathrm{A}) \qquad \text{(emission)}, \tag{6.7}$$

where $\langle\ldots\rangle_\mathrm{R}$ denotes the average with respect to the field's density operator. The latter does not involve the atom because we assume a weak atom-field coupling. The same result can be obtained from Fermi's Golden Rule (Wylie & Sipe, 1984). As we discussed in Section 5.3.2, the field is not necessarily a reservoir in equilibrium itself; in the near field of a 'hot' object, for example, only the object, but not the field will be in an equilibrium state.

The cross correlation spectrum of the field, taken at the atomic transition frequency, hence provides the time scale for field-induced transitions. We have assumed a broad field spectrum whose value at the eigenfrequencies of the system Hamiltonian does not differ significantly compared to the 'bare' transition frequency ω_A. This breaks down in a field with a strongly modulated spectrum like for a photonic band gap material (Mossberg & Lewenstein, 1993). The master equation (6.4) must then be modified to take into account memory effects, typically by replacing it with an integro-differential equation. We outline a more detailed theory in Section 6.1.3.

The master equation (6.4) reproduces the rate equations one would write down given the transition rates $\Gamma_\pm$. But it also gives the dynamics of off-diagonal elements of the atomic density matrix. Recall that these 'coherences' are nonzero for superposition states made from $|\mathrm{g}\rangle$ and $|\mathrm{e}\rangle$. We get for example

$$\frac{\mathrm{d}\rho_\mathrm{eg}}{\mathrm{d}t} = \frac{1}{\mathrm{i}\hbar}\langle\mathrm{e}|\,[H_\mathrm{S},\,\rho]\,|\mathrm{g}\rangle - \frac{\Gamma_+ + \Gamma_-}{2}\rho_\mathrm{eg}, \tag{6.8}$$

so that the coupling to the field damps the off-diagonal matrix elements — this is the hallmark of 'decoherence'. The corresponding time scale is in the present model determined by the transition rates for the populations. There are cases, however, where decoherence happens faster: reservoir-induced fluctuations of the atomic transition frequency, also called 'dephasing', are an example.

Classical calculation of spontaneous emission

Although spontaneous emission is a process triggered by quantum fluctuations, its rate is closely connected to classical quantities. At zero temperature, only spontaneous emission processes survive in (6.6, 6.7) because the correlations $\mathcal{E}_{ij}(\ldots;\omega_\mathrm{A})$, corresponding to normal order, vanish, while the anti-normally ordered ones $\mathcal{E}_{ij}(\ldots;-\omega_\mathrm{A})$ do not (see remarks after Eq.(5.41)). Using the fluctuation-dissipation theorem (5.42) at zero temperature, Eq.(6.7) can be

written

$$\Gamma_+(T=0) = \frac{2d_i\, d_j^*}{\hbar}\mathrm{Im}\, G_{ij}(\mathbf{r},\mathbf{r};\omega_\mathrm{A}) = \frac{2\,\mathrm{Re}\big[\mathrm{i}\omega_\mathrm{A}\mathbf{d}\cdot\mathbf{E}^*_\mathrm{dip}(\mathbf{r},\mathbf{r};\omega_\mathrm{A})\big]}{\hbar\omega_\mathrm{A}}. \tag{6.9}$$

In the second step, we have expressed the Green tensor in terms of the electric field of an oscillating point dipole with amplitude $\mathbf{d}$ and frequency ω_A. In the numerator of Eq.(6.9), we recognize the power radiated by the dipole and averaged over an oscillation period, according to the Poynting theorem. If this classical emission is normalized to the energy quantum $\hbar\omega_\mathrm{A}$, we get the spontaneous emission rate. We may thus regard this calculation as an application of the correspondence principle. It may be one of the fastest ways to get the spontaneous emission rate in free space. The imaginary part of the Green tensor is, using Eq.(5.8) and taking the limit $\mathbf{x}\to\mathbf{x}'$ (see footnote 11 on page 58),

$$\mathrm{Im}\, G_{ij}(\mathbf{x},\mathbf{x};\omega) = \frac{\omega^3}{6\varepsilon_0 c^3}\delta_{ij}. \tag{6.10}$$

The well-known result $\Gamma_+(\mathrm{vac}) = \mathbf{d}^2\omega_\mathrm{A}^3/(3\pi\varepsilon_0\hbar c^3)$ follows.

In the near field, the 'reflected' part of the Green tensor gives the modification of the spontaneous emission rate. Close to a metallic surface, for example, one gets an enhanced decay rate $\Gamma_+ \propto 1/z^3$ using the expansion (5.20). Note that the decay is in this limit dominated by 'nonradiative' processes: the energy of the excited state is absorbed by the surface without emission of a photon. The decay rate (6.9) does not separate these two channels. But the radiative contribution can be found using again the correspondence principle: computing the power emitted into the far field and normalizing to $\hbar\omega_A$.

Energy level shifts

For completeness, we also write down the energy shift of the atomic levels due to the coupling to the reservoir. To lowest order in the dipole moments, one gets (Agarwal, 1975b; Wylie & Sipe, 1984)

$$\begin{aligned}\alpha = \mathrm{e},\,\mathrm{g}: \quad \delta E_\alpha &= \sum_\beta d_i^{\alpha\beta} d_j^{\alpha\beta *}\mathcal{P}\int\frac{\mathrm{d}\omega}{2\pi\hbar}\frac{\mathcal{E}_{ij}(\mathbf{r},\mathbf{r};\omega)}{\omega-\omega_{\beta\alpha}} \\ &= \sum_\beta d_i^{\alpha\beta} d_j^{\alpha\beta *}\mathcal{P}\int\frac{\mathrm{d}\omega}{\pi}\frac{\mathrm{Im}\, G_{ij}(\mathbf{r},\mathbf{r};\omega)}{(\omega-\omega_{\beta\alpha})(\mathrm{e}^{\hbar\omega/k_\mathrm{B}T}-1)}\end{aligned} \tag{6.11}$$

where $\mathcal{P}$ denotes the principal value and β is any level connected to $|\mathrm{g}\rangle$ or $|\mathrm{e}\rangle$ via an electric dipole transition (transition frequency $\omega_{\beta\alpha} = (E_\beta - E_\alpha)/\hbar$, matrix element $\mathbf{d}^{\alpha\beta}$). At zero temperature, only negative frequencies contribute to the integral (see Eq.(5.43)). For the ground state, all Bohr frequencies $\omega_{\beta\alpha}$

are positive so that the energy shift is negative, as is well known from perturbation theory. For the excited state $|\mathrm{e}\rangle$, the transition to the ground state $|\mathrm{g}\rangle$ gives a resonant contribution. Using (at zero temperature) the Kramers-Kronig relations, this can be written in terms of the real part $\mathrm{Re}\, G_{ij}(\mathbf{r},\mathbf{r};\omega_{\mathrm{eg}})$. A similar frequency shift is experienced by a classical dipole coupled to the field (see Henkel & Sandoghdar (1998) for details).

6.1.3 Structured reservoirs and non Markovian dissipation

We relax in this Section the assumption that the field provides a broad-band reservoir and sketch the corresponding master equation. For simplicity, the weak coupling approximation is still made. We also assume that at some initial time $t = 0$, system and reservoir are uncorrelated, $\rho(0) = \rho_{\mathrm{S}}(0) \otimes \rho_{\mathrm{R}}(0)$.

Starting from the Liouville-von Neumann equation in an interaction picture with respect to the free evolution, we get a formal solution in terms of a time integral and insert it into the equation of motion. This leads to the integro-differential equation

$$\frac{\partial}{\partial t}\rho \;=\; \frac{1}{\mathrm{i}\hbar}\left[H_{\mathrm{int}}(t),\rho(0)\right] + \frac{1}{\mathrm{i}\hbar}\int_0^t \mathrm{d}\tau\, \left[H_{\mathrm{int}}(t),\left[H_{\mathrm{int}}(t-\tau),\rho(t-\tau)\right]\right]. \quad (6.12)$$

We get the master equation for the system density matrix by tracing out the reservoir degrees of freedom. This makes the first term disappear (a nonzero expectation value could be incorporated into the system Hamiltonian H_{S}). The second term, involving the integral, is already of second order in the interaction. Given the assumption of weak coupling, we shall replace the density matrix by $\rho(t-\tau) \approx \rho_{\mathrm{R}}(0) \otimes \rho_{\mathrm{S}}(t-\tau)$, where a finite memory time is allowed for by keeping the time argument $t-\tau$ in the system density matrix.

With the usual bilinear coupling $H_{\mathrm{int}} = -\mathbf{p}\cdot\mathbf{E}(\mathbf{r})$ where $\mathbf{p} = \sigma_+\mathbf{d} + \sigma_-\mathbf{d}^*$, the master equation that follows can be written in the form (Agarwal, 1975c)

$$\begin{aligned}\frac{\partial}{\partial t}\rho_{\mathrm{S}} = &-\frac{1}{2\hbar^2}\int_0^t \mathrm{d}\tau \Big\{ \langle\{E_i(\mathbf{r},t),\, E_j(\mathbf{r},t-\tau)\}\rangle_{\mathrm{R}}\,[p_i(t),\,[p_j(t-\tau),\,\rho_{\mathrm{S}}(t-\tau)]] \\ &+ \langle[E_i(\mathbf{r},t),\, E_j(\mathbf{r},t-\tau)]\rangle_{\mathrm{R}}\,[p_i(t),\,\{p_j(t-\tau),\,\rho_{\mathrm{S}}(t-\tau)\}]\Big\}. \end{aligned} \quad (6.13)$$

The time-dependence of the operators is that of the trivial free evolution. When the fluctuation-dissipation theorem holds for the field, the 'fluctuation kernels' occurring in this integral can be expressed in terms of the Green tensor (see also Eq.(5.44))

$$\langle[E_i(\mathbf{r},t),\, E_j(\mathbf{r},t-\tau)]\rangle_{\mathrm{R}} \;=\; -2\hbar\int_{-\infty}^{\infty}\frac{\mathrm{d}\omega}{2\pi}\,\mathrm{e}^{\mathrm{i}\omega\tau}\mathrm{Im}\, G_{ij}(\mathbf{r},\mathbf{r};\omega), \quad (6.14)$$

$$\langle\{E_i(\mathbf{r},t),\, E_j(\mathbf{r},t-\tau)\}\rangle_{\mathrm{R}} \quad = \quad 2\hbar \int\limits_{-\infty}^{\infty} \frac{\mathrm{d}\omega}{2\pi}\, \mathrm{e}^{\mathrm{i}\omega\tau}\, \coth(\hbar\omega/2k_{\mathrm{B}}T) \mathrm{Im}\, G_{ij}(\mathbf{r},\mathbf{r};\omega).$$

We recover the previous theory when the frequency range that effectively contributes to these integrals is so broad that the corresponding reservoir correlation time τ_{R} is smaller than all other time scales. Then the Markov approximation can be made, replacing the fluctuation kernels by δ-functions in τ. In this regime, it would be inconsistent to keep the time argument $\rho_{\mathrm{S}}(t-\tau)$, as pointed out by van Kampen (1992, ch. XVI.4). The opposite case is relevant for fields whose correlation spectrum shows significant structure, leading to long correlation or memory times. This occurs in high-finesse cavities (Lambropoulos & al., 2000) and close to a photonic band edge in periodic nanostructured dielectrics (John & Quang, 1994; Woldeyohannes & John, 2003). An example is worked out in Boedecker & al. (2004) for a simplified band edge model: close to the band edge, an excited dipole shows an essentially algebraic instead of exponential decay. We currently investigate whether this can also occur in finite nanostructures where the singularities in the density of field modes are smoothed.

6.2 Atomic spin coupling to magnetic fields

6.2.1 Magnetic moment

Atoms with a nonzero spin have a degenerate ground state whose magnetic sublevels provide a representation of both the spin operator[2] $\mathbf{J}$ and the magnetic dipole moment $\boldsymbol{\mu}$. The Hamiltonian for the coupling to a magnetic field reads

$$H_{\mathrm{AM}} = -\boldsymbol{\mu}\cdot\mathbf{B}(\mathbf{r},t) = -\hbar\mu\mathbf{J}\cdot\mathbf{B}(\mathbf{r},t), \tag{6.15}$$

where $\mu = \mu_{\mathrm{B}} g_J$ is the magnetic moment (expressed in terms of the Bohr magneton and the Landé factor). We normalize the spin to $\hbar$ so that $\mathbf{J}$ becomes dimensionless.

In a static magnetic field $\mathbf{B}_0(\mathbf{r})$, the magnetic moment precesses at the Larmor frequency $\omega_{\mathrm{L}} \equiv \mu|\mathbf{B}_0(\mathbf{r})|$ around the field direction. The corresponding eigenstates $|m_J\rangle$ of the Hamiltonian are characterized by the magnetic quantum number m_J and have energies $\hbar\omega_{\mathrm{L}} m_J$. They can be coupled by a time-dependent field $\mathbf{B}_\perp(\mathbf{r},t)$ orthogonal to $\mathbf{B}_0(\mathbf{r})$, a resonance then occurs at the Larmor frequency. In the rotating wave approximation, the off-resonant terms

[2] We use $\mathbf{J}$ instead of the more conventional $\mathbf{F}$ for the total spin (nuclear + orbital + electronic), to avoid confusion with the force.

are neglected,[3] and assuming a monochromatic driving at $\omega_{\rm B}$, one is led to a Hamiltonian similar to Eq.(6.3):

$$H_{\rm AM} = \hbar(\omega_{\rm B} - \omega_{\rm L})J_3 - \mu|\mathbf{B}_\perp(\mathbf{r})|\,(J_+ + J_-)\,, \tag{6.16}$$

where J_3 is chosen along the direction of $\mathbf{B}_0(\mathbf{r})$ and $J_\pm = J_1 \pm {\rm i}J_2$ are the usual ladder operators, with J_1 the component along $\mathbf{B}_\perp(\mathbf{r})$.

6.2.2 Processes in broad band fields

A framework identical to the master equation (6.4) can be formulated for the interaction with a broad band magnetic field (see Henkel & al. (1999b) for explicit formulas). The field induces processes like spin relaxation and decoherence. The transitions induced between magnetic sublevels $|m_J\rangle$ (defined with respect to the static field $\mathbf{B}_0(\mathbf{r})$) are called 'spin flips'. They play an important role in the context of magnetic traps because typically only some of the sublevels are trapped. Consider for simplicity a $J = 1/2$ spin. If the centre-of-mass motion is 'slow' compared to the Larmor frequency, one can introduce adiabatic potentials

$$V_{m_J}(\mathbf{x}) = -\hbar\mu m_J|\mathbf{B}_0(\mathbf{x})|. \tag{6.17}$$

The Maxwell equations do not forbid a minimum of $|\mathbf{B}_0(\mathbf{x})|$ so that sublevels with $\mu m_J < 0$ are trapped around such a minimum ('weak field seekers'). After a spin flip, however, m_J has changed sign, the atom finds itself close to a potential maximum and is expelled from the trap. This picture applies when the spin flip rate is small compared to the characteristic frequencies in the magnetic trap; this has to be checked after the calculation.

The trap loss rate due to spin flips, $|m_{\rm i}\rangle \to |m_{\rm f}\rangle$, corresponds to the rate Γ_+ introduced in Eq.(6.7) (the weak field seeking state has a higher energy) and is given by

$$\Gamma_{\rm flip} = \mu^2 \sum_{k,l} \langle m_{\rm i}|J_k|m_{\rm f}\rangle\langle m_{\rm f}|J_l|m_{\rm i}\rangle \mathcal{B}_{kl}(\mathbf{r},\mathbf{r};-\omega_{\rm L}) \tag{6.18}$$

where $\mathcal{B}_{kl}$ is the magnetic noise tensor and $\omega_{\rm L}$ the Larmor frequency at the trap centre $\mathbf{r}$. Regarding the field, this rate is averaged over its initial states (with the corresponding ensemble weight) and summed over the final states, see Wylie & Sipe (1984) and Henkel & al. (2003c). If the centre-of-mass motion is quantized as well, one has to average the noise tensor over the position distribution of the trap eigenstates and has to incorporate the trap eigenenergies in the transition frequency. For spin flips induced by the non-adiabatic motion in the trapping

[3] For magnetic interactions, this approximation is usually less well justified because the transverse field detuning may easily be comparable to the Larmor frequency. The analogous situation occurs for electric dipole transitions only in very strong laser fields.

potential, this has been studied by Bergeman & al. (1989); Sukumar & Brink (1997); Gov & al. (2000b); Hinds & Eberlein (2000).

The information obtained for the magnetic noise spectrum in the near field also characterizes the loss rate for trapped spins. For example, it is clear from the matrix elements of the spin operators in Eq.(6.18) that only magnetic fields polarized perpendicular to the static trapping field can drive spin flips. The dependence on the trap geometry is discussed in detail in the papers Henkel & Wilkens (1999); Henkel & al. (1999b); Henkel & Pötting (2001); Henkel & al. (2003c); Schroll & al. (2003). The most important result is that at close distance to a metal, magnetic noise has a strength orders of magnitude above the black body level,

$$\frac{\mathcal{B}_{ij}(\mathbf{r},\mathbf{r};\omega)}{\mathcal{B}_{ij\,(\mathrm{b.b.})}(\mathbf{r},\mathbf{r};\omega)} \sim \frac{\lambda^3}{\delta^2 z} \gg 1 \tag{6.19}$$

when both the skin depth δ and the trap distance z are much smaller than the wavelength λ. Typical Larmor frequencies are in the 1–100 MHz range, corresponding to wavelengths exceeding 1 m and skin depths of order 10–100 μm. Recently, the predictions of our theory could be confirmed quantitatively by the groups of Eric A. Cornell (Harber & al., 2003), Ed A. Hinds (Jones & al., 2003), and Vladan Vuletić (Lin & al., 2004), see page 20.

6.3 Centre of mass motion

We finally discuss the coupling of the atomic position to fluctuating electromagnetic fields. For simplicity, we focus on a single 'internal' state, for example the single weak field seeker for a magnetically trapped $J = 1/2$ atom. The centre-of-mass motion is then described by the Hamiltonian

$$H_{\mathrm{S}} = \frac{\mathbf{p}^2}{2m} + V(\mathbf{x},t) \tag{6.20}$$

where the potential $V(\mathbf{x},t)$ contains both the static trapping potential and the coupling to time-dependent fields. In a static magnetic field $\mathbf{B}_0(\mathbf{x})$, including to lowest order the contribution of magnetic field fluctuations $\mathbf{B}(\mathbf{x},t)$, we have

$$V(\mathbf{x},t) = \mu_{\mathrm{eff}}|\mathbf{B}_0(\mathbf{x})| + \mu_{\mathrm{eff}}\left(\mathbf{B}(\mathbf{x},t)\cdot\hat{\mathbf{B}}_0(\mathbf{x})\right) \tag{6.21}$$

where $\mu_{\mathrm{eff}} = -\hbar\mu m_J$ is the magnetic moment in the trapped state $|m_J\rangle$ and $\hat{\mathbf{B}}_0(\mathbf{x})$ is a unit vector. We have made the adiabatic approximation (Larmor frequency much larger than the vibration frequency of the centre of mass). Another example is a static trap perturbed by a random force, for example an ion trap subject to electric field noise. In that case,

$$V(\mathbf{x},t) = V_0(\mathbf{x}) - q\mathbf{x}\cdot\mathbf{E}(\mathbf{r},t), \tag{6.22}$$

where $\mathbf{x}$ denotes the ion displacement with respect to the trap centre $\mathbf{r}$.

6.3.1 Discrete spectrum

In terms of the eigenstates $\varphi_n(\mathbf{x})$ of the trapping potential, we can expand the density matrix for the centre-of-mass motion as

$$\rho_{nn'}(t) = \int \mathrm{d}^3x \mathrm{d}^3x' \, \varphi_n(\mathbf{x}) \langle \psi^*(\mathbf{x},t)\psi(\mathbf{x}',t)\rangle \varphi^*_{n'}(\mathbf{x}') \tag{6.23}$$

where the average is with respect to the fluctuations in the potential $V(\mathbf{x},t)$. In this basis, the structure of the master equation is similar to the previous cases: transitions between the trap eigenstates happen with rates characterized by the matrix elements of the fluctuating potential. In terms of the spatial correlation spectrum, we have in a magnetic trap

$$\Gamma_{n\to n'} = \frac{\mu_{\mathrm{eff}}^2}{\hbar^2} \sum_{kl} \int \mathrm{d}^3x \mathrm{d}^3x' \, M_{nn'}(\mathbf{x}) \hat{B}_{0k}(\mathbf{x}) \mathcal{B}_{kl}(\mathbf{x},\mathbf{x}';-\omega_{nn'}) \hat{B}_{0l}(\mathbf{x}') M^*_{nn'}(\mathbf{x}'), \tag{6.24}$$

where the wave function overlap is denoted as

$$M_{nn'}(\mathbf{x}) = \varphi^*_n(\mathbf{x})\varphi_{n'}(\mathbf{x}), \tag{6.25}$$

and $\omega_{nn'}$ is the transition frequency. The scaling of these rates with the trap geometry is discussed in detail in Folman & al. (2002); Henkel & al. (2003c). In a harmonic trap subject to a random force, the transition rates get simpler and one recovers the well-known selection rule $n \to n' = n \pm 1$. Calculations pertaining to ion traps can be found in Henkel & al. (1999b).

To summarize, field fluctuations heat the vibrational motion of trapped atoms and damp coherences between different trap eigenstates, similar to Eq.(6.8) for 'optical' coherences.

6.3.2 Decoherence of quasi-free motion

We finally address the impact of field fluctuations on the motion of a free particle. This situations occurs in very anisotropic traps where the confinement along one or two directions is very weak. In the paper reproduced in Appendix B, we use the spirit of the master equation in the Markov approximation to derive a 'transport equation' that is valid on length scales larger than the correlation length ℓ_{corr} of the fluctuating field. This equation is most easily formulated in terms of the Wigner transform of the atomic coherence function, *i.e.*,

$$W(\mathbf{x},\mathbf{p};t) = \int \frac{\mathrm{d}^d s}{(2\pi\hbar)^d} \mathrm{e}^{\mathrm{i}\mathbf{p}\cdot\mathbf{s}/\hbar} \langle \psi^*(\mathbf{x}+\tfrac{1}{2}\mathbf{s},t)\psi(\mathbf{x}-\tfrac{1}{2}\mathbf{s},t)\rangle \tag{6.26}$$

The atomic motion is described in d dimensions, $d = 1, 2$ being the most relevant cases in anisotropic traps. The key idea of the transport equation is to use the momentum variable $\mathbf{p}$ to capture the behaviour of the atomic coherence function on short scales (small distance $\mathbf{s}$ between two points in the de Broglie wave field). The Wigner function thus serves as a 'local Fourier transform'. 'Short scales' are comparable to the correlation length $\ell_{\rm corr}$ and on this scale, the 'large scale' variable $\mathbf{x}$ is supposed to vary slowly. This allows to disentangle the scattering from the locally corrugated noise potential from the otherwise ballistic motion of de Broglie wave packets.

In a broad-band field, one finds the following transport equation for the Wigner function (similar results have been obtained by Jayannavar & Kumar (1982); Kuklov & al. (2002))

$$\begin{aligned} &\left(\partial_t + \frac{\mathbf{p}}{m}\cdot\boldsymbol{\nabla}_{\mathbf{x}} + \mathbf{F}_0(\mathbf{x})\cdot\boldsymbol{\nabla}_{\mathbf{p}}\right) W(\mathbf{x},\mathbf{p};t) \\ &= \int d^d p'\, \Gamma(\mathbf{p}-\mathbf{p}';\mathbf{x})\,[W(\mathbf{x},\mathbf{p}';t) - W(\mathbf{x},\mathbf{p};t)] \end{aligned} \tag{6.27}$$

where $\mathbf{F}_0(\mathbf{x})$ is a static, slowly position-dependent force, due to a weak confinement for example. The 'collision integral' on the right hand side involves a transition rate per momentum transfer

$$\Gamma(\mathbf{p};\mathbf{x}) = \frac{1}{\hbar^2}\int \frac{\mathrm{d}^d s}{(2\pi\hbar)^d} \mathrm{e}^{\mathrm{i}\mathbf{p}\cdot\mathbf{s}/\hbar} \mathcal{C}(\mathbf{x}+\tfrac{1}{2}\mathbf{s}, \mathbf{x}-\tfrac{1}{2}\mathbf{s}) \tag{6.28}$$

that may weakly depend on $\mathbf{x}$. We assume a noise potential with zero correlation time

$$\langle V(\mathbf{x},t)V(\mathbf{x}',t')\rangle = \mathcal{C}(\mathbf{x},\mathbf{x}')\,\delta(t-t'). \tag{6.29}$$

This theory applies if the noise field is essentially at infinite temperature. Otherwise, a friction force would occur in Eq.(6.27) and establish thermal equilibrium against the scattering processes that broaden the momentum distribution Haake & Reibold (1985); Zurek (1991).

In a constant force field, the transport equation (6.27) can be solved analytically (Jayannavar & Kumar, 1982; Zurek, 1991). If we spatially average the resulting atomic coherence function, we get

$$\begin{aligned} \rho(\mathbf{s};t) &\equiv \int \mathrm{d}^d x \langle \psi^*(\mathbf{x}+\tfrac{1}{2}\mathbf{s},t)\psi(\mathbf{x}-\tfrac{1}{2}\mathbf{s},t)\rangle \\ &= \rho(\mathbf{s};0)\exp\left[-\Gamma(\mathbf{s})t - \mathrm{i}\mathbf{F}_0\cdot\mathbf{s}t/\hbar\right] \end{aligned} \tag{6.30}$$

where the 'decoherence rate' depends on the separation $\mathbf{s}$ between two points of the atomic de Broglie wave:

$$\Gamma(\mathbf{s}) = \frac{\mathcal{C}(\mathbf{x},\mathbf{x}) - \mathcal{C}(\mathbf{x}+\frac{1}{2}\mathbf{s},\mathbf{x}-\frac{1}{2}\mathbf{s})}{\hbar^2}. \tag{6.31}$$

This rate does not actually depend on the position $\mathbf{x}$ in the trap for statistically homogeneous noise. Such a situation occurs, for example, in a quasi one-dimensional atom guide parallel to a planar substrate. The decoherence rate depends of course parametrically on the guide-substrate distance. Note the saturation behaviour $\Gamma(\mathbf{s}) \to \Gamma_\infty = \mathcal{C}(\mathbf{x},\mathbf{x})/\hbar^2$ for points in the atom trap separated by a distance larger than the noise correlation length: the second term in Eq.(6.31) then vanishes. In the limit $\Gamma_\infty t \gg 1$, the atomic wave function therefore has lost coherence on scales exceeding $\ell_{\rm corr}$. This entails a broader momentum distribution with width $\Delta p \sim \hbar/\ell_{\rm corr}$: the random scattering from the potential fluctuations has increased the kinetic temperature of the atom. More details are summarized on page 24.

Part III

Appendices

Appendix A

Fluctuation dissipation theorem in QED

In this Appendix, we quote two simplified proofs of the fluctuation dissipation theorem (5.42) for quantized boson fields in macroscopic electrodynamics. The original paper by Callen & Welton (1951) focusses on simpler systems, but also contains the 'fermionic' generalization to two-level media. Stefano & al. (2000) have published a proof valid under more general conditions.

A.1 Mode expansion

Let us first consider a dielectric with a real, positive and frequency-independent permittivity. In this case, as shown for example by Carnaglia & Mandel (1971) and Glauber & Lewenstein (1991), the standard canonical quantization procedure can be carried over from the vacuum case. The wave equation (5.6) contains a differential operator which is self-adjoint with respect to a scalar product with weight function $\varepsilon(\mathbf{x})$. The corresponding orthonormal eigenfunctions provide a complete set of modes $\mathbf{E}_{\mathbf{k}\mu}$. The combined label $\mathbf{k}\mu$ generalizes the wave and polarization vectors of plane waves in free space. Without loss of generality we assume real mode functions in the following.

The calculation closely parallels the one in free space, and we only quote the main steps. We first secure the familiar mode expansion for the electric field operator

$$\mathbf{E}(\mathbf{x},t) = \mathrm{i}\int \mathrm{d}k \sum_{\mu} \sqrt{\frac{\hbar\omega_{\mathbf{k}\mu}}{2\varepsilon_0}}\mathbf{E}_{\mathbf{k}\mu}(\mathbf{x})\left(a_{\mathbf{k}\mu}(t) - \text{H.C.}\right). \tag{A.1}$$

The expression under the square root is fixed by the requirement that the mode

functions diagonalize the electromagnetic field energy and reduce it to a sum of quantized harmonic oscillators. The mode functions are normalized with respect to the scalar product

$$\int \mathrm{d}^3x\, \varepsilon(\mathbf{x})\, \mathbf{E}_{\mathbf{k}\mu}(\mathbf{x}) \cdot \mathbf{E}_{\mathbf{k}'\mu'}(\mathbf{x}) = \delta_{\mu\mu'}\delta(\mathbf{k},\mathbf{k}') \tag{A.2}$$

The annihilation operators $a_{\mathbf{k}\mu}$ in Eq.(A.1) satisfy the standard commutation relations.

In thermal equilibrium, the field density operator factorizes into modes and correlations between orthogonal modes vanish. Normally ordered averages, for example, are given by

$$\left\langle a^\dagger_{\mathbf{k}\mu}(t) a_{\mathbf{k}'\mu'}(t') \right\rangle = \delta_{\mu\mu'}\delta(\mathbf{k},\mathbf{k}') \frac{\mathrm{e}^{\mathrm{i}\omega_{\mathbf{k}\mu}(t-t')}}{\mathrm{e}^{\beta\omega_{\mathbf{k}\mu}}-1}, \tag{A.3}$$

where $\beta = \hbar/k_\mathrm{B}T$ is the inverse temperature. Calculating the temporal field correlation function and taking the Fourier transform, we get the spectrum

$$\mathcal{E}_{ij}(\mathbf{x},\mathbf{x}';\omega) = \frac{2\pi\hbar}{\varepsilon_0} \frac{\omega}{\mathrm{e}^{\beta\omega}-1} \int \mathrm{d}k \sum_\mu \omega_{\mathbf{k}\mu} E_{\mathbf{k}\mu,i}(\mathbf{x}) E_{\mathbf{k}\mu,j}(\mathbf{x}') \delta(\omega^2 - \omega^2_{\mathbf{k}\mu}) \tag{A.4}$$

Note that the diagonal elements $\mathcal{E}_{ii}(\mathbf{x},\mathbf{x};\omega) \geq 0$ at both positive and negative frequencies.

The Green tensor can also be expanded in modes. It solves the inhomogeneous wave equation (5.6)

$$\left(\delta_{ij}\boldsymbol{\nabla}^2 - \frac{\partial^2}{\partial x_i \partial x_j} + \delta_{ij}\varepsilon(\mathbf{x}) \frac{(\omega+\mathrm{i}0)^2}{c^2} \right) G_{jk} = -\frac{\omega^2}{c^2\varepsilon_0}\delta_{ik}\delta(\mathbf{x}-\mathbf{x}') \tag{A.5}$$

where the positive infinitesimal part of $\omega + \mathrm{i}0$ on the left hand side selects the causal (retarded) solution. Expanding the delta function source term in modes using the completeness relation, we get the coefficients of the mode expansion of the Green tensor:

$$G_{ij}(\mathbf{x},\mathbf{x}';\omega) = \frac{\omega^2}{\varepsilon_0} \int \mathrm{d}k \sum_\mu \frac{E_{\mathbf{k}\mu,i}(\mathbf{x}) E_{\mathbf{k}\mu,j}(\mathbf{x}')}{\omega^2_{\mathbf{k}\mu} - (\omega+\mathrm{i}0)^2}. \tag{A.6}$$

Taking into account the frequency sign, the imaginary part of this denominator is

$$\mathrm{Im} \frac{1}{\omega^2_{\mathbf{k}\mu} - (\omega+\mathrm{i}0)^2} = \frac{\pi\omega_{\mathbf{k}\mu}}{\omega} \delta(\omega^2 - \omega^2_{\mathbf{k}\mu}). \tag{A.7}$$

Comparing Eqs.(A.4) and (A.6), we read off the fluctuation dissipation theorem

$$\mathcal{E}_{ij}(\mathbf{x},\mathbf{x}';\omega) = \frac{2\hbar}{\mathrm{e}^{\beta\omega}-1} \mathrm{Im}\, G_{ij}(\mathbf{x},\mathbf{x}';\omega) \tag{A.8}$$

which has been stated in Eq.(5.42).

A.2 Noise source representation

The second proof we quote allows for a complex, frequency-dependent medium permittivity where the wave operator is no longer self-adjoint. For simplicity, we follow Knöll & al. (2001) and assume that $\mathrm{Im}\,\varepsilon > 0$ in the entire space. This damps any plane wave incident from infinity and suppresses the scattering solutions to the homogeneous wave equation. The field is generated by the noise polarization $\mathbf{P}_\mathrm{n}$ only, and using the Green tensor we have

$$E_i(\mathbf{x};\omega) = \int \mathrm{d}^3x' G_{ik}(\mathbf{x},\mathbf{x}';\omega) P_{\mathrm{n}k}(\mathbf{x}';\omega). \tag{A.9}$$

The noise correlations given by Eq. (5.46) are δ-correlated in position with a spectral density proportional to the medium absorption $\mathrm{Im}[\varepsilon_0\varepsilon(\mathbf{x};\omega)]$. For a homogeneous medium temperature, the field spectrum (5.47) thus becomes

$$\mathcal{E}_{ij}(\mathbf{x},\mathbf{x}';\omega) = \frac{2\hbar}{\mathrm{e}^{\hbar\omega/k_\mathrm{B}T}-1} \int \mathrm{d}^3x_1\, \mathrm{Im}[\varepsilon_0\varepsilon(\mathbf{x}_1;\omega)] G^*_{ik}(\mathbf{x},\mathbf{x}_1;\omega) G_{jk}(\mathbf{x}',\mathbf{x}_1;\omega) \tag{A.10}$$

Hence, the fluctuation dissipation theorem follows provided the following identity holds (Henry & Kazarinov, 1996; Knöll & al., 2001)

$$\int \mathrm{d}^3x_1\, \mathrm{Im}[\varepsilon_0\varepsilon(\mathbf{x}_1;\omega)] G^*_{ik}(\mathbf{x},\mathbf{x}_1;\omega) G_{jk}(\mathbf{x}',\mathbf{x}_1;\omega) = \mathrm{Im}\, G_{ij}(\mathbf{x},\mathbf{x}';\omega). \tag{A.11}$$

Via this identity, the fluctuation dissipation theorem is already contained in macroscopic electrodynamics. We note that Eq.(A.11) provides a nontrivial connection between expressions quadratic and linear in the Green tensor. (Another connections of this kind are the optical theorem and the Ward identities.)

We make again use of the reciprocity of the Green tensor, for example, $G_{jk}(\mathbf{x}',\mathbf{x}_1;\omega) = G_{kj}(\mathbf{x}_1,\mathbf{x}';\omega)$. Recall that reciprocity holds trivially for the scalar permittivity we focus on here, even if it is complex. As a first step in the proof of Theorem (A.11), we write down the wave equation (A.5) for $G_{kj}(\mathbf{x}_1,\mathbf{x}';\omega)$, multiply with the conjugate tensor $G^*_{ki}(\mathbf{x}_1,\mathbf{x};\omega)$ and integrate over $\mathbf{x}_1$. With partial integration, the terms involving the differential operators can be 'symmetrized'. The surface integrals over the sphere at infinity do not contribute because the Green tensor vanishes there.[1] We thus get the intermediate result

$$\begin{aligned} -\frac{\omega^2}{c^2} G^*_{ij}(\mathbf{x},\mathbf{x}') \;=\; & \int \mathrm{d}^3x_1 \Big[-\nabla_1 G^*_{ki}(\mathbf{x}_1,\mathbf{x}) \cdot \nabla_1 G_{kj}(\mathbf{x}_1,\mathbf{x}') \\ & + \frac{\partial}{\partial x_{1k}} G^*_{ki}(\mathbf{x}_1,\mathbf{x}) \frac{\partial}{\partial x_{1l}} G_{lj}(\mathbf{x}_1,\mathbf{x}') \end{aligned} \tag{A.12}$$

[1] This follows from the assumption that $\mathrm{Im}\,\varepsilon > 0$ everywhere. Otherwise, additional terms appear in the identity (A.11); they combine with the scattered field contribution to give the fluctuation dissipation theorem, see Stefano & al. (2000).

$$+ G^*_{ki}(\mathbf{x}_1,\mathbf{x})\varepsilon_0\varepsilon(\mathbf{x}_1)]\frac{(\omega+\mathrm{i}0)^2}{c^2}G_{kj}(\mathbf{x}_1,\mathbf{x}')\Big],$$

where repeated indices are summed over and frequency arguments have been suppressed.

In the second step of the proof, the complex conjugate of (A.5) is multiplied by the Green tensor and integrated over $\mathbf{x}_1$. Then both results are subtracted. On the left hand side of Eq.(A.12), the imaginary part of $G_{ij}(\mathbf{x},\mathbf{x}')$ appears. On the right hand side, only the term involving the complex permittivity survives and gives $\mathrm{Im}\,[\varepsilon(\mathbf{x}_1)(\omega+\mathrm{i}0)^2]$. The limit of real ω does not pose problems, and one arrives at (A.11).

Appendix B

Derivation of the transport equation

The paper that we reprint here has been published as

Carsten Henkel (2001), 'Coherent transport', *Comptes Rendus de l'Académie des Sciences (Paris)*, Série IV **2**(4), 573–80, special issue with the proceedings of the Euroconference 'Atom Optics and Interferometry' (Cargèse, France, 26–29 July 2000).

Abstract. We discuss the transport of matter waves in low-dimensional waveguides. Due to scattering from uncontrollable noise fields, the spatial coherence gets reduced and eventually lost. We develop a description of this decoherence process in terms of transport equations for the atomic Wigner function. We outline its derivation and discuss the special case of white noise where an analytical solution can be found.

Résumé. *Nous discutons ici du transport d'ondes de matière dans des guides de basse dimensionnalité. En raison de la diffusion par des champs aléatoires incontrôlables, la cohérence spatiale de l'onde décroît, pour être finalement complètement perdue. Nous développons une description de ce processus de décohérence en terme d'équations de transport pour la fonction de Wigner atomique. Nous donnons le principe de la dérivation de cette description et nous discutons le cas particulier du bruit blanc pour lequel nous donnons une solution analytique.*

1. Introduction

We discuss in this contribution the transport of atomic matter waves in a low-dimensional waveguide. Such structures may be created close to solid sub-

strates using electro-magnetic fields: the magnetic field of a current-carrying wire combined with a homogeneous bias field, e.g., gives rise to a linear waveguide [1–3]. Planar waveguides may be constructed with repulsive magnetic [4] or optical [5] fields that 'coat' the substrate surface. The atomic motion is characterised by bound vibrations in the 'transverse' direction(s) and an essentially free motion in the 'longitudinal' direction(s) along the waveguide axis (plane), respectively. Although direct contact with the substrate is avoided by the shielding potential, the atoms feel its presence through enhanced electromagnetic field fluctuations that 'leak' out of the thermal solid, typically held at room temperature. We have shown elsewhere that these thermal near fields are characterised by a fluctuation spectrum exceeding by orders of magnitude the usual blackbody radiation [6–9]. The scattering of the atoms off the near field fluctuations occurs at a rate that may be calculated using Fermi's Golden Rule. The consequences of multiple scattering is conveniently described by a transport equation that combines in a self-consistent way both ballistic motion and scattering.

The purpose of this contribution is to outline a derivation of this transport equation. The status of this equation is similar to that of the quantum-optical master equations allowing to describe the evolution of the reduced density matrix of an atomic system, on a time scale large compared to the correlation time of the reservoir the system is coupled to, typically the vacuum radiation field. In the case of transport in waveguides, we face both temporal and spatial dynamics and therefore restrict our attention to scales large compared to the correlation time and length of a fluctuating noise potential. Our analysis uses a multiple scale expansion adapted from [10]. Similar to the quantum-optical case, we make an expansion in the perturbing potential to second order. In the resulting transport equation, the noise is thus characterised by its second-order correlation functions or, equivalently, its spectral density. In the case of white noise, the transport equation can be explicitly solved. We have shown elsewhere [8] that this approximation holds quite well for thermal near field fluctuations. For technical noise, it also holds when the noise spectrum is flat on a frequency scale roughly set by the 'longitudinal' temperature of the atoms in the waveguide. The explicit solution yields an estimate for the spatial coherence of the guided matter waves as a function of time. The paper concludes with some remarks on the limits of validity of the present transport theory. It cannot describe, e.g., Anderson localisation in one dimension [11] because on the coarser spatial scale of the transport equation, the scattering from the noise field is assumed to take place locally; interferences between different scattering sequences are not taken into account. Decoherence in 'curved' or 'split' waveguides also needs a refined theory because of the cross-coupling between the transverse and longitudinal degrees of freedom, the former being 'frozen

out' in our framework.

2. Statistical matter wave optics

The simplest model for atom transport in a low-dimensional waveguide is based on the Schrödinger equation

$$\mathrm{i}\hbar\partial_t\psi(\mathbf{x},t) = -\frac{\hbar^2}{2m}\nabla^2\psi + V(\mathbf{x},t)\psi \tag{B.1}$$

The coordinate $\mathbf{x}$ describes the motion in the free waveguide directions. The transverse motion is 'frozen out' by assuming that the atom is cooled to the transverse ground state. Atom-atom interactions are neglected, too. $V(\mathbf{x},t)$ is the noise potential: for a magnetic waveguide, e.g., it is given by

$$V(\mathbf{x},t) = \langle s|\boldsymbol{\mu}\cdot\mathbf{B}(\mathbf{x},t)|s\rangle, \tag{B.2}$$

where $|s\rangle$ is the trapped internal state of the atom (we neglect spin-changing processes), and $\mathbf{B}(\mathbf{x},t)$ is the thermal magnetic field. The noise potential is a statistical quantity with zero mean and second-order correlation function

$$C_V(\mathbf{s},\tau) = \langle V(\mathbf{x}+\mathbf{s},t+\tau)\,V(\mathbf{x},t)\rangle, \tag{B.3}$$

where the average is taken over the realisations of the noise potential. We assume a statistically homogeneous noise, the correlation function being independent of $\mathbf{x}$ and t. As a function of the separation $\mathbf{s}$, thermal magnetic fields are correlated on a length scale l_c given approximately by the distance d between the waveguide axis and the solid substrate [8]. This estimate is valid as long as the wavelength $2\pi c/\omega$ corresponding to the noise frequency ω is large compared to d: for micrometre-sized waveguide structures, this means frequencies below the optical range. The relevant frequencies of the noise will be identified below and turn out to be much smaller than this.

The coherence properties of the guided matter waves are characterised by the noise-averaged coherence function (the time dependence is suppressed for clarity)

$$\rho(\mathbf{x};\mathbf{s}) = \langle\psi^*(\mathbf{x}-\tfrac{1}{2}\mathbf{s})\,\psi(\mathbf{x}+\tfrac{1}{2}\mathbf{s})\rangle. \tag{B.4}$$

In complete analogy to quantum-optical master equations, this coherence function may be regarded as the reduced density matrix of the atomic ensemble, when the degrees of freedom of the noise are traced over. The Wigner function gives a convenient representation of the coherence function:

$$W(\mathbf{x},\mathbf{p}) = \int\frac{d^D s}{(2\pi\hbar)^D}\mathrm{e}^{-\mathrm{i}\mathbf{p}\cdot\mathbf{s}/\hbar}\rho(\mathbf{x};\mathbf{s}), \tag{B.5}$$

where D is the waveguide dimension. This representation allows to make a link to classical kinetic theory: $W(\mathbf{x}, \mathbf{p})$ may be viewed as a quasi-probability in phase space. For example, the spatial density $n(\mathbf{x})$ and the current density $\mathbf{j}(\mathbf{x})$ of the atoms are given by

$$n(\mathbf{x}) = \int \mathrm{d}^D p \, W(\mathbf{x}, \mathbf{p}) \tag{B.6}$$

$$\mathbf{j}(\mathbf{x}) = \int \mathrm{d}^D p \, \frac{\mathbf{p}}{m} W(\mathbf{x}, \mathbf{p}) \tag{B.7}$$

We also obtain information about the spatial coherence: the spatially averaged coherence function $\Gamma(\mathbf{s}, t)$, for example, is related to the Wigner function by

$$\Gamma(\mathbf{s}, t) \equiv \int \mathrm{d}^D x \, \rho(\mathbf{x}; \mathbf{s}, t) \tag{B.8}$$

$$= \int \mathrm{d}^D x \, \mathrm{d}^D p \, \mathrm{e}^{\mathrm{i}\mathbf{p}\cdot\mathbf{s}/\hbar} \, W(\mathbf{x}, \mathbf{p}, t) \tag{B.9}$$

In the next section, we outline a derivation of a closed equation for the Wigner function in terms of the noise correlation function.

3. Transport equation

Details of the derivation of the transport equation may be found in the appendix.We quote here only the main assumptions underlying the theory.

(i) The noise potential is supposed to be *weak* so that a perturbative analysis is possible. As in quantum-optical master equations, a closed equation is found when the expansion is pushed to second order in the perturbation.

(ii) The scale l_c over which the noise is spatially correlated is assumed to be small compared to the characteristic scale of variation of the Wigner function. This implies a separation of the dynamics on short and large spatial scales, the dynamics on the large scale being 'enslaved' by certain averages over the short scale. Similarly, we assume that the potential fluctuates rapidly on the time scale for the evolution of the Wigner function. These assumptions correspond to the Markov approximation of quantum optics, where the master equation is valid on a coarse-grained time scale.

The derivation of the master equation is based on a multiple scale expansion. Functions $f(\mathbf{x})$ of the spatial coordinate are thus written in the form

$$f(\mathbf{x}) = f(\mathbf{X}, \boldsymbol{\xi}) \tag{B.10}$$

where $\mathbf{X}$ gives the 'slow' variation and the dimensionless variable $\boldsymbol{\xi} = \mathbf{x}/l_c$ gives the 'rapid' variation on the scale of the noise correlation length l_c. Spatial gradients are thus expanded using

$$\nabla_{\mathbf{x}} = \nabla_{\mathbf{X}} + \frac{1}{l_c}\nabla_{\boldsymbol{\xi}} \tag{B.11}$$

By construction, the first term is much smaller than the second one. Finally, the Wigner function is expanded as

$$W(\mathbf{x}, \mathbf{p}, t) = W_0(\mathbf{X}, \mathbf{p}, t) + \eta^{1/2} W_1(\mathbf{X}, \boldsymbol{\xi}, \mathbf{p}, t) + \mathcal{O}(\eta) \tag{B.12}$$

where $\eta \ll 1$ is the ratio between the correlation length l_c and a 'macroscopic' scale on which the coordinate $\mathbf{X}$ varies. The expansion allows to prove self-consistently that the zeroth order approximation W_0 does not depend on the short scale $\boldsymbol{\xi}$, and to fix the exponent $1/2$ for the first order correction.

The resulting transport equation specifies the evolution of the Wigner function W_0. Dropping the subscript 0, it reads

$$\begin{aligned} &\Big(\partial_t + \frac{\mathbf{p}}{m} \cdot \nabla_{\mathbf{x}}\Big) W(\mathbf{x}, \mathbf{p}) = \\ &\int \mathrm{d}^D p' \, S_V(\mathbf{p}' - \mathbf{p}, E_{\mathbf{p}'} - E_{\mathbf{p}}) \left[W(\mathbf{x}, \mathbf{p}') - W(\mathbf{x}, \mathbf{p}) \right], \end{aligned} \tag{B.13}$$

where S_V, the *spectral density* of the noise, is essentially the spatial and time Fourier transform of the noise correlation function

$$S_V(\mathbf{q}, \Delta E) = \frac{1}{\hbar^2} \int \frac{\mathrm{d}^D s \, \mathrm{d}\tau}{(2\pi\hbar)^D} C_V(\mathbf{s}, \tau) \, \mathrm{e}^{-i(\mathbf{q}\cdot\mathbf{s} - \Delta E \tau)/\hbar}. \tag{B.14}$$

The left hand side of the transport equation gives the free ballistic motion of the atoms in the waveguide. If an external force were applied, an additional term $\mathbf{F} \cdot \nabla_{\mathbf{p}}$ would appear. The right hand side describes the scattering from the noise potential. $E_{\mathbf{p}} = p^2/2m$ is the de Broglie dispersion relation for matter waves. We observe that scattering processes $\mathbf{p} \to \mathbf{p}'$ occur at a rate given by the noise spectrum at the Bohr frequency $(E_{\mathbf{p}} - E_{\mathbf{p}'})/\hbar$. If the potential noise is static (as would be the case for a 'rough potential'), then its spectral density is proportional to $\delta(\Delta E)$, and energy is conserved. If we are interested in the scattering between guided momentum states, then the initial and final energies $E_{\mathbf{p}}$, $E_{\mathbf{p}'}$ are typically of the order of the (longitudinal) temperature kT of the ensemble. The relevant frequencies in the noise spectral density are thus comparable to $kT/\hbar$.

4. Results

4.1. White noise

White noise is characterised by a constant spectral density, i.e., the noise spectrum $S_V(\mathbf{q}, \Delta E)$ is independent of ΔE. Equivalently, the noise correlation is δ-correlated in time:

$$C_V(\mathbf{s}, \tau) = B_V(\mathbf{s})\, \delta(\tau). \tag{B.15}$$

The integration over the momentum $\mathbf{p}'$ in (B.13) is now not restricted by energy conservation, and the right hand side of the transport equation becomes a convolution. One therefore obtains a simple solution using Fourier transforms. Denoting $\mathbf{k}$ (dimension: wavevector) and $\mathbf{s}$ (dim.: length) the Fourier variables conjugate to $\mathbf{x}$ and $\mathbf{p}$, we find the equation

$$\Big(\partial_t + \frac{\hbar\mathbf{k}}{m} \cdot \nabla_{\mathbf{s}}\Big)\tilde{W}(\mathbf{k}, \mathbf{s}) = -\gamma(\mathbf{s})\tilde{W}(\mathbf{k}, \mathbf{s}). \tag{B.16}$$

where we have introduced the rate

$$\gamma(\mathbf{s}) = \frac{1}{\hbar^2}\left(B_V(\mathbf{0}) - B_V(\mathbf{s})\right). \tag{B.17}$$

Eq.(B.16) is easily solved using the method of characteristics, using $\mathbf{s} - \hbar\mathbf{k}t/m$ as a new variable. One finds

$$\begin{aligned} \tilde{W}(\mathbf{k}, \mathbf{s}; t) \;&=\; \tilde{W}_i(\mathbf{k}, \mathbf{s} - \hbar\mathbf{k}t/m) \times \\ &\quad \times \exp\left[-\int_0^t \mathrm{d}t' \gamma(\mathbf{s} - \hbar\mathbf{k}t'/m)\right], \end{aligned} \tag{B.18}$$

where $\tilde{W}_i(\mathbf{k}, \mathbf{s})$ is the Wigner function at $t = 0$.

We observe in particular that the spatially averaged coherence function (B.8) shows an exponential decay as time increases:

$$\Gamma(\mathbf{s}; t) = \Gamma_i(\mathbf{s}) \exp\Big[-\gamma(\mathbf{s})t\Big]. \tag{B.19}$$

We can thus give a physical meaning to the quantity $\gamma(\mathbf{s})$: it is the rate at which two points in the matter wave field, that are separated by a distance $\mathbf{s}$, lose their mutual coherence. This rate saturates to $\gamma = \gamma(\infty) = B_V(\mathbf{0})/\hbar^2$ for distances $s \gg l_c$ large compared to the correlation length of the noise field (the correlation $B_V(\mathbf{s})$ then vanishes). This saturation has been discussed, e.g., in [12]. As shown in [9], the rate γ is equal to the total scattering rate from the noise potential, as obtained from Fermi's Golden Rule. For distances smaller than l_c, the decoherence rate $\gamma(\mathbf{s})$ decreases since the two points of the matter wave field 'see' essentially the same noise potential. The exact solution (B.19) thus

implies that after a time of the order of the scattering time $1/\gamma$, the spatial coherence of the atomic ensemble has been reduced to the correlation length l_c. The estimates given in [9] imply a time scale of the order of a fraction of a second for waveguides at a micrometre distance from a (bulk) metallic substrate. Significant improvements can be made using thin metallic layers or wires, non-conducting materials or by mounting the waveguide at a larger distance from the substrate [9].

At timescales longer than the scattering time $1/\gamma$, the spatial coherence length of the atoms decreases more slowly, approximately as $l_c/\sqrt{\gamma t}$ [9]. This is due to a diffusive increase of the width of the atomic momentum distribution, with a diffusion constant of the order of $D = \hbar^2\gamma/l_c^2$. This constant is in agreement with a random walk in momentum space: for each scattering time $1/\gamma$, the atoms absorb a momentum $q_c = \hbar/l_c$ from the noise potential. The momentum step q_c follows from the fact that the noise potential is smooth on scales smaller than l_c, its Fourier transform therefore contains momenta up to $\hbar/l_c$.

4.2. Fokker-Planck equation

The momentum diffusion estimate given above can also be retrieved from the transport equation, making an expansion of the Wigner distribution as a function of momentum. We assume that the typical momentum transfer q_c absorbed from the noise is small compared to the scale of variation of the Wigner distribution, and expand the latter to second order. This manipulation casts the transport equation into a Fokker-Planck form

$$\Big(\partial_t + \frac{\mathbf{p}}{m}\cdot\nabla_{\mathbf{x}} + \mathbf{F}_{\rm dr}(\mathbf{p})\cdot\nabla_{\mathbf{p}}\Big)W(\mathbf{x},\mathbf{p}) = \sum_{ij} D_{ij}(\mathbf{p})\frac{\partial^2}{\partial p_i \partial p_j}W(\mathbf{x},\mathbf{p}), \tag{B.20}$$

where the drift force and the diffusion coefficient are given by

$$\mathbf{F}_{\rm dr}(\mathbf{p}) = -\int \mathrm{d}^D q\, \mathbf{q}\, S_V(\mathbf{q}, E_{\mathbf{p}+\mathbf{q}} - E_{\mathbf{p}}) \tag{B.21}$$

$$D_{ij}(\mathbf{p}) = \int \mathrm{d}^D q\, q_i q_j\, S_V(\mathbf{q}, E_{\mathbf{p}+\mathbf{q}} - E_{\mathbf{p}}). \tag{B.22}$$

In the special case of white noise, the $\mathbf{p}$-dependence of these quantities drops out. Also the drift force is then zero because the noise correlation function is real and the spectrum $S_V(\mathbf{q})$ even in $\mathbf{q}$. Since q_c gives the width of the spectrum, the diffusion coefficient turns out to be of order $q_c^2\gamma$, as estimated before.

Casting the transport equation into Fokker-Planck form, one can easily take into account the scattering from the noise field in (classical) Monte Carlo sim-

ulations of the atomic motion: one simply has to add a random force whose correlation is given by the diffusion coefficient.

We note, however, that the Fokker-Planck equation cannot capture the initial stage of the decoherence process, starting from a wave field that is coherent over distances larger than the correlation length l_c. Indeed, it may be shown (neglecting the $\mathbf{p} \cdot \nabla_{\mathbf{x}}$ term and the drift force, assuming an isotropic diffusion tensor for simplicity) that (B.20) yields a spatially averaged coherence function

$$\Gamma_{FP}(\mathbf{s}, t) = \Gamma_i(\mathbf{s}) \, \exp\left[-Ds^2 t/\hbar^2\right] \tag{B.23}$$

This result implies a decoherence rate proportional to s^2 without saturation. It is hence valid only at large times (compared to the scattering time $1/\gamma$) where the exponentials in both solutions (B.19, B.23) are essentially zero for $s \geq l_c$.

5. Concluding remarks

We have given an outline of a transport theory for dilute atomic gases trapped in low-dimensional waveguides. This theory allows to follow the evolution of the atomic phase-space distribution (more precisely, the atomic, noise-averaged Wigner function) when the atoms are subject to a noise potential with fluctuations in space and time. The spatial coherence of the gas can be tracked over temporal and spatial scales larger than the correlation scale of the noise, in a manner similar to the master equations of quantum optics. We have given explicit results in the case of white noise, highlighting spatial decoherence and momentum diffusion.

The transport equation has to be taken with care for strong noise potentials because its derivation is based on second-order perturbation theory. It is certainly not valid when the 'mean free path' $\sim \bar{v}/\gamma$ ($\bar{v}$ is a typical velocity of the gas) is smaller than the noise correlation length l_c because then the Wigner distribution changes significantly over a small spatial scale. (In technical terms, the approximation of a local scattering kernel in (B.13) is no longer appropriate.) Also, the theory cannot describe Anderson localisation in 1D waveguides with static noise [11]. This can be seen by working out the scattering kernel with $S_V(q, \Delta E) = S_V(q)\, \delta(\Delta E)$:

$$\begin{aligned} &2m \int \mathrm{d}p' \, S_V(p' - p) \, \delta(p'^2 - p^2) \, [W(x, p') - W(x, p)] \\ &= \frac{m S_V(2p)}{p} \, [W(x, -p) - W(x, p)] \, . \end{aligned} \tag{B.24}$$

We find a divergence of the scattering rate at $p \to 0$ since the spectrum $S_V(2p)$ is finite in this limit. The one-dimensional, static case therefore merits further

investigation. We also mention that is has been found recently that Anderson localisation is destroyed when time-dependent fluctuations are superimposed on the static disorder [13, 14]. In this context, transport (or master) equations similar to our approach have been used.

Acknowledgements. We thank S. A. Gardiner, S. Pötting, M. Wilkens, and P. Zoller for constructive discussions. Continuous support from M. Wilkens is gratefully acknowledged.

Appendix
Multiple scale derivation of the transport equation

The Schrödinger equation (B.1) gives the following equation for the Wigner function

$$\begin{aligned}&(\partial_t + \mathbf{p}\cdot\nabla_{\mathbf{x}})\, W(\mathbf{x},\mathbf{p}) = \\ &-\frac{\mathrm{i}}{\hbar}\int \frac{\mathrm{d}^D q}{(2\pi\hbar)^D}\tilde{V}(\mathbf{q},t)\,\mathrm{e}^{\mathrm{i}\mathbf{q}\cdot\mathbf{x}}\left[W(\mathbf{x},\mathbf{p}+\tfrac{1}{2}\mathbf{q}) - W(\mathbf{x},\mathbf{p}-\tfrac{1}{2}\mathbf{q})\right]\end{aligned} \tag{B.25}$$

where $\tilde{V}(\mathbf{q},t)$ is the spatial Fourier transform of the noise potential. Since this potential is assumed weak and varies on a scale given by the correlation length l_c, we introduce the following scaling

$$\tilde{V}(q_c\mathbf{u},t) = \int \mathrm{d}^D x\,\mathrm{e}^{-\mathrm{i}q_c\mathbf{u}\cdot\mathbf{x}/\hbar}V(\mathbf{x},t) = l_c^D\eta^\beta\hat{V}(\mathbf{u},t) \tag{B.26}$$

where $q_c \equiv \hbar/l_c$ is the typical momentum width of $\tilde{V}(\mathbf{q},t)$ and $\mathbf{u}$ is a dimensionless vector. The parameter η is given by the ratio between the small scale l_c and the 'macroscopic' scale of the position distribution, the (positive) exponent β remains to be determined. We assume $\eta \ll 1$ and make the multiple scale expansion (B.12) for the Wigner function. Using the expansion (B.11) for the spatial gradient, we get

$$\begin{aligned}&\left[\partial_t + \frac{\mathbf{p}}{m}\cdot\left(\nabla_{\mathbf{X}} + \frac{1}{l_c}\nabla_{\boldsymbol{\xi}}\right)\right](W_0 + \eta^\alpha W_1) = \\ &-\frac{\mathrm{i}\eta^\beta}{q l_c}\int\frac{\mathrm{d}^D u}{(2\pi)^D}\hat{V}(\mathbf{u},t)\,\mathrm{e}^{\mathrm{i}\mathbf{u}\cdot\mathbf{x}/l_c}\left[W(\mathbf{x},\mathbf{p}+q_c\mathbf{u}/2) - W(\mathbf{x},\mathbf{p}-q_c\mathbf{u}/2)\right]\end{aligned} \tag{B.27}$$

We now take the limit $\eta \to 0$, $l_c \to 0$ at fixed q_c. The most divergent term on the left hand side is the one with $(1/l_c)\nabla_{\boldsymbol{\xi}}W_0$. It could only be balanced with a term on the right hand side involving W_0, but due to the small factor η^β, this term cannot have the same order of magnitude. We must therefore require

that $(1/l_c)\nabla_{\boldsymbol{\xi}} W_0$ vanishes individually: the zeroth order Wigner function is independent of the short scale variable $\boldsymbol{\xi}$.

The next terms on the left hand side contain $(\eta^\alpha/l_c)\nabla_{\boldsymbol{\xi}} W_1$ and $\nabla_{\mathbf{X}} W_0$, while on the right hand side the leading order is $(\eta^\beta/l_c)W_0$. We look for a connection between W_0 and W_1, and therefore, the left hand W_1 term must be more divergent than the W_0 term. This is the case if $\eta^\alpha \mathcal{O}(1/l_c) \gg \mathcal{O}(1/X) \sim \eta\mathcal{O}(1/l_c)$. We thus conclude that $\alpha < 1$. Comparing powers of η on the left and right hand side, we find $\alpha = \beta$, since the vector $\mathbf{u}$ and the scaled distance $\boldsymbol{\xi}$ are of order unity. Therefore we get the equation

$$\left(l_c\partial_t + \frac{\mathbf{p}}{m}\cdot\nabla_{\boldsymbol{\xi}}\right) W_1(\mathbf{X},\boldsymbol{\xi},\mathbf{p}) = \tag{B.28}$$
$$-\frac{\mathrm{i}}{q_c}\int\frac{\mathrm{d}^D u}{(2\pi)^D}\hat{V}(\mathbf{u},t)\,\mathrm{e}^{\mathrm{i}\mathbf{u}\cdot\boldsymbol{\xi}}\left[W_0(\mathbf{X},\mathbf{p}+q_c\mathbf{u}/2) - W_0(\mathbf{X},\mathbf{p}-q_c\mathbf{u}/2)\right]$$

In the exponential, only the short length scale $\boldsymbol{\xi} = \mathbf{x}/l_c$ occurs. We thus find that the large scale variable $\mathbf{X}$ is a parameter in this equation, and get a solution via Fourier transforms with respect to $\boldsymbol{\xi}$ and t. In the spirit of the Markov approximation, we take the slowly varying W_0 (as a function of time) out of the time integral

$$\int_{-\infty}^{\infty}\mathrm{d}t\,\mathrm{e}^{\mathrm{i}\omega t}\hat{V}(\mathbf{u},t)\,W_0(\ldots,t) \approx W_0(\ldots,t)\hat{V}[\mathbf{u},\omega] \tag{B.29}$$

where $\hat{V}[\mathbf{u},\omega]$ denotes the double space and time Fourier transform of the potential. We note $\boldsymbol{\kappa}$, ω the conjugate variables for the spatial Fourier transform and find the following solution for the first order Wigner function

$$W_1(\mathbf{X},\boldsymbol{\xi},\mathbf{p}) = -\frac{\mathrm{i}}{q_c}\int\frac{\mathrm{d}\omega}{2\pi}\int\frac{\mathrm{d}^D\kappa}{(2\pi)^D}\frac{\mathrm{e}^{\mathrm{i}\boldsymbol{\kappa}\cdot\boldsymbol{\xi}-\mathrm{i}\omega t}\hat{V}[\boldsymbol{\kappa},\omega]}{\mathrm{i}\boldsymbol{\kappa}\cdot\mathbf{p}/m - \mathrm{i}l_c\omega + 0}\times \tag{B.30}$$
$$(W_0(\mathbf{X},\mathbf{p}+q_c\boldsymbol{\kappa}/2) - W_0(\mathbf{X},\mathbf{p}-q_c\boldsymbol{\kappa}/2))$$

The $+0$ prescription in the denominator is related to causality: it ensures that the poles in the complex ω-plane are moved into the lower half plane, avoiding a blow-up of W_1.

This result will be inserted into the next order equation that also links W_0 to W_1:

$$\left(\partial_t + \frac{\mathbf{p}}{m}\cdot\nabla_{\mathbf{X}}\right) W_0 =$$
$$-\frac{\mathrm{i}\eta^{2\alpha}}{q_c l_c}\int\frac{\mathrm{d}^D u}{(2\pi)^D}\hat{V}(\mathbf{u},t)\,\mathrm{e}^{\mathrm{i}\mathbf{u}\cdot\boldsymbol{\xi}}\left[W_1(\mathbf{X},\boldsymbol{\xi},\mathbf{p}+q_c\mathbf{u}/2) - W_1(\mathbf{X},\boldsymbol{\xi},\mathbf{u}-q_c\mathbf{u}/2)\right]$$

Note that this equation is scaled consistently if $\mathcal{O}(1/X) \sim \eta^{2\alpha}\mathcal{O}(1/l_c) =$

$\eta^{2\alpha-1}\mathcal{O}(1/X)$. This determines the exponent $\alpha = \frac{1}{2}$. The result is an equation for W_0 only. We take the statistical average and make the factorisation

$$\langle \hat{V}(\mathbf{u},t)\,\hat{V}[\boldsymbol{\kappa},\omega]\,W_0(\mathbf{X},\mathbf{p})\rangle = \langle \hat{V}(\mathbf{u},t)\,\hat{V}[\boldsymbol{\kappa},\omega]\rangle\,W_0(\mathbf{X},\mathbf{p}). \tag{B.31}$$

This may be justified heuristically as follows: it seems reasonable that the statistical average can also be performed via 'spatial coarse graining', *i.e.,* taking an average over the small-scale fluctuations of the medium. This is precisely the picture behind transport theory: the individual scattering events are not resolved but only the behaviour of the matter wave on larger scales. The lowest order Wigner function W_0 may be taken out of the coarse grain average because it does not depend on the short scale $\boldsymbol{\xi}$ by construction.

Finally, we introduce the spectral density $\hat{S}(\mathbf{u},\omega)$ of the (scaled) noise potential

$$\langle \hat{V}(\mathbf{u},t)\,\hat{V}[\boldsymbol{\kappa},\omega]\rangle = (2\pi)^D \hat{S}(\mathbf{u},\omega)\,\mathrm{e}^{\mathrm{i}\omega t}\,\delta(\mathbf{u}+\boldsymbol{\kappa}) \tag{B.32}$$

This allows to perform the integration over $\boldsymbol{\kappa}$ when (B.30) is inserted into (B.31). The result still contains a frequency integral where denominators of the following form appear

$$\frac{1}{\mathrm{i}(\mathbf{u}/m)\cdot(\mathbf{p}+q_c\mathbf{u}/2) - \mathrm{i}l_c\omega + 0} = \frac{-\mathrm{i}q_c}{E_{\mathbf{p}+q_c\mathbf{u}} - E_{\mathbf{p}} - \hbar\omega - \mathrm{i}0} \tag{B.33}$$

A second term contains the sign-reversed energy difference. These denominators ensure that the kinetic energy change occurring in the scattering is compensated by a 'quantum' $\hbar\omega$ from the noise potential.

We write the denominators (B.33) as a δ-function plus a principal part. For the classical noise potential considered here, the power spectrum $\hat{S}(\mathbf{u},\omega)$ is even in ω, so that the δ-functions combine and the principal parts drop out. We finally get

$$\begin{aligned}&\left(\partial_t + \frac{\mathbf{p}}{m}\cdot\nabla_{\mathbf{X}}\right) W_0 = \\ &\frac{\eta}{\hbar^2}\int \frac{\mathrm{d}^D u}{(2\pi)^D}\hat{S}(\mathbf{u},\Delta E/\hbar)\,[W_0(\mathbf{X},\mathbf{p}+q_c\mathbf{u}) - W_0(\mathbf{X},\mathbf{p})]\end{aligned} \tag{B.34}$$

where $\Delta E = E_{\mathbf{p}+q_c\mathbf{u}} - E_{\mathbf{p}}$. It is easily checked that this is the transport equation (B.13), taking into account the relation between the scaled and non-scaled noise spectra

$$\frac{\eta l_c^3}{\hbar^2}\hat{S}_V(\mathbf{u},\Delta E/\hbar) = S_V(q_c\mathbf{u},\Delta E) \tag{B.35}$$

that follows from (B.14) and (B.26).

References

[1] J. Schmiedmayer, Eur. Phys. J. D **4**, 57 (1998).
[2] D. Müller, D. Z. Anderson, R. J. Grow, P. D. D. Schwindt, and E. A. Cornell, Phys. Rev. Lett. **83**, 5194 (1999).
[3] N. H. Dekker *et al.*, Phys. Rev. Lett. **84**, 1124 (2000).
[4] E. A. Hinds, M. G. Boshier, and I. G. Hughes, Phys. Rev. Lett. **80**, 645 (1998).
[5] H. Gauck, M. Hartl, D. Schneble, H. Schnitzler, T. Pfau, and J. Mlynek, Phys. Rev. Lett. **81**, 5298 (1998).
[6] C. Henkel and M. Wilkens, Europhys. Lett. **47**, 414 (1999).
[7] C. Henkel, S. Pötting, and M. Wilkens, Appl. Phys. B **69**, 379 (1999).
[8] C. Henkel, K. Joulain, R. Carminati, and J.-J. Greffet, Opt. Commun. **186** (2000) 57.
[9] C. Henkel and S. Pötting, Appl. Phys. B **72** (2001) 73 (selected papers of the Bonn 2000 DPG meeting).
[10] L. Ryzhik, G. Papanicolaou, and J. B. Keller, Wave Motion **24**, 327 (1996).
[11] P. W. Anderson, Phys. Rev. **109**, 1492 (1958).
[12] C.-C. Cheng and M. G. Raymer, Phys. Rev. Lett. **82**, 4807 (1999).
[13] J. C. Flores, Phys. Rev. B **60**, 30 (1999).
[14] S. A. Gurvitz, Phys. Rev. Lett. **85**, 812 (2000).

Appendix C

List of papers

Note added in proof (07 June 2004). This list contains updated bibliographic information.

C. Henkel and J.-Y. Courtois (1998), "Atomic recoil and momentum diffusion close to a vacuum–dielectric interface", *Eur. Phys. J. D* **3**, 129.

C. Henkel and V. Sandoghdar (1998), "Single-molecule spectroscopy near structured dielectrics", *Opt. Commun.* **158**, 250.

C. Henkel, S. Pötting, and M. Wilkens (1999b), "Loss and heating of particles in small and noisy traps", *Appl. Phys. B* **69**, 379. (**Invited paper**.)

C. Henkel, H. Wallis, N. Westbrook, C. I. Westbrook, A. Aspect, K. Sengstock, and W. Ertmer (1999a), "Theory of atomic diffraction from evanescent waves", *Appl. Phys. B* **69**, 277. (**Review paper**.)

C. Henkel and M. Wilkens (1999), "Heating of trapped atoms near thermal surfaces", *Europhys. Lett.* **47**, 414.

C. Henkel, K. Joulain, R. Carminati, and J.-J. Greffet (2000), "Spatial coherence of thermal near fields", *Opt. Commun.* **186**, 57.

C. Henkel (2001), "Coherent transport", *C. R. Acad. Sci. (Paris), Série IV* **2**, 573.

C. Henkel and S. Pötting (2001), "Coherent transport of matter waves", *Appl. Phys. B* **72**, 73. (**Invited paper**.)

R. Folman, P. Krüger, J. Schmiedmayer, J. H. Denschlag, and C. Henkel (2002), "Microscopic atom optics: from wires to an atom chip", *Adv. At. Mol. Opt. Phys.* **48**, 263, edited by B. Bederson (Academic Press, New York). (**Review paper**.)

C. Henkel, K. Joulain, J.-P. Mulet, and J.-J. Greffet (2002), "Radiation forces on small particles in thermal near fields", *J. Opt. A: Pure Appl. Opt.* **4**, S109.

G. Boedecker and C. Henkel (2003), "All-frequency effective medium theory for a photonic crystal", *Opt. Express* **11**, 1590.

C. Henkel, P. Krüger, R. Folman, and J. Schmiedmayer (2003c), "Fundamental Limits for Coherent Manipulation on Atom Chips", *Appl. Phys. B* **76**, 173 (**Invited paper**.)

L. Rogobete, H. Schniepp, V. Sandoghdar, and C. Henkel (2003b), "Spontaneous emission in nanoscopic dielectric particles", *Opt. Lett.* **28** (2003) 1736.

C. Henkel and S. A. Gardiner (2004), "Decoherence of Bose-Einstein condensates in microtraps", *Phys. Rev. A* **69** (2004) 043602.

C. Henkel, S. A. Gardiner, and A. Negretti (2004a), "(De)coherence physics with condensates in microtraps", *Las. Phys.* **14** (2004) 615, proceedings of the 12th International Workshop on Laser Physics, Hamburg 2003.

C. Henkel, K. Joulain, J. P. Mulet, and J. J. Greffet (2004b), "Coupled surface polaritons and the Casimir force", *Phys. Rev. A* **69** (2004) 023808.

L. Rogobete, V. Sandoghdar, and C. Henkel (2003a), "Modifications of spontaneous emission in nanoscopic environments", unpublished.

G. Boedecker, C. Henkel, C. Hermann, O. Hess (2004), "Spontaneous emission in photonic structures: theory and simulation", ch. 2 of "Photonic crystals – advances in design, fabrication and characterization", K. Busch et al., eds. (Wiley-VCH, Berlin), pp.23-42. (**Invited contribution**.)

Bibliography

G. S. Agarwal (1975a). Quantum electrodynamics in the presence of dielectrics and conductors. I. Electromagnetic-field response functions and black-body fluctuations in finite geometries, *Phys. Rev. A* **11**, 230–242.

G. S. Agarwal (1975b). Quantum electrodynamics in the presence of dielectrics and conductors. II. Theory of dispersion forces, *Phys. Rev. A* **11**, 243–252.

G. S. Agarwal (1975c). Quantum electrodynamics in the presence of dielectrics and conductors. IV. General theory for spontaneous emission in finite geometries, *Phys. Rev. A* **12**, 1475–1497.

G. S. Agarwal (1977). Interaction of electromagnetic waves at rough dielectric surfaces, *Phys. Rev. B* **15**, 2371–2383.

Y. Aharonov & A. Stern (1992). Origin of the geometric forces accompanying Berry's geometric potentials, *Phys. Rev. Lett.* **69** (25), 3593–97.

P. W. Anderson (1958). Absence of diffusion in certain random lattices, *Phys. Rev.* **109**, 1492–1505.

N. W. Ashcroft & N. D. Mermin (1976). *Solid State Physics*. Saunders, Philadelphia.

R. Bancroft (1996). *Understanding electromagnetic scattering using the Moment Method: a practical approach*. Artech House Inc., Norwood Mass.

W. L. Barnes (1998). Fluorescence near interfaces: the role of photonic mode density, *J. mod. Optics* **45**, 661–699.

G. Barton (1991). On the fluctuations of the Casimir force, *J. Phys. A: Math. Gen.* **24** (5), 991–1005.

T. H. Bergeman, P. McNicholl, J. Kycia, H. Metcalf & N. Balazs (1989). Quantized Motion of Atoms in a Quadrupole Magnetostatic Trap, *J. Opt. Soc. B* **6**, 2249–56.

E. Betzig & R. J. Chichester (1993). Single molecules observed by near-field scanning optical microscopy, *Science* **262**, 1422–25.

A. Beveratos, R. Brouri, T. Gacion, J.-P. Poizat & P. Grangier (2001). Nonclassical radiation from diamond nanocrystals, *Phys. Rev. A* **64**, 061802(R).

G. Boedecker & C. Henkel (2003). All-frequency effective medium theory for a photonic crystal, *Opt. Express* **11** (13), 1590–95.

G. Boedecker, C. Henkel, C. Hermann & O. Hess (2004). Spontaneous emission in photonic structures: theory and simulation, in K. Busch, S. Lölkes, R. Wehrspohn & H. Föll, editors, *Photonic crystals – advances in design, fabrication and characterization*, chapter 2, pp.23–42. Wiley-VCH, Weinheim Berlin.

C. J. Bordé (1989). Atomic interferometry with internal state labelling, *Phys. Lett. A* **140**, 10–12.

C. J. Bordé (1997). Matter-wave interferometers: a synthetic approach. in P. R. Berman, editor, *Adv. At. Mol. Opt. Phys.*, volume 37, Suppl. 3, pages 257–92. Academic Press, New York.

M. Born & E. Wolf (1959). *Principles of Optics*. Pergamon Press, Oxford, 6th edition.

E. Buks & M. L. Roukes (2001). Stiction, adhesion energy, and the Casimir effect in micromechanical systems, *Phys. Rev. B* **63**, 03 3402.

K. Busch, N. Vats, S. John & B. C. Sanders (2000). Radiating dipoles in photonic crystals, *Phys. Rev. E* **62** (3), 4251–60.

H. B. Callen & T. A. Welton (1951). Irreversibility and generalized noise, *Phys. Rev.* **83** (1), 34–40.

R. Carminati & J.-J. Greffet (1995a). Influence of dielectric contrast and topography on the near field scattered by an inhomogeneous surface, *J. Opt. Soc. Am. A* **12**, 2716–25.

R. Carminati & J.-J. Greffet (1995b). Two-dimensional numerical simulation of the photon scanning tunneling microscope. Concept of transfer function., *Opt. Commun.* **116**, 316–21.

R. Carminati & J.-J. Greffet (1999). Near-field effects in spatial coherence of thermal sources, *Phys. Rev. Lett.* **82**, 1660–63.

C. K. Carnaglia & L. Mandel (1971). Quantization of evanescent electromagnetic waves, *Phys. Rev. D* **3**, 280–296.

H. B. Casimir & D. Polder (1948). The influence of retardation on the London-van der Waals forces, *Phys. Rev.* **73**, 360–372.

H. B. G. Casimir (1948). On the attraction between two perfectly conducting plates, *Proc. Kon. Ned. Akad. Wet.* **51**, 793–95.

Y. Castin & R. Dum (1996). Bose-Einstein condensates in time dependent traps, *Phys. Rev. Lett.* **77**, 5315–5319.

H. B. Chan, V. A. Aksyuk, R. N. Kleiman, D. J. Bishop & F. Capasso (2001). Quantum mechanical actuation of microelectromechanical systems by the Casimir force, *Science* **291** (5510), 1941–44.

R. R. Chance, A. Prock & R. Silbey (1978). Molecular fluorescence and energy transfer near interfaces. in I. Prigogine & S. A. Rice, editors, *Advances in Chemical Physics XXXVII*, pages 1–65. Wiley & Sons, New York.

S. Chandrasekhar (1960). *Radiative Transfer*. Dover, New York.

C.-C. Cheng & M. G. Raymer (1999). Long-range saturation of spatial decoherence in wave-field transport in random multiple-scattering media, *Phys. Rev. Lett.* **82**, 4807–4810.

H. Chew (1988). Radiation and lifetimes of atoms inside dielectric particles, *Phys. Rev. A* **38** (7), 3410–16.

M. E. Crenshaw & C. M. Bowden (2000). Effects of local fields on spontaneous emission in dielectric media, *Phys. Rev. Lett.* **85** (9), 1851–54.

P. de Vries, D. V. van Coevorden & A. Lagendijk (1998). Point scatterers for classical waves, *Rev. Mod. Phys.* **70** (2), 447–66.

J. P. Dowling & J. Gea-Banacloche (1997). Evanescent light-wave atom mirrors, resonators, waveguides, and traps. in P. R. Berman, editor, *Adv. At. Mol. Opt. Phys.*, volume 37, Suppl. 3, pages 1–94. Academic Press, New York.

H. T. Dung, S. Y. Buhmann, L. Knöll, D.-G. Welsch & S. Scheel (2003). Electromagnetic-field quantization and spontaneous decay in left-handed media, *Phys. Rev. A* **68**, 043816.

H. T. Dung, L. Knöll & D.-G. Welsch (2000). Spontaneous decay in the presence of dispersing and absorbing bodies: general theory and application to a spherical cavity, *Phys. Rev. A* **62**, 053804.

R. C. Dunn (1999). Near-field scanning optical microscopy, *Chem. Rev.* **99**, 2891–2927.

C. Eberlein (1992). Fluctuations of Casimir forces on finite objects. I. Spheres and hemispheres, *J. Phys. A: Math. Gen.* **25** (10), 3015–37.

P. J. Feibelman (1982). Surface electromagnetic fields, *Progr. Surf. Sci.* **12**, 287–408.

A. L. Fetter (1999). Theory of a dilute low-temperature trapped Bose condensate. in M. Inguscio, S. Stringari & C. E. Wieman, editors, *Bose-Einstein condensation in atomic gases*, Amsterdam Oxford. IOS Press. Proceedings of the International School of Physics "Enrico Fermi" (Course CXL, Varenna July 1998).

R. Folman, P. Krüger, J. Schmiedmayer, J. H. Denschlag & C. Henkel (2002). Microscopic atom optics: from wires to an atom chip, *Adv. At. Mol. Opt. Phys.* **48**, 263–356.

G. W. Ford & W. H. Weber (1984). Electromagnetic interactions of molecules with metal surfaces, *Phys. Rep.* **113**, 195–287.

J. Fortágh, H. Ott, S. Kraft & C. Zimmermann (2002). Surface effects on a Bose-Einstein condensate in a magnetic microtrap, *Phys. Rev. A* **66**, 041604(R).

A. Franchini & V. Bartolani (1994). Inelastic He-atom scattering from metal surfaces, *Comp. Phys. Commun.* **80**, 90–118.

R. Frisch & E. Segré (1933). *Zeitschr. für Physik* **75**, 610.

J. L. Gall, M. Olivier & J.-J. Greffet (1997). Experimental and theoretical study of reflection and coherent thermal emission by a SiC grating supporting a surface-phonon polariton, *Phys. Rev. B* **55**, 10105–10114.

E. Gerlach (1971). Equivalence of can der Waals forces between solids and the surface-plasmon interaction, *Phys. Rev. B* **4** (2), 393–96.

C. Girard, O. J. F. Martin & A. Dereux (1995). Molecular lifetime changes induced by nanometer scale optical fields, *Phys. Rev. Lett.* **75**, 3098–3101.

R. J. Glauber & M. Lewenstein (1991). Quantum optics of dielectric media, *Phys. Rev. A* **43**, 467–491.

J. P. Gordon & A. Ashkin (1980). Motion of Atoms in a Radiation Trap, *Phys. Rev. A* **21**, 1606–1617.

S. Gov, S. Shtrikman & H. Thomas (1998). Magnetic Trapping of Neutral Particles: A Study of a Physically Realistic Model, preprint quant-ph/9812079.

S. Gov, S. Shtrikman & H. Thomas (2000a). 1D toy model for magnetic trapping, *Am. J. Phys.* **68** (4), 334–43.

S. Gov, S. Shtrikman & H. Thomas (2000b). Magnetic trapping of neutral particles: classical and quantum-mechanical study of a Ioffe-Pritchard type trap, *J. Appl. Phys.* **87** (8), 3989–3998.

J.-J. Greffet (1988). Scattering of electromagnetic waves at rough dielectric surfaces, *Phys. Rev. B* **37**, 6436–6441.

J.-J. Greffet, R. Carminati, K. Joulain, J.-P. Mulet, S. Mainguy & Y. Chen (2001). Coherent emission of light by thermal sources, *Nature* **416**, 61–64.

J.-J. Greffet, A. Sentenac & R. Carminati (1995). Surface profile reconstruction using near-field data, *Opt. Commun.* **116**, 20–24.

R. Grimm, M. Weidemüller & Y. B. Ovchinnikov (2000). Optical dipole traps for neutral atoms, *Adv. At. Mol. Opt. Phys.* **42**, 95–170.

T. Gruner & D.-G. Welsch (1995). Correlation of radiation-field ground-state fluctuations in a dispersive and lossy dielectric, *Phys. Rev. A* **51**, 3246–3256.

T. L. Gustavson, P. Bouyer & M. Kasevich (1997). Precision rotation measurements with an atom interferometer gyroscope, *Phys. Rev. Lett.* **78**, 2046–2049.

F. Haake & R. Reibold (1985). Strong damping and low-temperature anomalies for the harmonic oscillator, *Phys. Rev. A* **32** (4), 2462–75.

F. D. M. Haldane (2002). Electromagnetic surface modes at interfaces with negative refractive index make a "not-quite-perfect" lens, preprint cond-mat/0206420.

M. Hammes, D. Rychtarik, B. Engeser, H.-C. Nägerl & R. Grimm (2003). Evanescent-wave trapping and evaporative cooling of an atomic gas near two-dimensionality, *Phys. Rev. Lett.* **90**, 173001.

W. Hänsel, P. Hommelhoff, T. W. Hänsch & J. Reichel (2001). Bose-Einstein condensation on a microelectronic chip, *Nature* **413**, 498–501.

D. M. Harber, J. M. McGuirk, J. M. Obrecht & E. A. Cornell (2003). Thermally induced losses in ultra-cold atoms magnetically trapped near room-temperature surfaces, *J. Low Temp. Phys.* **133**, 229–38.

S. Haroche (1992). Cavity Quantum Electrodynamics. in J. Dalibard, J.-M. Raimond & J. Zinn-Justin, editors, *Fundamental Systems in Quantum Optics (Les Houches, Session LIII)*, pages 767–940, Amsterdam. North-Holland.

R. F. Harrington (1993). *Field computation by moment methods*. IEEE Press, Piscataway.

C. Henkel (2001). Coherent transport, *C. R. Acad. Sci. (Paris), Série IV* **2**, 573–80. Proceedings of the 'Euroconference on Atom Optics and Interferometry' (Cargese, France 26-29 july 2000).

C. Henkel & J.-Y. Courtois (1998). Atomic recoil and momentum diffusion close to a vacuum–dielectric interface, *Eur. Phys. J. D* **3**, 129–153.

C. Henkel, K. Joulain, R. Carminati & J.-J. Greffet (2000). Spatial coherence of thermal near fields, *Opt. Commun.* **186**, 57–67.

C. Henkel & S. Pötting (2001). Coherent transport of matter waves, *Appl. Phys. B* **72** (1), 73–80. Selected papers of the Bonn 2000 DPG meeting.

C. Henkel & V. Sandoghdar (1998). Single-molecule spectroscopy near structured dielectrics, *Opt. Commun.* **158**, 250–262.

C. Henkel, H. Wallis, N. Westbrook, C. I. Westbrook, A. Aspect, K. Sengstock & W. Ertmer (1999a). Theory of atomic diffraction from evanescent waves, *Appl. Phys. B* **69**, 277–289. Special issue 'Atom optics with laser cooled atoms'.

C. Henkel & S. A. Gardiner (2004). Decoherence of Bose-Einstein condensates in microtraps, *Phys. Rev. A* **69**, 043602.

C. Henkel, S. A. Gardiner & A. Negretti (2004a). (De)coherence physics with condensates in microtraps, *Laser Physics* **14**, 615–20. Proceedings of the 12th International Workshop on Laser Physics, Hamburg 2003.

C. Henkel, K. Joulain, J.-P. Mulet & J.-J. Greffet (2002). Radiation forces on small particles in thermal near fields, *J. Opt. A: Pure Appl. Opt.* **4** (5), S109–14. Special issue "Electromagnetic Optics" (EOS Topical Meeting, Paris 26–30 august 2001).

C. Henkel, K. Joulain, J.-P. Mulet & J.-J. Greffet (2004b). Coupled surface polaritons and the Casimir force, *Phys. Rev. A* **69**, 023808.

C. Henkel, P. Krüger, R. Folman & J. Schmiedmayer (2003c). Fundamental Limits for Coherent Manipulation on Atom Chips, *Appl. Phys. B* **76**, 173–82. Selected papers of the DPG spring meeting "Quantum Optics" (Osnabrück, 04–08 march 2002).

C. Henkel, S. Pötting & M. Wilkens (1999b). Loss and heating of particles in small and noisy traps, *Appl. Phys. B* **69**, 379–387. Selected papers of the Heidelberg 1999 DPG meeting.

C. Henkel & M. Wilkens (1999). Heating of trapped atoms near thermal surfaces, *Europhys. Lett.* **47**, 414–420.

C. H. Henry & R. F. Kazarinov (1996). Quantum noise in photonics, *Rev. Mod. Phys.* **68**, 801.

N. R. Hill, M. Haller & V. Celli (1982). Van der Waals forces and molecular diffraction from metal surfaces, with application to Ag(111), *Chem. Phys.* **73** (3), 363–75.

E. A. Hinds & C. Eberlein (2000). Quantum propagation of neutral atoms in a magnetic quadrupole guide, *Phys. Rev. A* **61**, 033614 (13 pages). Erratum: Phys. Rev. A **64** (2001) 039902(E).

E. A. Hinds & I. G. Hughes (1999). Magnetic atom optics: mirrors, guides, traps, and chips for atoms, *J. Phys. D: Appl. Phys.* **32** (18), R119–R146.

B. Huttner, J. J. Baumberg & S. M. Barnett (1991). Canonical quantization of light in a linear dielectric, *Europhys. Lett.* **16**, 177–182.

IEEE J. Quant. El. (2002) **38** (7). Feature Section: Photonic Crystal Structures and Applications, T. F. Krauss & T. Baba, editors.

J. Microsc. (March 2003) **209** (3), 149–276. Topical Issue on Near Field Optics, L. Novotny, editor.

J. D. Jackson (1975). *Classical Electrodynamics*. Wiley & Sons, New York, second edition.

A. M. Jayannavar & N. Kumar (1982). Nondiffusive quantum transport in a dynamically disordered medium, *Phys. Rev. Lett.* **48** (8), 553–56.

J. D. Joannopoulos, R. D. Meade & J. N. Winn (1995). *Photonic Crystals*. Princeton University Press, Princeton, Chichester.

S. John (1987). Strong localization of photons in certain disordered dielectric superlattices, *Phys. Rev. Lett.* **58**, 2486–2489.

S. John & T. Quang (1994). Spontaneous emission near the edge of a photonic band gap, *Phys. Rev. A* **50**, 1764–1769.

S. John & J. Wang (1990). Quantum electrodynamics near a photonic band gap: photon bound states and dressed atoms, *Phys. Rev. Lett.* **64**, 2418–2421.

M. P. A. Jones, C. J. Vale, D. Sahagun, B. V. Hall & E. A. Hinds (2003). Spin coupling between cold atoms and the thermal fluctuations of a metal surface, *Phys. Rev. Lett.* **91**, 080401 (4 pages).

K. Joulain, R. Carminati, J.-P. Mulet & J.-J. Greffet (2003). Definition and measurement of the local density of electromagnetic states close to an interface, *Phys. Rev. B* **68**, 245405 (10 pages).

N. G. V. Kampen, B. R. A. Nijboer & K. Schram (1968). On the macroscopic theory of van der Waals forces, *Phys. Lett.* **26A** (7), 307–08.

M. Kasevich & S. Chu (1992). Measurement of the gravitational acceleration of an atom with a light-pulse atom interferometer, *Appl. Phys. B* **54**, 321–332.

O. Kenneth, I. Klich, A. Mann & M. Revzen (2002). Repulsive Casimir forces, *Phys. Rev. Lett.* **89**, 033001.

L. Knöll, S. Scheel & D.-G. Welsch (2001). QED in dispersing and absorbing media, in J. Peřina, editor, *Coherence and Statistics of Photons and Atoms*. John Wiley & Sons, Inc., New York.

S. Kraft, A. Günther, H. Ott, D. Wharam, C. Zimmermann & J. Fortágh (2002). Anomalous longitudinal magnetic field near the surface of copper conductors, *J. Phys. B: Atom. Molec. Phys.* **35**, L469–74.

A. B. Kuklov, N. Chensincki & J. L. Birman (2002). Symmetries and decoherence of two-component confined atomic clouds: study of the atomic echo in the two-component Bose-Einstein condensate, *Laser Physics* **12** (1), 127–44. Proceedings of the 10th International Workshop on Laser Physics.

D. V. Labeke & D. Barchiesi (1993). Probes for scanning tunneling optical microscopy: a theoretical comparison, *J. Opt. Soc. Am. A* **10**, 2193–2201.

A. Lagendijk, B. Nienhuis, B. A. van Tiggelen & P. de Vries (1997). Microscopic approach to the Lorentz cavity in dielectrics, *Phys. Rev. Lett.* **79**, 657–660.

A. Lambrecht & S. Reynaud (2000). Casimir force between metallic mirrors, *Eur. Phys. J. D* **8**, 309–318.

A. Lambrecht (2002). The Casimir effect: a force from nothing, *Physics World* **15** (9), 29–32.

P. Lambropoulos, G. M. Nikolopoulos, T. R. Nielsen & S. Bay (2000). Fundamental quantum optics in structured reservoirs, *Rep. Prog. Phys.* **63** (4), 455–503.

S. K. Lamoreaux (1997). Demonstration of the Casimir force in the 0.6 to 6 μm range, *Phys. Rev. Lett.* **78**, 5–8. Erratum: **81** (1998) 5475.

A. E. Leanhardt, Y. Shin, A. P. Chikkatur, D. Kielpinski, W. Ketterle & D. E. Pritchard (2003). Bose-Einstein condensates near a microfabricated surface, *Phys. Rev. Lett.* **90**, 100404.

A. Lenef, T. D. Hammond, E. T. Smith, M. S. Chapman, R. A. Rubenstein & D. E. Pritchard (1997). Rotation sensing with an atom interferometer, *Phys. Rev. Lett.* **78**, 760–763.

M. Lewenstein, J. Zakrzewski & T. W. Mossberg (1988). Spontaneous emission of atoms coupled to frequency-dependent reservoirs, *Phys. Rev. A* **38**, 808–819.

E. M. Lifshitz (1956). The theory of molecular attractive forces between solids, *Soviet Phys. JETP* **2**, 73–83. [*J. Exper. Theoret. Phys. USSR* **29**, 94 (1955)].

Y.-J. Lin, I. Teper, C. Chin & V. Vuletić (2004). Impact of Casimir-Polder potential and Johnson noise on Bose-Einstein condensate stability near surfaces, *Phys. Rev. Lett.* **92**, 050404.

L. Mandel & E. Wolf (1995). *Optical coherence and quantum optics*. Cambridge University Press, Cambridge.

P. Markoš & C. M. Soukoulis (2003). Structures with negative index of refraction, *phys. stat. sol. (a)* **197** (3), 595–604.

C. Menotti, J. R. Anglin, J. I. Cirac & P. Zoller (2001). Dynamic splitting of a Bose-Einstein condensate, *Phys. Rev. A* **63** (2), 023601.

P. Meystre (2001). *Atom Optics*. Springer, Berlin.

J. Michaelis, C. Hettich, J. Mlynek & V. Sandoghdar (2000). Optical microscopy using a single-molecule light source, *Nature* **405**, 325–328.

J. Michaelis, C. Hettich, A. Zayats, B. Eiermann, J. Mlynek & V. Sandoghdar (1999). Mapping an optical standing wave with a single molecule, *Opt. Lett.* **24**, 581–583.

U. Mohideen & A. Roy (1998). Precision measurement of the Casimir force from 0.1 to 0.9 μm, *Phys. Rev. Lett.* **81** (21), 4549–52.

T. W. Mossberg & M. Lewenstein (1993). Radiative properties of strongly driven atoms in the presence of photonic bands and gaps, *J. Opt. Soc. Am. B* **10** (2), 340–45.

V. M. Mostepanenko & N. N. Trunov (1997). *The Casimir Effect and Its Applications*. Oxford Science Publications, Oxford.

J. H. Müller, O. Morsch, D. Ciampini, M. Anderlini, R. Mannella & E. Arimondo (2000). Atomic micromotion and geometric forces in a triaxial magnetic trap, *Phys. Rev. Lett.* **85** (21), 4454–57.

M. Nieto-Vesperinas (1982). Depolarization of electromagnetic waves scattered from slightly rough random surfaces: a study by means of the extinction theorem, *J. Opt. Soc. Am.* **72**, 539–547.

M. Nieto-Vesperinas (1991). *Scattering and Diffraction in Physical Optics*. Wiley & Sons, New York.

L. Novotny (1996). Single molecule fluorescence in inhomogeneous environments, *Appl. Phys. Lett.* **69**, 3806–3808.

Opt. Express (2001) **8** (3), 166–222. Focus Issue: Photonic Bandgap Calculations, M. de Sterke & K. Busch, editors.

Opt. Quantum Electr. (2002) **34** (1–3), 1–310. Special Issue: Photonic and Electromagnetic Crystals, R. M. De La Rue, editor. Proceedings of the Sendai workshop (March 2000).

H. Ott, J. Fortagh, G. Schlotterbeck, A. Grossmann & C. Zimmermann (2001). Bose-Einstein condensation in a surface microtrap, *Phys. Rev. Lett.* **87**, 230401.

G. Parent, D. V. Labeke & D. Barchiesi (1999a). Fluorescence lifetime of a molecule near a corrugated interface: application to near-field microscopy, *J. Opt. Soc. Am. A* **16**, 896–908.

G. Parent, D. V. Labeke & D. Barchiesi (1999b). Surface imaging in near-field optical microscopy by using the fluorescence decay rate: a theoretical study, *J. Microsc.* **194** (2–3), 281–90.

J. B. Pendry (2000). Negative refraction index makes a perfect lens, *Phys. Rev. Lett.* **85** (18), 3966–69. Comments by G. W. t'Hooft, Phys. Rev. Lett. 87 (2001) 249701; J. M. Williams, Phys. Rev. Lett. 87 (2001) 249703.

A. Peters, K. Y. Chung & S. Chu (1999). Measurement of gravitational acceleration by dropping atoms, *Nature* **400**, 849–852.

phys. stat. sol. (a) (2003) **197** (3), 589–702. Photonic Crystals: Optical Materials for the 21st Century, K. Busch & R. Wehrspohn, editors.

C. Raabe, D.-G. Welsch & L. Knöll (2003). Three-dimensional Casimir force between absorbing multilayer dielectrics, *Phys. Rev. A* **68**, 033810 (19 pages).

H. Raether (1988). *Surface Plasmons on Smooth and Rough Surfaces and on Gratings*, volume 111 of *Springer Tracts in Modern Physics*. Springer, Berlin, Heidelberg.

A. Rahmani (2002). Local-field correction for an interstitial impurity in a crystal, *Opt. Lett.* **27** (6), 430–32.

A. Rahmani, P. C. Chaumet & F. de Fornel (2001). Environment-induced modification of spontaneous emission: Single-molecule near-field probe, *Phys. Rev. A* **63** (2), 023819.

A. Rahmani, P. C. Chaumet, F. de Fornel & C. Girard (1997). Field propagator of a dressed junction: fluorescence lifetime calculations in confined geometry, *Phys. Rev. A* **56**, 3245–3254.

L. Rayleigh (1907). On the dynamical theory of gratings, *Proc. R. Soc. London A* **79**, 399–416.

J. Reichel, W. Hänsel, P. Hommelhoff & T. W. Hänsch (2001). Applications of integrated magnetic microtraps, *Appl. Phys. B* **72**, 81–89.

F. Riehle, T. Kisters, A. Witte, J. Helmcke & C. J. Bordé (1991). Optical Ramsey spectoscopy in a rotating frame: Sagnac effet in a matter-wave interferometer, *Phys. Rev. Lett.* **67**, 177–180.

L. Rogobete, V. Sandoghdar & C. Henkel (2003a). Modification of spontaneous emission in nanoscopic environments. In preparation.

L. Rogobete, H. Schniepp, V. Sandoghdar & C. Henkel (2003b). Spontaneous emission in nanoscopic dielectric particles, *Opt. Lett.* **28** (19), 1736–38.

D. Rychtarik, B. Engeser, H.-C. Ngerl & R. Grimm (2004). Two-dimensional Bose-Einstein condensate in an optical surface trap, *Phys. Rev. Lett.* **92**, 173003.

S. M. Rytov, Y. A. Kravtsov & V. I. Tatarskii (1989). *Elements of Random Fields*, volume 3 of *Principles of Statistical Radiophysics*. Springer, Berlin.

K. Sakoda (2001). *Optical Properties of Photonic Crystals*. Springer, Berlin Heidelberg.

C. Santori, D. Fattal, J. Vučković, G. S. Solomon & Y. Yamamoto (2002). Indistinguishable photons from a single-photon device, *Nature* **419**, 594–97.

S. Savasta, O. D. Stefano & R. Girlanda (2002). Light quantization for arbitrary scattering systems, *Phys. Rev. A* **65**, 043801.

S. Scheel, L. Knöll, D.-G. Welsch & S. M. Barnett (1999). Quantum local-field corrections and spontaneous decay, *Phys. Rev. A* **60**, 1590–1597.

F. Schmidt-Kaler, H. Häffner, M. Riebe, S. Gulde, G. P. T. Lancaster, T. Deuschle, C. Becher, C. F. Roos, J. Eschner & R. Blatt (2003). Realization of the Ciac-Zoller controlled-NOT quantum gate, *Nature* **422**, 408–11.

H. Schniepp & V. Sandoghdar (2002). Spontaneous emission of europium ions embedded in dielectric nanospheres, *Phys. Rev. Lett.* **89**, 257403.

C. Schroll, W. Belzig & C. Bruder (2003). Decoherence of cold atomic gases in magnetic micro-traps, *Phys. Rev. A* **68**, 043618.

F. J. P. Schuurmans, P. de Vries & A. Lagendijk (2000). Local-field effects on spontaneous emission of impurity atoms in homogeneous dielectrics, *Phys. Lett. A* **264**, 472–77.

T. Setälä, A. Shevchenko, M. Kaivola & A. T. Friberg (2002a). Degree of polarization for optical near fields, *Phys. Rev. E* **66**, 016615 (7 pages).

T. Setälä, M. Kaivola & A. T. Friberg (2002b). Degree of polarization in near fields of thermal sources: effects of surface waves, *Phys. Rev. Lett.* **88**, 123902.

A. V. Shchegrov, K. Joulain, R. Carminati & J.-J. Greffet (2000). Near-field spectral effects due to electromagnetic surface excitations, *Phys. Rev. Lett.* **85**, 1548–1551.

J. A. Sidles, J. L. Garbini, W. M. Dougherty & S.-H. Chao (2003). The classical and quantum theory of thermal magnetic noise, with applications in spintronics and quantum microscopy, *Proc. IEEE* **91** (5), 799–816.

E. Snoeks, A. Lagendijk & A. Polman (1995). Measuring and modifying the spontaneous emission rate of Erbium near an interface, *Phys. Rev. Lett.* **74**, 2459–2462.

C. Soukoulis, editor (2001). *Photonic Crystals and Light Localization in the 21th Century*, volume 563 of *NATO Science Series C*. Kluwer, Dordrecht.

O. D. Stefano, S. Savasta & R. Girlanda (1999). Electromagnetic-field quantization in absorbing confined systems, *Phys. Rev. A* **60**, 1614–1625.

O. D. Stefano, S. Savasta & R. Girlanda (2000). Three-dimensional electromagnetic field quantization in absorbing and dispersive bounded dielectrics, *Phys. Rev. A* **61**, 02 3803.

H. T. C. Stoof (1999). Coherent versus incoherent dynamics during Bose-Einstein condensation in atomic gases, *J. Low Temp. Phys.* **114** (1–2), 11–108.

C. V. Sukumar & D. M. Brink (1997). Spin-flip transitions in a magnetic trap, *Phys. Rev. A* **56**, 2451–2454.

A. Tip (1997). Canonical formalism and quantization for a class of classical fields with application to radiative atomic decay in dielectrics, *Phys. Rev. A* **56** (6), 5022–41.

A. Tip, A. Moroz & J. M. Combes (2000). Band structure of absorptive photonic crystals, *J. Phys. A: Math. Gen.* **33** (35), 6223–52.

Q. A. Turchette, D. Kielpinski, B. E. King, D. Leibfried, D. M. Meekhof, C. J. Myatt, M. A. Rowe, C. A. Sackett, C. S. Wood, W. M. Itano, C. Monroe & D. J. Wineland (2000). Heating of trapped ions from the quantum ground state, *Phys. Rev. A* **61**, 063418.

H. van Kampen, V. A. Sautenkov, C. J. C. Smeets, E. R. Eliel & J. P. Woerdman (1999). Measurement of the excitation dependence of the Lorentz local-field shift, *Phys. Rev. A* **59** (1), 271–74.

N. G. van Kampen (1992). *Stochastic Processes in Physics and Chemistry*. Elsevier, Amsterdam, revised edition.

T. Varpula & T. Poutanen (1984). Magnetic field fluctuations arising from thermal motion of electric charge in conductors, *J. Appl. Phys.* **55**, 4015–21.

V. G. Veselago (1968). The electrodynamics of substances with simultaneously negative values of ϵ and μ, *Sov. Phys. Usp.* **10** (4), 509–14. [*Usp. Fiz. Nauk.*, **92** (1967) 517–26].

D.-W. Wang, M. D. Lukin & E. Demler (2003). Disordered Bose-Einstein condensates in quasi one-dimensional magnetic microtraps, *Phys. Rev. Lett.* **92**, 076802.

D. J. Wineland, C. Monroe, W. M. Itano, D. Leibfried, B. E. King & D. M. Meekhof (1998). Experimental issues in coherent quantum-state manipulation of trapped atomic ions, *J. Res. Natl. Inst. Stand. Technol.* **103**, 259–328.

M. Woldeyohannes & S. John (2003). Coherent control of spontaneous emission near a photonic band edge, *J. Opt. B: Quantum Semicl. Opt.* **5** (2), R43–R82.

P. T. Worthing, R. M. Amos & W. L. Barnes (1999). Modification of the spontaneous emission rate of Eu^{3+} ions embedded within a dielectric layer above a silver mirror, *Phys. Rev. A* **59**, 865–872.

J. M. Wylie & J. E. Sipe (1984). Quantum electrodynamics near an interface, *Phys. Rev. A* **30**, 1185–1193.

E. Yablonovitch (1987). Inhibited spontaneous emission in solid-state physics and electronics, *Phys. Rev. Lett.* **58**, 2059–2062.

S.-Y. Zhu, Y. Yang, H. Chen, H. Zheng & M. S. Zubairy (2000). Spontaneous Radiation and Lamb shift in three-dimensional photonic crystals, *Phys. Rev. Lett.* **84**, 2136–39.

R. W. Ziolkowski & E. Heyman (2001). Wave propagation in media having negative permittivity and permeability, *Phys. Rev. E* **64**, 056625.

W. H. Zurek (1991). Decoherence and the transition from quantum to classical, *Physics Today* **44** (October 1991), 36–44.